SAINT PETERSBURG STATE UNIVERSITY

Prokhorova Daria Sergeevna

Initial configurations and fusion of colour strings as origin of collective signatures in $p + p$ interactions at high energies

Specialisation 1.3.3. Theoretical physics

Dissertation is submitted for the degree
of Candidate of Physical and Mathematical Sciences

Thesis supervisor:
Grigory Aleksandrovich Feofilov
Candidate of Physical and Mathematical Sciences

Saint Petersburg
2024

Contents

Introduction

Relevance of the research topic.

Living in the era of RHIC (Relativistic Heavy Ion Collider) and LHC (Large Hadron Collider), one has access to the unprecedentedly huge amount of data on particle production in relativistic collisions of hadrons and ions recorded by the state-of-the-art experimental facilities. It is a profound collaboration between theoreticians and experimentalists in high energy physics that moves us towards solving the mysteries of the Universe.

In recent decades, a significant effort has been made in the study of a unique state of matter called quark-gluon plasma (QGP) [1]. It was suggested that QGP could be produced in central ion-ion ($A + A$) collisions if the critical energy density, $\varepsilon_{\text{crit}} \sim 1$ GeV/fm^3, and the critical temperature, $T_{\text{crit}} \sim 150$ – 160 MeV (that is equivalent to more than 10^{12} K), are exceeded. It was initially thought that the QGP formed under such conditions is in the weak coupling regime, that is, it represents a gas of asymptotically free quarks and gluons [2, 3]. However, further studies have shown that the emerging QGP is better described in the strong coupling regime and represents a nearly perfect fluid [4]. In this paradigm, the locally equilibrated QGP expands and cools down (hydrodynamic phase), evolving into a gas state of individual particles through a freeze-out mechanism [5]. This results in the formation of the plethora of hadrons that fly into detectors.

On the one hand, from the first principles of the theory of strong interaction, the description of such a multi-particle production is complicated by the fact that the majority of the particles are produced in soft processes that are characterised by the small momentum transferred. It leads to the transverse momenta of produced particles, p_T, generally not exceeding ~ 1 GeV. Therefore, the perturbative calculations in quantum chromodynamics (QCD) are inapplicable in this regime. This forces us to work in phenomenological approaches that can effectively describe the

transition, for instance, from a few colliding hadrons to hundreds and thousands of particles produced.

On the other hand, the first experimental evidence of QGP formation has been already claimed by CERN (Conseil Européen pour la Recherche Nucléaire) in 2000 [6] after analysing lead-lead and lead-gold collision events at SPS (Super Proton Synchrotron). In 2005, this statement was quantitatively confirmed by RHIC experiments [7, 8, 9, 10], whose studies raised questions about the properties of QGP produced in gold-gold collisions. Among many predicted QGP signals [11], e.g. strangeness enhancement [12], jet quenching [13, 14] etc., they focused on the observation [8] of the azimuthal anisotropy of produced particles [15, 16] which by that time had already been studied for a long time in nucleus-nucleus collisions [17, 18]. It has been proposed to express the magnitude of the effect in terms of Fourier coefficients, v_n, corresponding to the harmonics [19] of transverse flow of different orders, n : directed flow (v_1), elliptic flow (v_2), triangular flow (v_3) etc. Surprisingly, at RHIC, the values of elliptic flow harmonic appeared to be comparable to the calculations [20] assuming the presence of a relativistic viscous fluid in the early times of the ion collisions. This led to the hypothesis that it is the collective motion of thermally equilibrated partonic degrees of freedom that converts the spatial anisotropies of peripheral ion-ion collisions into momentum asymmetries of produced particles under the pressure gradients of the compressed medium.

It is worth noting that many results for $A + A$ collisions are traditionally presented with respect to proton-proton ($p + p$) data. In particular, it is believed that most similar and/or trivial effects or dependencies will cancel each other in the ratio of quantities measured in $A + A$ and $p + p$ reactions, and, thus, the collective behaviour of the produced particles, expected due to the formation of QGP in $A + A$ collisions, will manifest itself clearly. In this sense, inelastic proton-proton interactions are often assumed to be a baseline measurement in comparison to ion-ion collisions.

However, recently the QGP-like behaviour was observed also in small colliding systems. Namely, the relative yields of strange baryons measured by ALICE [21] in high-multiplicity $p+p$ interactions reach the values obtained for $p+Pb$ and $Pb+Pb$ collisions. Thus, the observed strangeness enhancement speaks in favour [22] of the existence of a common mechanism, for example, the QGP formation, in both $p + p$

and $A + A$ collisions. In addition, analysis of two-particle angular correlations in high-multiplicity $p + p$ interactions at LHC energies revealed [23, 24] the enhanced yields of particle pairs with the small difference in the azimuthal angles and arbitrarily large difference in pseudorapidities (the so-called near-side ridge structure). The associated transverse flow harmonics [25] unexpectedly appeared to be of the same order as the ones seen in peripheral heavy ion collisions [8].

On the one hand, there are successful attempts [26] to describe the collimated production of particles over the large rapidity range (the so-called long-range correlations) observed in $p+p$ reactions [23, 24] in the same manner as in $A+A$ collisions. On the other hand, there is a hot discussion [27] whether the hydro-description is justified for the matter produced in such a small droplet since it should not be able to reach local thermodynamic equilibrium prior to hadronisation [28].

From an alternative perspective, this phenomenon can be elucidated in the following manner. The long-range pseudorapidity correlations that form the measured near-side ridge [25] can arise only at the early times of the collision [29]. Thus, the problem of the origin of the ridge structure in $p+p$ collisions can be addressed in the complex frameworks based on the longitudinally extended objects of the colour field, so-called colour strings or colour flux tubes, formed at initial stages of collisions (e.g. Dual Parton Model [30], String percolation model [31], Colour-Glass Condensate + Glasma model [32]). In general, particle production in these approaches is carried out through the fragmentation of the colour field tubes, which gives a uniform distribution of particles in rapidity [33, 34] and can provide the long-range correlations that are intrinsic to this picture. Plenty of widely used Monte-Carlo event generators are based on certain ideas of these approaches, such as EPOS [35], PYTHIA [36], HIJING [37], AMPT [38] etc.

In turn, this thesis is also devoted to the development of the Monte-Carlo model of multi-particle production based on the colour string formation scenario and aimed to study the collective effects in small systems. What in principle differentiates our approach from the aforementioned event generators and from the original string model is the set of applied mechanisms that are responsible for string-string interactions and the resulting correlated particle yields. The obvious advantage of a specifically designed model is that it has only a few parameters, as opposed to hundreds of them in the full-chain event generators that include many physical pro-

cesses. Thus, we anticipate that our preliminary estimates will demonstrate whether the nature of collective effects observed in $p+p$ collisions can be revealed using new simplified model.

Elaboration of the topic.

The aforementioned class of colour string models traces its origin back to the pre-QCD Regge-Gribov effective field theory [39]. In this approach, the scattering amplitude is expanded in the series of poles in the complex angular momentum related to the exchange of particles belonging to a certain Regge trajectory [40]. In the high energy limit, the existence of the leading pole, called pomeron [41, 42], contribution to the scattering amplitude was suggested. Thus, a high-energy proton-proton inelastic interaction can be viewed via the multiple exchanges of pomerons.

With the advent of QCD, it has been shown [43, 44, 45] that the contributions to the $1/N_c$ and $1/N_f$ expansion of the amplitude in the limit of simultaneously large number of colours, N_c, and large number of flavours, N_f, (such that $N_c/N_f = \text{const}$) can be classified by the topologies of the corresponding diagrams. Thus, they can be grouped to obtain the leading order contribution to the S-matrix and to find the infrared spectrum of the theory. It turned out that the dominant contribution is given by the cylindrical diagrams. Moreover, the correspondence between such topological expansion and the Pomeron exchange in the non-perturbative Regge-Gribov approach was found.

An important step forward was the space-time localisation of the pomeron in papers [30, 46, 47, 48, 49]. Namely, it was stated that the unitarity cut of the cylindrical pomeron exchange diagram is to form two strings fragmenting into observed soft hadrons. This is how the transition was made from the hypothetical concept of pomeron exchange to the idea of the formation of colour strings due to the colour reconnection between partons of colliding hadrons. The colour field that confines them at distance r is described by the Cornell potential [50]

$$V(r) = -\frac{4}{3} \cdot \frac{\alpha_s}{r} + \sigma_T \cdot r, \tag{0.0.1}$$

where α_s is the QCD running coupling and the large-distance term is proportional to the string tension, σ_T, that also defines the linear Regge trajectories. Thus, a colour

field, gathered in the limited area of a flux tube [51] due to gluon self-interaction, has the constant amount of energy per unit length of a string, σ_T. However, there are assumptions [52] that σ_T might fluctuate, which would lead to the modification of the particle production characteristics of a string.

It is suggested that the colour strings are not static objects: the longitudinal dynamics of a massless one-dimensional string is described by the yo-yo mode solution [51], with string ends approaching and departing at the speed of light. The picture is more complicated if one considers massive partons at string's ends. In this case, the string's length oscillates with the periodic transition of the potential energy of the colour field to the kinetic energy of a massive quark and antiquark at the ends of a string. And what is more important is that the trajectories of their motion will be hyperbolic [53] instead of straight lines in $z(t)$ plane. Moreover, the motion of the string's ends becomes asymmetric if their masses are different. This is the case that is considered in this thesis.

In the collision of two partons, the string stretched between moving apart quark and antiquark subsequently fragments. This can be accounted by the probabilistic break-up of the colour field via the Schwinger mechanism of quark-antiquark creation [54] in analogy with pair production in an external electric field in QED. It results in the decay of a string into colourless hadrons [49] uniformly distributed over rapidity, y,

$$y = \frac{1}{2} \ln \frac{p_0 + p_z}{p_0 - p_z}, \tag{0.0.2}$$

where $p_0 = \sqrt{m^2 + p_T^2 + p_z^2}$, m is a particle's mass, p_z is a longitudinal component of particle's momentum, $p_T = \sqrt{p_x^2 + p_y^2}$ is the transverse momentum of the particle, p_x and p_y are its components. Produced hadrons, on average, are ordered in rapidity with respect to the part of a string they were produced by. Therefore, there is a correspondence between rapidities of emitted particles and string's rapidity coordinates (see one of the conventional string fragmentation scenario in Ref. [55]).

In the string model, simultaneously with the rapidity for the particle one finds its transverse momentum, p_T, mass, m, and azimuthal angle, $\phi = \tan^{-1}(p_y/p_x)$, under which the particle propagates in the transverse plane. Thus, instead of the Cartesian coordinate system (p_x, p_y, p_z), the (y, ϕ, p_T) system is often used in high energy physics. Along with the rapidity, another kinematic variable is used - the

pseudorapidity, η, defined as

$$\eta = \frac{1}{2}\ln\frac{|\vec{p}| + p_z}{|\vec{p}| - p_z}, \tag{0.0.3}$$

where $|\vec{p}| = \sqrt{p_T^2 + p_z^2}$. The pseudorapidity is often used in the analysis of experimental data, since it does not require the mass of the particle to be known to measure it. Eq. (0.0.3) is equivalent to:

$$\eta = -\ln\left[\tan\left(\frac{\theta}{2}\right)\right], \tag{0.0.4}$$

where θ is the polar angle between the particle momentum vector and the beam axis, i.e. η determines the direction of motion of the particle in the forward or backward hemispheres. Thus, in the string model it is also convenient to use the coordinate system (η, ϕ, p_T).

It is interesting to note that, in the models, strings that are infinite in rapidity are usually considered [56]. In this approximation, one neglects the effects of the oscillation of massive or massless string ends and studies particles that are produced at mid-rapidity. It considerably simplifies the calculations since the model is boost invariant. Although most experimental results are also usually limited by the central rapidity acceptance of the detectors, the impact of this rough approximation on various correlation measures has not been adequately estimated. The thesis is devoted to these important studies since the colour strings formed between sea partons are, on average, shorter in rapidity and their contribution increases for $A + A$ and high-energy $p + p$ collisions.

It is also important to note that the mean number of pomeron exchanges grows with the collision energy [57], which results in the remarkable string density even for $p + p$ interactions at high energies. In the meantime, lattice QCD calculations show [58] that the presence of a colour string modifies the QCD vacuum and leads to the partial restoration of the chiral symmetry. This fact can be interpreted as the existence of the scalar field of σ-mesons with Yukawa potential surrounding a string [59]. This σ-cloud defines string-string attractive potential, with the smallness of string-string coupling being compensated by the high string density [60]. Thus, the string system tends to collapse, which results in the formation of string clusters and large string density fluctuations that determine initial configurations of $p + p$ events. This consideration fits well within the scope of this dissertation.

With or without the abovementioned mechanism of string clustering due to their attraction, strings may overlap having the finite transverse size due to colour confinement [61]. There are very different estimates of string thickness: from about 1 fm in the bag model [62] to 0.3 - 0.5 fm in lattice calculations [63, 64]. Moreover, there is the analogy between a QCD string and the vortex lines in superconductors [65, 66, 64]. There is also speculation about fluctuating string width [67], but consideration of this effect is beyond the scope of this thesis.

The string percolation model [31] suggests that string fusion rearranges the colour fields [68]. In addition, in lattice QCD calculations, the possible modification of the colour charges at the ends of the string changes its tension [69]. Thus, string fusion leads to the formation of string clusters whose particle production characteristics vary with the degree of string overlap: mean particle multiplicity produced by rapidity unit of the cluster of k strings decreases [68] in comparison to the superposition of k free strings, while the mean transverse momentum of produced particles increases [70]. Moreover, string fusion increases the probability to produce heavier particles.

In addition, string fusion can be viewed in the colour space, where the colour field inside each flux tube is directed from quark to antiquark. It is postulated [71] that the partially overlapped strings with co-directed colour fluxes attract each other in the transverse plane, while ones with the oppositely directed colour fields repeal each other. Thus, the fusion of k overlapped strings with randomly directed colour fields is treated, on average, as the random walk in the SU(3) colour space, which results in the factor $\sqrt{k}$ for the newly shaped colour field of the cluster of k fused strings [68]. Therefore, if one considers the fusion of k co-directed colour flux tubes the colour field and tension will be increased for the string cluster, $\sigma_T\sqrt{k}$, in comparison to a free string, σ_T. Fusion of oppositely directed colour flux tubes will, on the contrary, decrease the field and the tension [71].

In such a picture of fusion, strings' overlap causes a redistribution of their potential and kinetic energy, which ensures the conservation of the total energy of the system of strings in an event. Therefore, the partial overlap of k strings leads to a decrease in the potential energy of each of them in this region, which causes an opposite change in their kinetic energies, pulling them towards each other [71]. In this thesis, it is assumed that this momenta is transmitted to the particles produced

in the string rest frame, which boosts them to the laboratory frame in analogy with [72, 73].

It is important to note that, in general, the colour string formation approach simplifies the event picture: the universal timeline in an event is neglected. In other words, there is no information on which strings fragment into particles sooner or later. Thus, one considers an event as a superposition of particle producing strings and string clusters and, in the same time, propagating particles that have already been produced. Another interaction effect, proposed in Refs. [74, 75, 76], can be on average taken into account based on the assumption mentioned above. One can consider that hadrons emit gluons while passing through the colour strings. It is an analogy to the QED process that describes charged particles moving in the external electromagnetic field and radiating photons. To be precise, the proposed QCD interaction should be accounted for more accurately at the level of quarks emitting gluons. Eventually, it results in the quenching of particle's transverse momentum in the string medium and creates the azimuthal anisotropy in their production. The impact of this particle-string interaction is to be estimated in the model, developed in this thesis, especially because, in the proposed machinery, an event looks like a strongly heterogeneous string environment with the varying density of the colour field along the path of a produced particle.

Applying the aforementioned mechanisms, one may contribute to the understanding of the origin of collective effects observed in inelastic $p + p$ interactions by estimating the influence of the complex structure of fluctuating event's initial conditions on the correlations between various measured observables.

For example, to probe the peculiar dependence of the number of charged particles produced in some rapidity region of the backward hemisphere, N_B, on the number of particles produced in some rapidity region of the forward hemisphere, N_F, one can study the slope of the $N_F - N_B$ correlation function [77]

$$b_{B-F} = \left. \frac{d\langle N_B(N_F)\rangle}{dN_F} \right|_{N_F=\langle N_F\rangle}, \tag{0.0.5}$$

where $\langle..\rangle$ denotes averaging over events.

For the case of the linear correlation function, $\langle N_B(N_F)\rangle$, b_{B-F} can be trans-

formed [78] into $b_{\rm corr}[N_F, N_B]$ - the correlation coefficient

$$b_{\rm corr}[N_F, N_B] = \frac{\langle N_F N_B\rangle - \langle N_F\rangle\langle N_B\rangle}{\langle N_B^2\rangle - \langle N_B\rangle^2}. \tag{0.0.6}$$

There are more sophisticated correlation measures, such as strongly intensive quantities [79] that are constructed in a way to be independent of both system volume and its fluctuations event-by-event in the models of independent particle production. Let us clarify that in the colour string models, the volume of the system is defined by the number of strings in an event. For example, studying the strongly intensive variable $\Sigma[N_F, N_B]$ [80] will remove the influence of trivial (volume) fluctuations to which the correlation coefficient $b_{\rm corr}[N_F, N_B]$ is subject. $\Sigma[N_F, N_B]$ is defined for the joint distribution $N_F - N_B$ as

$$\Sigma[N_F, N_B] = \frac{\langle N_F\rangle\omega[N_B] + \langle N_B\rangle\omega[N_F] - 2(\langle N_F N_B\rangle - \langle N_F\rangle\langle N_B\rangle)}{\langle N_F\rangle + \langle N_B\rangle}, \tag{0.0.7}$$

where $\omega[A] = \big(\langle A^2\rangle - \langle A\rangle^2\big)/\langle A\rangle$ is a scaled variance of an extensive event variable A distribution.

One can also study the correlations and fluctuations of multiplicity and transverse momentum in the common rapidity acceptance. It is, first of all, the $\langle p_T\rangle - N$ correlation function that shows the dependence of the event mean transverse momentum on the event charged particle multiplicity.

More profound are strongly intensive measures defined [79] for the joint distribution of the event transverse momentum, P_T, found as a scalar sum of particles' p_T, and event multiplicity, N, as

$$\Sigma[P_T, N] = \frac{1}{\langle N\rangle\omega\langle\langle p_T\rangle\rangle}\cdot\Big[\langle N\rangle\omega[P_T] + \langle P_T\rangle\omega[N] - 2\left(\langle P_T N\rangle - \langle P_T\rangle\langle N\rangle\right)\Big], \tag{0.0.8}$$

$$\Delta[P_T, N] = \frac{1}{\langle N\rangle\omega\langle\langle p_T\rangle\rangle}\cdot\Big[\langle N\rangle\omega[P_T] - \langle P_T\rangle\omega[N]\Big], \tag{0.0.9}$$

where $\langle\langle..\rangle\rangle$ denotes the averaging over all particles in all events. $\Sigma[P_T, N]$ and $\Delta[P_T, N]$ are expected to be sensitive to the hypothetical QCD critical point [81], while in general the studies of p_T distribution could shed some light on the form of the equation of state of the produced medium in the QGP framework [82]. In the colour string model approach, string clusterization causes p_T fluctuations [83], thus, addressing them is a promising approach in the study of the properties of the particle producing sources.

The study of correlations can be extended by considering not only the rapidity, but also the azimuthal angle of particles. The two-particle angular correlation function [84] can be defined as

$$C(\Delta\eta, \Delta\phi) = \frac{S(\Delta\eta, \Delta\phi)}{B(\Delta\eta, \Delta\phi)}, \tag{0.0.10}$$

where S and B represent the $\Delta\eta - \Delta\phi$ distributions calculated for particle pairs from the same simulated events and from the mixed events, respectively. The experimental analysis of this observable revealed the impressive near-side ridge structure in both peripheral $A + A$ collisions [85, 86] and high-multiplicity $p + p$ interactions [23, 24].

To measure the strength of azimuthal correlations, another method [87] is to compute the two-particle cumulant, $c_2\{2\}$, defined as

$$c_2\{2\} = \langle\langle e^{2i(\phi_1 - \phi_2)} \rangle\rangle, \tag{0.0.11}$$

where ϕ_1 and ϕ_2 are the azimuthal angles of the two particles, $\langle\langle ... \rangle\rangle$ is the average over all pairs of particles in the event that is then averaged over all events. Moreover, the estimate, $v_2\{2\}$, of the elliptic flow harmonic, v_2, can be found as

$$v_2\{2\} = \sqrt{c_2\{2\}} \tag{0.0.12}$$

under the assumption of independent particle production (when particle transverse flow is the only source of correlations, providing that all non-flow effects are suppressed), which implies that $c_2\{2\}$ should be positive. There are also techniques [88] to suppress the remaining contributions from non-flow (coming from resonance decays, jets, and momentum conservation laws) by calculating cumulants in subevents separated in rapidity.

Thus, the study of rapidity and azimuthal correlations belongs to the actively developing realm of high energy physics. The role of this thesis is to establish the possibility of describing collective behaviour in small colliding systems only by taking into account the interaction and fusion of quark-gluon strings and without using the hydro-dynamical phase that is still questionable in application to $p + p$ data.

Goal and objectives of the work.

The main goal of this thesis is to develop the model of interacting colour strings finite in rapidity that describes multi-particle production and collective phenomena observed in inelastic $p + p$ interactions.

To achieve this goal the following objectives were accomplished:

1. To consider longitudinal dynamics of strings finite in rapidity and find its influence on multiplicity correlations in separated rapidity regions.

2. To derive the analytic relations between strongly intensive quantity $\Sigma[N_F, N_B]$ and widely used (factorial) cumulants and asymmetry coefficient of $N_F - N_B$ distribution.

3. To consider the impact of transverse dynamics of strings and their fusion on $\langle p_T \rangle - N$ correlation function.

4. To search for possible collectivity signatures in the behaviour of strongly intensive variables in the model with string clusters finite in rapidity, and compare the results with experimental data.

5. To estimate the interplay of the two proposed mechanisms of azimuthal anisotropy of particles in the model: particle boosts by overlapped fused strings and particle's momentum quenching in the inhomogeneous string environment.

Scientific novelty.

This thesis is inspired by a set of breakthrough ideas within the colour string formation and fragmentation approach to describe strong interaction. The concept that motivated the author to conduct this study is primarily to consider strings that are finite in rapidity. In addition, the thesis for the first time proposes to simultaneously consider also the attraction potential between colour strings and their fusion, leading to particle boosts and quenching of their momentum in the string medium. Thus, the scientific novelty of the study consists in a multistage consideration of the interaction of some number of colour strings formed in $p + p$

event, taking into account their transverse and longitudinal dynamics, as well as their fusion into clusters.

The obtained results show that these refinements of the colour string model induce the appearance of the non-trivial long-range contributions to the correlation and fluctuation measures as well as particular azimuthal anisotropies consistent with the experimental observations.

Theoretical and practical significance.

This work addresses the unresolved issue of describing multi-particle production in the processes of strong interaction. This problem is of particular importance in the modern high energy physics since there is no established mechanism of the transition from the quarks and gluons appearing in the QCD Lagrangian to the observed colourless hadrons.

The dissertation proposes a phenomenological solution to the identified problem faced in inelastic proton-proton interactions. It uses the Monte-Carlo method based on the model of interacting colour strings that are finite in rapidity and whose fusion causes boosts of produced particles. The results are in qualitative agreement with the experimental data at LHC energies.

On the one hand, it is important to find the influence of the discussed processes on the correlation and fluctuation measures that are widely used in the experimental studies and, therefore, predict the possible bias in the interpretation of the results. On the other hand, by comparison of the model results in different regimes with the experimental data one could extract the information about possible characteristics of the particle emitting sources and types of their interactions.

The developed framework can be extended to be more sensitive to the details of particle production, however, its main advantage in the current implementation is the relative simplicity and the elegantly small number of parameters to be extracted from the comparison with experimental data. In future, the model can be used to perform calculations in the energy domain of NICA (Nuclotron-based Ion Collider fAcility) collider, which makes it useful for the prediction of the experimental results.

The reliability of the results obtained.

The majority of calculations in this thesis are performed within the developed Monte-Carlo model realised in C++ language. In the limiting case of non-interacting (free) strings, the results for correlation and fluctuation measures were calculated analytically. The comparison of the Monte-Carlo method with the direct analytical calculations shows the reliability of the application of numerical calculations.

In addition, model results were compared to published experimental data, which allows one to examine the general behaviour of the studied quantities. The possibility of such a comparison is an indisputable advantage of work in this area of theoretical physics that is constantly fed by experimental results.

Thesis structure.

The thesis consists of Introduction, three Chapters, Conclusion, two Appendices and Bibliography. The thesis contains 138 pages, 26 figures. The list of references includes 162 items.

- In **Introduction,** the relevance of the topic, its elaboration, the purpose and main objectives of the research, its novelty, significance and methods are described. The main scientific results and statements to be defended are formulated and the approbation of the research is presented.

- In **Chapter 1** the simplified toy-model of multi-particle production is presented that takes into account fusion of strings finite in rapidity. The preliminary results for correlation coefficient and strongly intensive quantity are presented and qualitatively compared with the experimental data. The benefits of considering this refinement of the original colour string model are discussed. The obtained intermediate conclusions support the continuation of the research in this direction.

- In **Chapter 2** the substantially developed version of the model is presented. It contains the detailed longitudinal dynamics of the oscillating colour strings, the attractive transverse evolution of string density in each event and string fusion in the dynamically defined string configuration. The inference of

model parameters is accomplished based on data. Model results are quantitatively compared with ALICE data for inelastic $p + p$ interactions at $\sqrt{s} = 900$ GeV. The conclusions about the influence of the fluctuations of the three-dimensional colour string density on correlation measures are formulated.

- In **Chapter 3** the model formalism is additionally extended by the mechanisms crucial for considering azimuthal particles' flows in our approach. It is the implementation of particle boosts caused by string fusion and the quenching of particle momentum in the dense string medium that allows one to study the azimuthal asymmetry of their production in the model formalism. The inference of model parameters is accomplished from comparison with the data. The observed near-side ridge and the obtained values of the elliptic flow harmonics are in qualitative agreement with ATLAS data for high-multiplicity $p + p$ interactions at $\sqrt{s} = 13$ TeV.

- **Conclusion** presents the main results of this work.

- Two **Appendices** contain technical information that complements some procedures presented in the core of this thesis, while at the same time not obstructing reading of the main text.

Personal contribution of the author.

All of the main findings submitted for defence were obtained personally by the applicant.

Acknowledgements

The author would like to express her deepest gratitude to her scientific advisor Dr. Grigory Aleksandrovich Feofilov for his kind attitude and support, as well as for the fact that he always generously shared his vision of beauty both in science and in life. The applicant would like to gratefully thank his article co-authors, Evgeny Vladimirovich Andronov and Vladimir Nikolaevich Kovalenko, without whom this work would also have been hardly possible. Special gratitude is expressed to Prof.

Vladimir Victorovich Vechernin for his valuable comments, conceptual proposals and careful participation in the discussions of the model results.

The applicant appreciates the hospitality of Saint Petersburg University, where this work was carried out. The applicant also thanks the members of the Laboratory of ultra-high energy physics of SPbU and the staff of the Department of High Energy and Elementary Particles Physics at SPbU, who participated in discussions of the results presented here.

Immense gratitude to my mother and grandmother, who believed in me unconditionally and always supported me, and to my father who pushed me to write the thesis.

Approbation of the research.

The findings of the investigation were reported and discussed at the following conferences:

1. 2019 3 - 7 June, Dubna, Russia: XIV Workshop on Particle Correlations and Femtoscopy

2. 2019 21 - 30 June, Erice, Italy: International School of Subnuclear Physics 57th Course "In Search for the Unexpected"

3. 2019 1 - 5 July, Dubna, Russia: LXIX International Conference "Nucleus-2019": Fundamental Problems of Nuclear Physics, Nuclei at Borders of Nucleon Stability, High Technologies

4. 2019 2 - 6 December, Budapest, Hungary: 19 Zimanyi school "Winter workshop on heavy ion physics"

5. 2021 20 - 25 September, SPbSU, online: LXXI International conference "NUCLEUS – 2021. Nuclear physics and elementary particle physics. Nuclear physics technologies"

6. 2022 11 - 16 July, Moscow, Russia: LXXII International conference "NUCLEUS – 2022: Fundamental problems and applications"

7. 2022 10 - 14 October, St.Petersburg, Russia: VII International Conference "Models in Quantum Field Theory"

8. 2022 24 - 28 October, Dubna, Russia: The XXVI International Scientific Conference of Young Scientists and Specialists (AYSS-2022)

9. 2022 29 November - 2 December, Moscow, Russia: The 6th International Conference on Particle Physics and Astrophysics (ICPPA-2022)

10. 2023 13 - 18 March, Luga, Russia: 55th PNPI Winter School

11. 2023 24 - 30 August, Moscow, Russia: The 21st Lomonosov Conference on Particle Physics

12. 2023 18 - 23 September, Dubna, Russia: The XXVth International Baldin Seminar on High Energy Physics Problems "Relativistic Nuclear Physics and Quantum Chromodynamics"

In addition, the results were reported and discussed at the seminars of the Laboratory of Ultra-high energy physics of St. Petersburg University and at the meetings of the High Energy and Elementary Particles Physics Department of St. Petersburg University.

Publications.

The results obtained within this study were published in 8 papers (and are included in the RSCI, Web of Science and Scopus databases):

1. D. Prokhorova, V. Kovalenko, *Study of forward-backward multiplicity fluctuations and correlations with pseudorapidity,* Phys. Part. Nucl. **51** 3, 323 (2020)

2. D. Prokhorova, V. Kovalenko, *Pseudorapidity dependence of multiplicity fluctuations in the model of interacting quark-gluon strings of finite rapidity length,* Bull. Russ. Acad. Sci. Phys. **84** 10, 1261 (2020)

3. D. Prokhorova, E. Andronov, *Role of String Fusion Mechanism in Fluctuation Studies,* Phys. Atom. Nucl. **85** 6, 1063 (2022)

4. D. Prokhorova, E. Andronov, G. Feofilov, *Interacting Colour Strings Approach in Modelling of Rapidity Correlations,* MDPI Physics **5**, 636 (2023)

5. D. Prokhorova, E. Andronov, *Study of Multiplicity and Transverse Momentum Fluctuations in the Monte-Carlo Model of Interacting Quark-Gluon Strings,* Phys. Part. Nucl. **54**, 3, 412 (2023)

6. E. Andronov, D. Prokhorova, A. Belousov, *Influence of quark–gluon string interactions on particle correlations in p+p collisions,* Theor. Math. Phys. **216**, 3, 1265 (2023)

7. D. Prokhorova, E. Andronov, *String Fusion Mechanism and Studies of Correlations,* Phys. Part. Nucl. Lett. **20**, 6, 1496 (2023)

8. D. Prokhorova, E. Andronov, *Emergent flow signal and the colour string fusion,* MDPI Physics, **6(1)**, 264 (2024)

The main scientific results.

1. In the developed theoretical approach, based on the formation of the colour strings finite in rapidity in hadronic collisions at high energies, the growth of the strongly intensive variable $\Sigma[N_F, N_B]$ with the distance between rapidity intervals F and B, where multiplicities N_F and N_B were calculated, was obtained (see paper №1 from the list of publications of the applicant, p. 325). This result was obtained by the applicant personally.

2. In the developed theoretical approach, based on the formation of the colour strings finite in rapidity in hadronic collisions at high energies, the decrease of the correlation coefficient $b_{\rm corr}[N_F, N_B]$ with the distance between rapidity intervals F and B, where multiplicities N_F and N_B were calculated, was obtained (see paper №2 from the list of publications of the applicant, p. 1264). This result was obtained by the applicant personally.

3. The analytical relationship of the strongly intensive variable $\Sigma[N_F, N_B]$ with cumulants, factorial cumulants, and the asymmetry coefficient of $N_F - N_B$ distribution is proved (see paper №4 from the list of publications of the applicant, pp. 647-650). This result was obtained by the applicant personally.

4. In the developed theoretical approach, based on the formation of the colour strings finite in rapidity in hadronic collisions at high energies, that form string clusters due to fusion, the following experimental distributions are described: the pseudorapidity distributions for inelastic $p+p$ interactions at $\sqrt{s} = 53, 900, 13000$ GeV (see papers from the list of publications of the applicant: №3, p. 1065, №4, p. 643 and №8, p. 278), the p_T-spectrum for inelastic $p+p$ interactions at $\sqrt{s} = 13000$ GeV (see paper №8 from the list of publications of the applicant, p. 278), and the multiplicity distributions for inelastic $p+p$ interactions at $\sqrt{s} = 900, 13000$ GeV (see papers from the list of publications of the applicant: №4, p. 643 and №8, p. 278). These results were obtained by the applicant personally.

5. In the developed theoretical approach, based on the formation of the colour strings finite in rapidity in hadronic collisions at high energies, that form string clusters due to attraction and fusion, the experimental slope of the $\langle p_T \rangle - N$ correlation function for inelastic $p+p$ interactions at $\sqrt{s} = 900, 13000$ GeV is described (see papers from the list of publications of the applicant: №4, p. 644 and №8, p. 278). This result was obtained by the applicant personally.

6. In the developed theoretical approach, based on the formation of the colour strings finite in rapidity in hadronic collisions at high energies, that form string clusters due to fusion, there is a weakening of $N_F - N_B$ correlations, manifested as a decrease of the values of $b_{\rm corr}[N_F, N_B]$ in comparison with the results of the model with independent sources (see papers from the list of publications of the applicant: №4, pp. 645-646, №6, p. 1273 and №7, p. 1497). This result was obtained by the applicant personally.

7. In the developed theoretical approach, based on the formation of the colour strings finite in rapidity in hadronic collisions at high energies, that form string clusters due to fusion, there is a weakening of $N_F - N_B$ correlations manifested as a decrease of the values of the strongly intensive variable $\Sigma[N_F, N_B]$ in comparison with the results of the model with independent sources (see papers from the list of publications of the applicant: №5, pp. 415-416 and №6, p. 1273). This result was obtained by the applicant personally.

8. In the developed theoretical approach, based on the formation of the colour strings finite in rapidity in hadronic collisions at high energies, that form string clusters due to fusion, there is an increase of $P_T - N$ correlations manifested as an increase in the values of the strongly intensive variables $\Sigma[P_T, N]$ and $\Delta[P_T, N]$ in comparison with the results of the model with independent sources (see papers from the list of publications of the applicant: №5, p. 415 and №6, p. 1274). This result was obtained by the applicant personally.

9. In the developed theoretical approach, based on the formation of the colour strings finite in rapidity in hadronic collisions at high energies, that form string clusters due to attraction and fusion, and taking into account the particle boosts caused by string fusion, as well as the losses of particle momentum in the string medium, the signal of azimuthal correlations in the form of the so-called "near-side ridge" and two-particle cumulants was obtained, that qualitatively describes the results of the ATLAS experiment for high-multiplicity $p + p$ interactions at $\sqrt{s} = 13000$ GeV (see paper №8 from the list of publications of the applicant, pp. 280-283). This result was obtained by the applicant personally.

The statements and results put forward for defence.

1. We show that the longitudinal dynamics of colour strings finite in rapidity, formed in $p + p$ collisions at high energies, changes the string density configuration and creates a rapidity-dependent background contribution to the multiplicity correlation coefficient $b_{\rm corr}[N_F, N_B]$ and to the strongly intensive variable $\Sigma[N_F, N_B]$ measured in separated rapidity intervals F and B.

2. It has been shown that strongly intensive quantity $\Sigma[N_F, N_B]$, cumulants, factorial cumulants and asymmetry coefficient of $N_F - N_B$ distribution form a family of measures that are robust to trivial fluctuations and allows one to study either of them, while $b_{\rm corr}[N_F, N_B]$ provides complementary information on correlated particle production.

3. It has been shown that the attractive transverse dynamics of strings and formation of string clusters due to their fusion give the origin to the mechanism

that describes the behaviour of $\langle p_T \rangle - N$ correlation function observed in $p+p$ interactions at high energies.

4. It is shown that in contrast to free colour strings, the consideration of the clustering of strings finite in rapidity and their fusion significantly changes the values of the correlation measures: it decreases the values of $b_{\rm corr}[N_F, N_B]$ and $\Sigma[N_F, N_B]$ and increases the values of $\Sigma[P_T, N]$ and $\Delta[P_T, N]$. The results obtained in this new approach for $p+p$ collisions at high energies are in qualitative agreement with experimental results, making it a confident alternative to the Colour Reconnection mechanism used in the PYTHIA event generator.

5. It is shown that the so-called near-side ridge – collimated in azimuthal angle and extended in pseudorapidity particle yield, observed in the two-particle correlation function in $p+p$ events with high multiplicity at high energies, can be described using the mechanism of string fusion as a source of particle boost and quenching of their momenta due to interaction with the string medium.

CHAPTER 1

Toy-model of interacting strings finite in rapidity

The study begins with the consideration of the simplified toy-model of multi-particle production that is based on the concept of formation, fusion and fragmentation of colour strings finite in rapidity. This Chapter presents methods and results, published in Refs. [89, 90].

1.1 Toy-model description

The developed model follows one of the conventional frameworks [49, 51] for the phenomenological representation of strong interaction between hadrons colliding at high energies. This approach is originally viewed in two stages: at the first stage, the longitudinally extended objects of the colour field are produced and, at the second stage, they fragment into observed hadrons. In this thesis, we introduce additional step as in Ref. [31] at which the fusion of initially stretched strings is considered.

To simplify the Monte-Carlo workflow, we ignore the step of simulating the collision itself. In our approach, an event starts with some number of strings already being formed. Thus, in this first implementation, we do not enforce the conservation of energy and momentum for the partons of colliding objects. It is because we neglect the possible presence of beam remnants (spectator partons) not participating in the collision. Moreover, we do not even focus on whether it is a high-multiplicity proton-proton or a peripheral nucleus-nucleus collision, but rather rely on the total number of strings formed, n_{str}. We sample it from the Poisson distribution with the given mean, $\langle n_{\mathrm{str}} \rangle$, regardless the collision energy.

To set up the first stage of the interaction, one has to define the positions of particle-producing sources in the rapidity dimension and in the transverse coordinate space. The rapidities of strings' ends are sampled from the uniform distribution from

$-Y$ to Y in a way that one string end has positive rapidity and another one has negative rapidity. Thus, strings always cross the $y = 0$ region. It is assumed that the found rapidity coordinates of a string correspond to its length and position just before the hadronisation.

The intermediate stage of the collision corresponds to the string interaction in the form of fusion [68]. It occurs because strings have finite size in the transverse dimension and, therefore, can overlap.

To simplify the calculations, we follow the cellular string fusion approach [91] that is more CPU-efficient. In this method, only those strings are to fuse whose centres lie in the same cell of the grid applied to a transverse plane (Fig. 1.1, upper left corner). This simplification replaces the explicit calculation of the areas of strings' overlaps that have complex shapes especially for multiple intersections. In this implementation, we assume the correspondence between the collision transverse area and the transverse cell size. Thus, only the serial number of the cell in which the centre of the string falls is generated, thus, one obtains a uniform distribution of $n_{\rm str}$ strings in the transverse plane.

However, it is clearly seen that this procedure may introduce some bias in the fusion picture. Namely, the pair of overlapped strings that are shown in the middle of the schematic transverse picture of an event (Fig. 1.1, upper left corner), are overlapped to approximately the same degree as the pair in the upper right corner of the transverse grid (centres are highlighted in red). But since the centres of the first pair of strings belong to the different cells of the grid their fusion will not be considered in contrast to the second pair. The possible cure is to re-run the simulations with the slightly displaced grid in the transverse plane, which will result in other sets of strings to be fused. By calculating the quantities of interest for a few grid positions, one can average the results obtained in different configurations, which will compensate for the bias of string fusion introduced by cell boundaries.

The novelty of our approach is that finite strings' length in rapidity implies the consideration of the 3D (three-dimensional) picture of string fusion. Namely, after finding strings whose centres belong to the same cell in the transverse grid, following the well-established procedure [91], one has to additionally search for their overlaps in the rapidity dimension (see the schematic representation in Fig. 1.1, upper right corner). In the projection on the rapidity axis, one has to find the degree of overlap,

k, for each intersection of strings (Fig. 1.1, bottom).

In this work, taking into account 3D string fusion, firstly, changes the number of particle sources, and secondly, both the parts of the original strings that remain free and the resulting string clusters become "shorter" in rapidity compared to independent sources (without fusion). It is schematically shown in Fig. 1.1 for some local fluctuation of increased string density, which leads to the fusion of these overlapped strings: $n'_{\rm str} = 3$ becomes $\tilde{n}'_{\rm str} = 5$ and some of them, being now string clusters, have higher tension. Thus, taking into account string fusion creates a sophisticated interplay between shortening of strings in rapidity and increasing their tension.

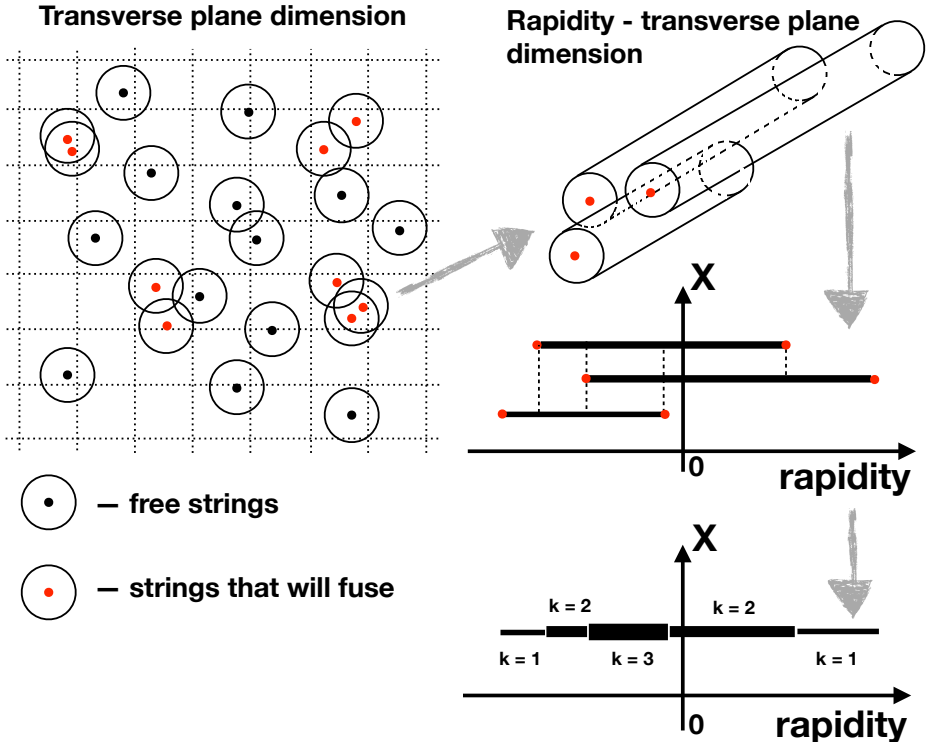

Figure 1.1: Schematic picture of the developed approach of three-dimensional fusion of strings and accounting for the degrees of their overlaps, k.

In our approach, the effective string hadronisation is applied: each string is split in rapidity in equal parts of length ε that produce particles independently. Particles produced from some string segment ε are assigned with rapidity y that is found from the Gaussian distribution with the mean that is the mean value of this ε unit in the absolute rapidity coordinates and the variance that is also equal to ε. This is how we ensure the correspondence between the rapidity coordinates of the string unit and the rapidities of particles that are produced by it.

From the assumption that a quark-gluon string has the constant energy of the

colour field, σ_T, per length unit it follows that a free string, on average, produces μ_0 charged particles per rapidity unit. The picture becomes more complex once one takes into account the string fusion that affects particle production: string cluster of length ε in rapidity, consisting of k overlapped strings, produces on average μ_k particles defined [68] as

$$\mu_k = \mu_0 \varepsilon \sqrt{k}, \tag{1.1.1}$$

where the case with $k = 1$ gives the mean multiplicity for ε rapidity interval of a free string.

In this thesis, following [92], we assume that the number of particles from a single string follows the Poisson distribution. The fact is that the Poisson distribution well describes the multiplicity distribution in $e+e-$ annihilation without hard processes, where a single string is supposed to be formed [93]. Remarkably, using the Poisson distribution of the number of particles from every ε piece of a string will provide us with the final multiplicity distribution from a single string also according to this law [94]. We note, that if in each $p+p$ interaction (also without hard processes) the same number of free (without fusion) strings is formed, each of which giving a Poisson contribution to the event multiplicity, then the event multiplicity distribution will coincide with the Poisson distribution. In our approach, we account for string fusion but do not change the type of distribution: the number of particles from a cluster of k strings will also follow a Poisson distribution, but with the different mean (see Eq. (1.1.1) for the ε interval). However, the fact that the number of strings fluctuates event-by-event, and the fact that we take into account the finiteness of strings in rapidity and their 3D fusion, leads to fluctuations in the number of string clusters and their degrees of overlap with rapidity. Thus, convolution of these distributions with the Poisson distribution from each particle source modifies the final multiplicity distribution in the model.

Taking into account the aforementioned, we sample the number of particles, N_ε, produced by ε unit of a string from the Poisson distribution with the mean μ_k from Eq. (1.1.1). The number of particles, N_i, produced by i-th string, is the sum of the number of particles produced by its ε units

$$N_i = \sum_{\varepsilon} N_\varepsilon. \tag{1.1.2}$$

The total event multiplicity, $N_{\rm ch}$, is obtained from the contributions of all particle

sources in the event, $\tilde{n}_{\rm str}$, including free strings and string clusters

$$N_{\rm ch} = \sum_{i=1}^{\tilde{n}_{\rm str}} N_i. \tag{1.1.3}$$

In our approach, no short-range correlations are introduced: particles produced from a string are uncorrelated in rapidity in contrast to how it was done, for example, in Ref. [95]. Here, our goal, on the contrary, is to separately estimate the impact of the formation of finite in rapidity strings on the correlation measures. Also, to clearly see the effect of string fusion, the calculation results are presented for two options: free strings (string overlaps are ignored) and with string fusion.

1.2 Toy-model results

To test the predictions of the proposed toy-model with strings finite in rapidity and string fusion, we calculate correlation and fluctuation quantities defined for multiplicities, measured in rapidity intervals in forward and backward hemispheres. Calculations were performed for one million generated events.

1.2.1 N_F-N_B correlation coefficient

In the presented approach, we calculate the correlation coefficient $b_{\rm corr}[N_F, N_B]$, Eq. (0.0.6), as a function of the distance Δy, between forward and backward rapidity intervals (F-B) of width $\delta y = 0.7$, where N_F and N_B multiplicities are calculated.

Fig. 1.2, left, shows model results for different considered configurations: (i) infinite free (fragmenting independently) strings (dashed brown line), (ii) free strings limited in rapidity (full symbols) and (iii) strings limited in rapidity with their fusion taken into account (solid lines). Colours and symbols depict the results calculated with different string density: for each event a number of strings is sampled from the Poisson distribution with the mean, $\langle n_{\rm str}\rangle$, mentioned on the legend, to be distributed over the transverse area of the same size. Fig. 1.2, right, presents the notations for the plots in Fig. 1.2, left: Δy is a rapidity gap between F-B windows of width δy, where multiplicities N_F and N_B are calculated; Δy can be varied, which allows one to analyse the distribution of charged particle multiplicity over rapidity, dN/dy, as a function of y.

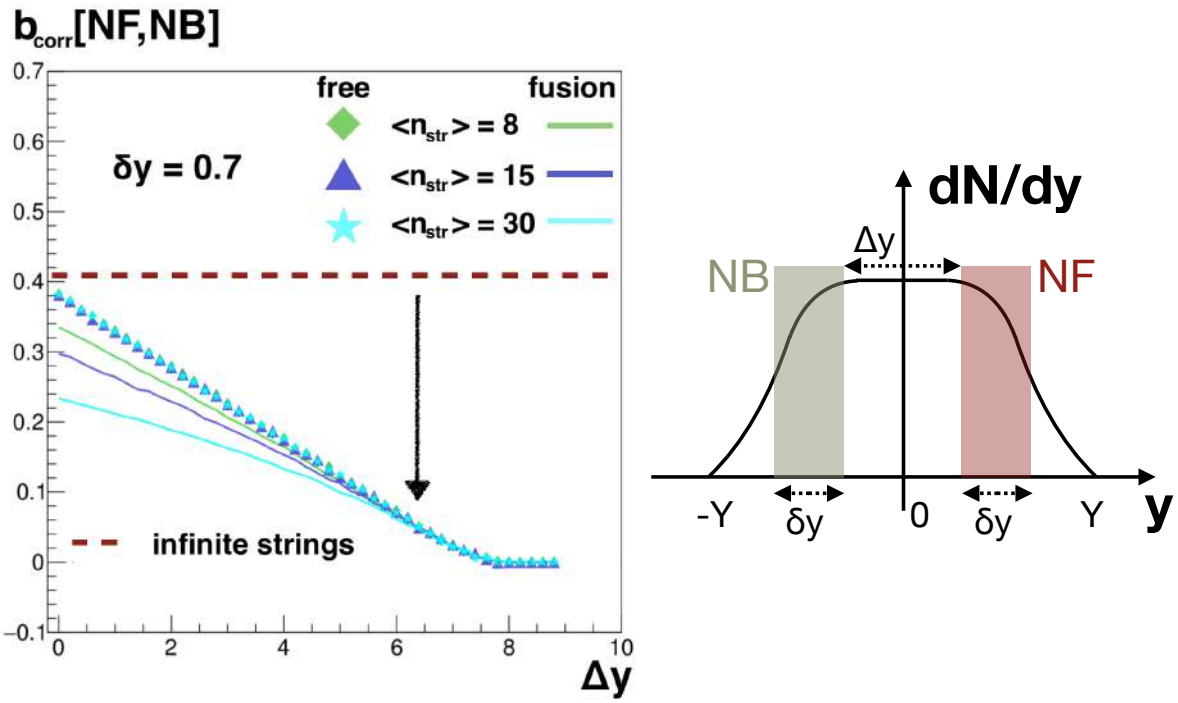

Figure 1.2: Left: model results for the correlation coefficient $b_{\rm corr}[N_F, N_B]$ defined for multiplicities N_F and N_B measured in forward and backward rapidity acceptances of width $\delta y = 0.7$ separated by the varying rapidity gap, Δy. Brown dashed line shows the reference result for the model with strings infinite in rapidity. Symbols (lines) denote the values of $b_{\rm corr}[N_F, N_B]$ calculated for free (fused) strings with the mean number of strings per event equal to 8 (green, diamonds), 15 (blue, triangles) and 30 (cyan, stars). **Right:** schematic picture of the forward-backward windows definition over the hand drawn rapidity distribution, dN/dy: multiplicities N_F and N_B are measured in forward (dark red area) and backward (dark green area) rapidity acceptances of width δy symmetrically spaced around $y = 0$ by the distance Δy.

For infinite free strings (Fig. 1.2, left, dashed brown line) the value of $b_{\rm corr}[N_F, N_B] \approx 0.4$ is constant with Δy. It is because, in the model, there are no mechanisms responsible for the formation of short-range correlations whose contribution would depend on the rapidity gap between measured N_F and N_B. In turn, the long-range contribution to $b_{\rm corr}[N_F, N_B]$ is defined solely by the fluctuations in the number of strings, $n_{\rm str}$, that produce particles in forward and backward acceptances. For infinite strings, it does not depend on the y-gap.

Our results for finite free strings (symbols) start at the same level for all $\langle n_{\rm str}\rangle$: around $b_{\rm corr}[N_F, N_B] \approx 0.4$ at $\Delta y = 0$. It is because all strings cross $y = 0$ region and produce particles in both forward and backward windows at $\Delta y = 0$. The small deviation (of about 0.02) from the infinite strings level arises due to boundary effects caused by the finite binning of strings in rapidity dimension (ε). Another

special area on this plot starts at $\Delta y \sim 8$, which corresponds to the maximum y-gap between F-B windows after which the rapidity distribution, dN/dy (for which the width 8 was arbitrarily chosen), ends. Here, the correlation is zero for any mean number of strings. In between the two limiting cases ($\Delta y = 0$ and $\Delta y \approx 8$), one observes the monotonic decrease of $b_{\rm corr}[N_F, N_B]$ since the number of strings that produce particles simultaneously in F-B windows reduces with the increase of the rapidity distance between them. Thus, for free strings the values of $b_{\rm corr}[N_F, N_B]$ are almost independent of the $\langle n_{\rm str}\rangle$ and coincide (diamonds, triangles, stars).

The situation is opposite if one considers string fusion. The values of $b_{\rm corr}[N_F, N_B]$ split already at $\Delta y = 0$: the higher the string density, the more often the fusion occurs, the smaller the correlation. This is in agreement with the results obtained in Ref. [96] where the model with infinite strings and short-range rapidity correlations, introduced for particles from one string, is considered. There, the similar decrease of $b_{\rm corr}[N_F, N_B]$ is explained as the shortening of the correlation length with the increase of string tension that occurs due to string fusion. In the approach presented here, the similar behaviour of $b_{\rm corr}[N_F, N_B]$ is caused by completely different reasons of the decrease of the contribution of long-range correlations. The effect of fusion is the highest at mid-rapidity where the string density is the largest for any $\langle n_{\rm str}\rangle$ and it disappears when the sliding F-B windows reach the boundaries of the rapidity dN/dy distribution.

1.2.2 Strongly intensive quantity and N_F-N_B fluctuations

Another measure of $N_F - N_B$ multiplicity correlations and fluctuations is strongly intensive quantity $\Sigma[N_F, N_B]$, Eq. (0.0.7). Fig. 1.3 shows the dependence of $\Sigma[N_F, N_B]$ on the distance between F-B windows (same definition as in Fig. 1.2, right) of width $\delta y = 0.5$ (left) and $\delta y = 1.0$ (right). The values of $\Sigma[N_F, N_B]$ grow with the size of rapidity acceptance δy (Fig. 1.3).

In the developed simplified approach, the values of $\Sigma[N_F, N_B]$ for free strings coincide for different string density (different $\langle n_{\rm str}\rangle$). It confirms its property of strong intensity for independent particle-producing sources: $\Sigma[N_F, N_B]$ is independent of both system volume (mean number of strings) and it's event-by-event fluctuations (actual number of strings is found for each event from the Poisson distribution with the given mean, thus, it fluctuates).

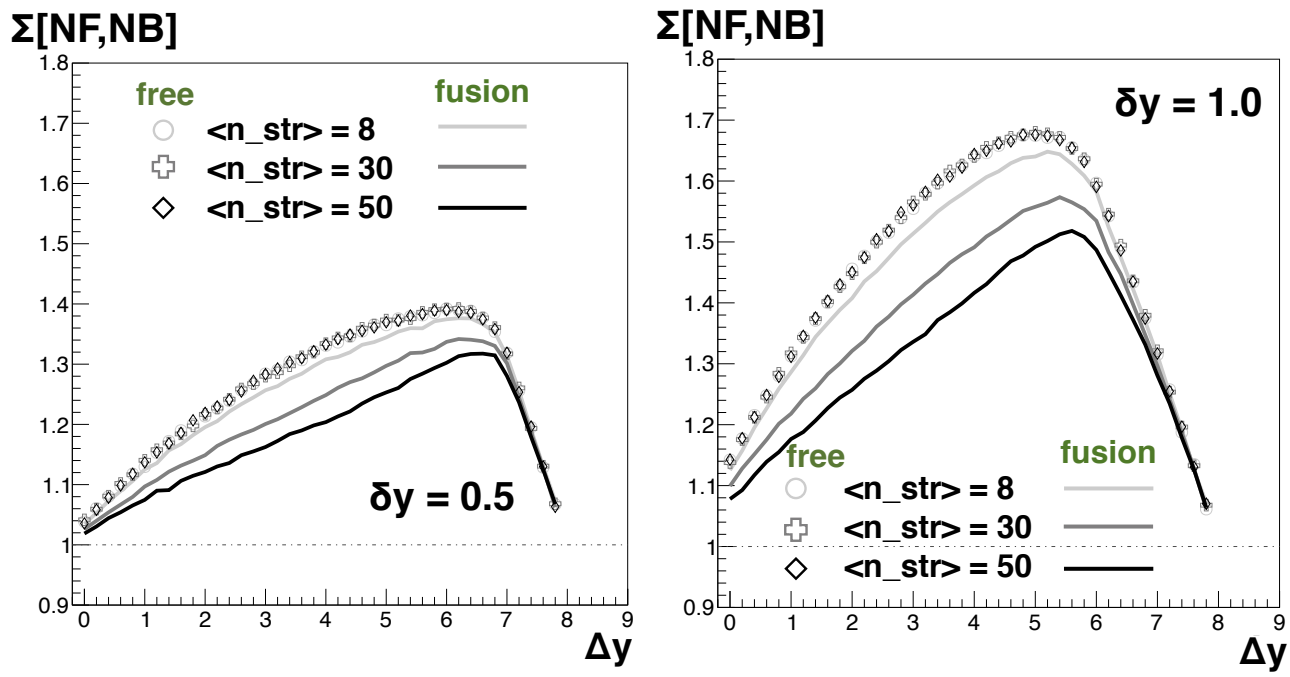

Figure 1.3: Model results for the strongly intensive quantity $\Sigma[N_F, N_B]$ defined for multiplicities N_F and N_B measured in forward and backward rapidity acceptances of width δy separated by the varying rapidity gap, Δy. Empty symbols (lines) denote the values of $\Sigma[N_F, N_B]$ calculated for free (fused) strings with the mean number of strings per event equal to 8 (light grey, circles), 30 (grey, crosses) and 50 (dark grey, diamonds). **Left:** $\delta y = 0.5$, **Right:** $\delta y = 1.0$ (see the schematic picture of the forward-backward windows definition over the dN/dy distribution in Fig. 1.2, right).

For both model regimes (of free strings and with string fusion), the $\Sigma[N_F, N_B]$ starts at unity at $\Delta y = 0$ and grows with Δy (see next subsection). At large Δy the sharp decrease of the $\Sigma[N_F, N_B]$ plots corresponds to the boundaries of the dN/dy rapidity distribution reached by the acceptance windows. Thus, at large Δy less and less particles enter the F-B acceptance windows, which corresponds to a Poisson distributions of N_F and N_B multiplicities for which $\Sigma[N_F, N_B]$ by definition is equal to unity [97].

With string fusion, the values of $\Sigma[N_F, N_B]$ split: the higher the string density is, the more often the string fusion occurs, the smaller the values of $\Sigma[N_F, N_B]$ are obtained (Fig. 1.3, solid lines of different brightness). Thus, string fusion violates the property of strong intensity of $\Sigma[N_F, N_B]$, which was also obtained earlier in the model with infinite strings and the correlation between particles from a string [96].

This result shows an advantage of studying $\Sigma[N_F, N_B]$, since, one the one hand, it, by construction, excludes the contributions from trivial fluctuations (in this model it is the fluctuations in the number of strings). On the other hand, $\Sigma[N_F, N_B]$

turns out to be sensitive to the types of particle sources (various degrees of strings' overlaps and string clusters formation due to fusion). Therefore, by studying the behaviour of $\Sigma[N_F, N_B]$, one can obtain more reliable results in the study of multiplicity fluctuations and, in the same time, to extract the valuable information on particle-producing sources.

In general, the obtained dependence of $\Sigma[N_F, N_B]$ on Δy is consistent with its behaviour in the model with infinite strings and short-range correlations [98]. However, our approach shows that the source of the $\Sigma[N_F, N_B]$ rise with Δy, as it was mentioned for the decrease of $b_{\rm corr}[N_F, N_B]$ with Δy, might equally be the long-range correlations that appear from the fluctuations in the number of finite in rapidity strings producing particles in forward and backward windows. This suggests that these two approaches should be considered as complementary.

1.3 Discussion

In the developed toy-model of interacting strings, finite in rapidity, the obtained behaviour of forward-backward multiplicity correlations and fluctuations with Δy qualitatively resembles the published ALICE data at LHC, namely:

1. the gradual decrease of $b_{\rm corr}[N_F, N_B]$ with the gap between forward and backward rapidity acceptances Δy [99],

2. the gradual increase of $\Sigma[N_F, N_B]$ with the gap between forward and backward rapidity acceptances Δy [100].

This result is of particular interest since in the models with infinite strings in rapidity this behaviour of $b_{\rm corr}[N_F, N_B]$ and $\Sigma[N_F, N_B]$ with Δy can only be obtained by introducing short-range correlations to the model [96]. Their impact fades with Δy, while the long-range contribution is fully defined by the number of strings producing particles in both forward and backward acceptance windows [56], thus, is constant with Δy in that models.

In the developed approach, on the contrary, this particular behaviour was obtained in the simplest scenario without short-range correlation introduced but with fluctuating number of strings that produce particles in the F-B rapidity acceptances.

Thus, one can conclude that it is important to take into account both the short-range correlations that were modelled, for instance, in Ref. [95] and the initial conditions that are considered in this model, e.g. strings of short length and/or shifted with respect to midrapidity, as these two mechanisms give similar impacts on $b_{\rm corr}[N_F, N_B]$ and $\Sigma[N_F, N_B]$ that cannot be easily disentangled.

The comparison of the result for $\Sigma[N_F, N_B]$ with string fusion in our model with finite strings [89, 90] and in models with infinite in rapidity strings and short-range correlations [95, 96] makes it even more preferable to consider strings of finite length in rapidity for further studies. The point is that when string fusion is taken into account in models with infinite in rapidity strings and short-range correlations [95], $\Sigma[N_F, N_B]$ loses its property of strong intensity and begins to depend on the string density and string cluster formation [96]. Moreover, the values of $\Sigma[N_F, N_B]$ with string fusion in these models [95, 96] increase compared to the results for free strings. This observation is supported by the ALICE result for inelastic $p + p$ interactions [101]: $\Sigma[N_F, N_B]$ grows with "centrality" (particle multiplicity).

On the other hand, in the model we developed, the result is the opposite: $\Sigma[N_F, N_B]$ decreases with string fusion (see Fig. 1.3). This statement can be supported by the observed decrease of $\Sigma[N_F, N_B]$ with increasing centrality, also measured by ALICE but in $A + A$ collisions [100]. Thus, we can assume that accounting for the formation of "short" strings in nucleus-nucleus collisions will compensate for the increase in $\Sigma[N_F, N_B]$ due to string fusion and short-range correlations. As a result, it is believed that the total effect on $\Sigma[N_F, N_B]$ in $A + A$ collisions will give a behaviour of $\Sigma[N_F, N_B]$ that coincides with its experimental dependence on centrality: a decrease of $\Sigma[N_F, N_B]$ for more central $A + A$ events. This is a plausible scenario, since in $A + A$ collisions the formation of strings between sea quarks (that are shorter than the ones formed between valence partons) is enhanced in comparison to $p + p$ collisions.

Thus, the first evaluative part of the thesis has shown the promise of using the model of interacting strings, finite in rapidity, to describe correlation data in hadron collisions at high energies. For the detailed study of string formation mechanisms, it is necessary to first evaluate the applicability of such a model to the description of proton-proton interactions and only then move on to nucleus-nucleus collisions.

CHAPTER 2

Elaborated model of interacting strings finite in rapidity with transverse and longitudinal dynamics

An initial assessment showed (see Chapter 1) that the phenomenological model of multi-particle production by colour strings of finite length in rapidity dimension gives results that are qualitatively consistent with the experimental data. In addition, the model turned out to be a promising tool to be applied to the description of $A+A$ collisions. However, we decided to continue the development of our approach, concentrating explicitly on the description of $p+p$ collisions at high energies in order to consider in more details the machinery of the formation of colour strings. This Chapter presents results published in Refs. [102, 103] that were obtained within the extended model whose mechanisms of string dynamics and interactions were consistently developed and tested in our investigations [104, 105, 106].

2.1 Description of $p+p$ interactions via multi-pomeron exchange

In this Chapter, we consider inelastic $p+p$ interactions in the framework of the pomeron exchange approach. Each pomeron is represented by the cylindrical Feynman diagram [43, 44, 45]. The uncut diagrams contribute to the elastic cross-section, while the unitarity cut of each cylinder creates two colour strings [30], that fragment into observed particles. Moreover, at high energies the diagrams of the multiple parallel exchanges of pomerons predominate.

Thus, in this approach, we replace an arbitrary number of stings in an event (as it was implemented in the toy-model presented in Chapter 1) by the number of strings, $n_{\rm str}$, arising from the number of exchanged pomerons, $n_{\rm pom}$, defined as

$$n_{\rm str} = 2n_{\rm pom}. \tag{2.1.1}$$

With the natural assumption of the Gaussian distribution of the transverse positions of partons inside the proton, one can calculate a probability of parton-parton interaction that can be interpreted as the probability of string formation [107]. The resulting distribution on the number of pomeron exchanges coincides with the Regge-theory parametrization [57] that neglects the three-pomeron vertices

$$P\left(n_{\mathrm{pom}}\right) = A\left(z\right) \frac{1}{z n_{\mathrm{pom}}} \left(1 - \exp\left(-z\right) \sum_{l=0}^{n_{\mathrm{pom}}-1} \frac{z^l}{l!}\right), \tag{2.1.2}$$

where $z = \frac{2C\gamma s^{\Delta}}{R^2 + \alpha' \ln s}$, $C = 1.5$ is the quasi-eikonal parameter related to the small-mass diffraction dissociation of incoming hadrons, $\Delta = \alpha(0) - 1 = 0.2$ is the residue of the pomeron trajectory, $\alpha(0)$ is the intercept of the pomeron trajectory, $\gamma = 1.035$ GeV^{-2} and $R^2 = 3.3$ GeV^{-2} characterise the coupling of the pomeron trajectory with the initial hadrons, the slope of the pomeron trajectory $\alpha' = 0.05$ GeV^{-2}, s is the square of the collision centre-of-mass energy, and $A(z)$ is a normalising coefficient. Fig. 2.1 presents the example event distribution in the number of strings, n_{str}, obtained with these parameters for $\sqrt{s} = 13$ TeV. One can see that the number of colour strings formed in $p + p$ collisions can reach the impressive values.

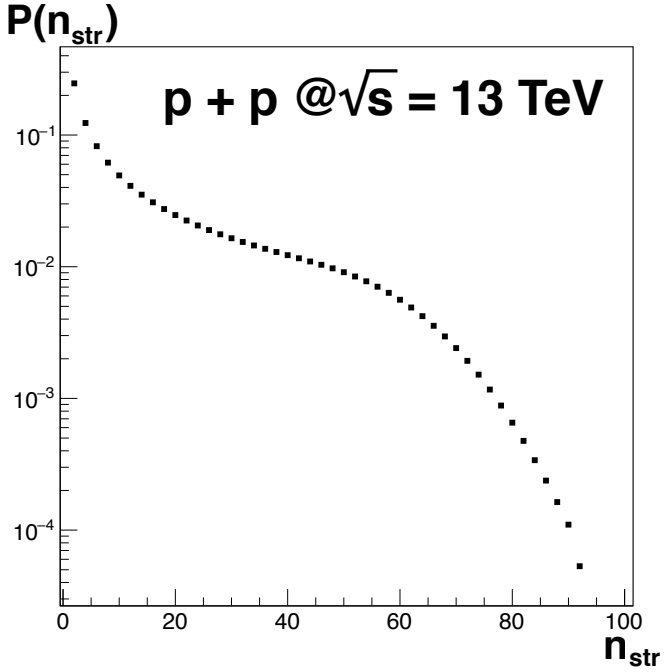

Figure 2.1: Model event distribution in the number of strings, $P(n_{\mathrm{str}})$, for inelastic $p + p$ interactions at $\sqrt{s} = 13$ TeV.

In this thesis, the values of parameters listed above and substituted into Eq. (2.1.2) were taken from Ref. [108]. In that investigation, they were found by fitting the data on multiplicity distributions and cross sections under assumption that strings that were initially formed in an event can overlap to various degrees and fuse, forming the string clusters with the modified fragmentation characteristics, which changes the model multiplicity.

This is in contrast to another approach used in Ref. [109], where the string fusion is effectively taken into account already at the moment of string formation. Therefore, there are a number of free strings in Ref. [108] and a number of string clusters in Ref. [109]. The values of parameters that are to be substituted in Eq. (2.1.2) for these two methods will differ, but they should both describe the same charged particle multiplicity distribution, $P\left(N_{\mathrm{ch}}\right)$, corresponding to the data. We follow the first approach that allows us to track the 3D evolution of string density before string fusion and, thus, to consider additional string dynamics.

Therefore, in our approach, a proton no longer consists only of a single pair of a quark and a diquark. Moreover, it is not only two strings that are formed in inelastic $p+p$ interaction, as we move away from the constituent picture. Instead, we take into account the multi-parton configurations of protons given by sea quarks whose independent and simultaneous interactions result in the exchange of some number of pomerons in an event.

This complication obliges us to monitor the fulfilment of the law of conservation of energy and momentum for partons forming a proton.

2.1.1 Parton composition of protons and string formation

In this Chapter, we consider only strings stretched between valence and sea quarks (anti-quarks) of colliding protons and no diquarks are considered. Moreover, we do not take into account spectator-partons, whose fragmentation would occur without the formation of longitudinal strings. Therefore, it is supposed that the number of partons in each of the colliding protons, n_{part}, is equal to the initial number of strings, n_{str}, that should be formed in an event according to Eq. (2.1.1).

It is the essential problem: to form two colliding protons with a given number of partons, on the one hand, respecting the energy and momentum conservation laws and, on the other hand, keeping the parton distribution functions (PDFs) uncor-

rupted. To meet these requirements in the Monte-Carlo simulation, the algorithm of partons' permutations was developed and used (see Appendix A).

Once an extensive set of protons with correctly selected partons is created, we proceed to the formation of the given number of strings in an event, Eq. (2.1.1). A string should be stretched between two randomly selected partons belonging to two randomly selected protons (but with the given number of partons equal to the number of strings in an event). However, the found string is accepted only if its energy is sufficient to decay at least into two pions at rest [110]

$$\sqrt{sx_1x_2} \geq 2m_\pi, \tag{2.1.3}$$

with x_1 and x_2 being the fractions of the protons' momenta that are carried by partons forming a string, m_π denoting the pion mass. An additional condition is that all partons from the two colliding protons should form such strings. Otherwise, another random proton pair to be sought.

Thus, at this step of the model, an event is represented by the number of parallel strings that are stretched between parton pairs of colliding protons.

2.2 Partial chiral symmetry restoration in the presence of a colour string

In general, the colour confinement in QCD, a non-abelian gauge theory, is viewed as the appearance of the colour field between two colour charges enclosed in the flux tube of finite transverse size [111]. However, some lattice QCD results demonstrate that the presence of a colour string modifies the QCD vacuum. For example, the correlator between the quark-antiquark chiral condensate, $\langle q\bar{q}\rangle$, and the Wilson loop, W, is appeared to be not a constant as a function of the transverse distance from a string [112]. Indeed, only at large distances $\langle q\bar{q}\rangle$ and W become uncorrelated, meaning that there is no string influence. In the meantime, the values of the correlation function decrease in the vicinity of the string, which indicates a partial restoration of chiral symmetry in this region of the space.

In this dissertation, we follow the approach developed in Refs. [59, 60], where the authors interpret these lattice results, Eq. (2.2.1), left, as the influence of a scalar field created by a cloud of σ-mesons, Eq. (2.2.1), right, that surrounds a string in

the transverse plane and creates the Yukawa potential

$$\frac{\langle q\bar{q}\,(r_\perp)\,W\rangle}{\langle q\bar{q}\rangle\langle W\rangle} = 1 - K_0\,(m_\sigma \widetilde{r_\perp})\,, \tag{2.2.1}$$

where $\widetilde{r_\perp} = \sqrt{r_\perp^2 + s_{\rm str}^2}$ is the regularised distance in the transverse plane, $r_\perp$ is a 2D distance between a pair of strings, $s_{\rm str} = 0.176$ fm [59] is a genuine string width, which differs from the effective string width resulting from quantum fluctuations, K_0 is zero-th modified second-kind Bessel function corresponding to a massive scalar propagator in two dimensions and $m_\sigma = 0.6$ GeV [59] is the mass of the σ-meson that is proposed to be a mediator of the force between strings.

In this paradigm, the string-string interaction appears in the created Yukawa potential, which results in the non-relativistic attraction between them similar to nuclear forces [60]. The problem is two-dimensional since the strings are viewed infinite in rapidity and the interaction between them manifests itself in the transverse dimension only.

The authors argue [59] that this attractive effect is most pronounced at high string densities and may lead to their collapse into a many-string hot spot. Moreover, some sufficient string density inside this region would lead to the ultimate restoration of the chiral symmetry and, thus, to the formation of the QGP fireball.

In this dissertation, we are interested in exploring whether it is possible to consider such string attraction as an effective determination of the initial event conditions: the formation of complex transverse distribution of the string density prior to hadronisation.

2.3 Transverse evolution of string density due to string attraction

In this thesis, it is assumed that the attractive interaction between strings occurs right after they are formed. Thus, the transverse dynamics of strings in an event, determined by their attraction, is first realized, and only after that the fusion of some of them is taken into account.

The non-relativistic equations of motion, Eq. (2.3.1), for all strings in an event are defined by the 2D Yukawa interaction [59] and are viewed as the motion of 2D

gas of particles

$$\ddot{\vec{r}}_i = \sum_{j \neq i} \vec{f}_{ij} = 2m_\sigma (g_N \sigma_T) \sum_{j \neq i} \frac{\vec{r}_{ij}}{\tilde{r}_{ij}} K_1(m_\sigma \tilde{r}_{ij}), \tag{2.3.1}$$

where $\vec{r}_{ij}$ and $\tilde{r}_{ij}$ correspond to $r_\perp$ and $\widetilde{r_\perp}$ from Eq. (2.2.1). The i and j subscripts indicate that the quantities are constructed for the i-th and j-th strings. The $g_N \sigma_T = 0.2$ is the string self-interaction coupling in units of string tension [60], K_1 is the first modified second-kind Bessel function. Strings are considered to be moving as a whole according to Eq. (2.3.1). This simplification assumes that there are no kinks that, for example, are taken into account in PYTHIA [36] event generator and affect the string characteristics (e.g. by changing the p_T spectrum of emitted particles).

To solve Eq. (2.3.1), one has to provide initial conditions and limit the time of system evolution to transfer it to the final state.

The 2D Gaussian distribution of width 0.5 (model parameter respecting the cross-section area of a proton) is used to sample the initial 2D transverse coordinates of string centres in an event (Fig. 2.2, left). This simplification is to decrease the program's running time: instead of applying the Glauber approach at the partonic level and finding which partons are to collide and form strings, we assume that some configuration of strings has already been created in an event and straightaway set their coordinates. It is the consequent motion of strings according to the system of Eqs. (2.3.1) that will complicate this picture.

Under the influence of Yukawa attraction according to Eq. (2.3.1), the strings come closer, fly through each other (since at this stage we neglect the surface tension of the string [113]), slow down, stop and begin to move in the opposite directions (Fig. 2.2, left, depicts the initial positions of string centres (squares) and their trajectories (lines)). Therefore, strings oscillate like a pendulum in the transverse plane and the proper time, τ, after which the system evolution, governed by Eq. (2.3.1), will be stopped crucially affects the final string density. In this part of the dissertation, we test two scenarios.

In the first scenario, the system of strings is frozen at the conventional time (same for all events) before the start of string fragmentation at $\tau = 1.5$ fm [59] (Fig. 2.2, right).

In the second case, the topology of the system is fixed at τ_{deepest} time that varies

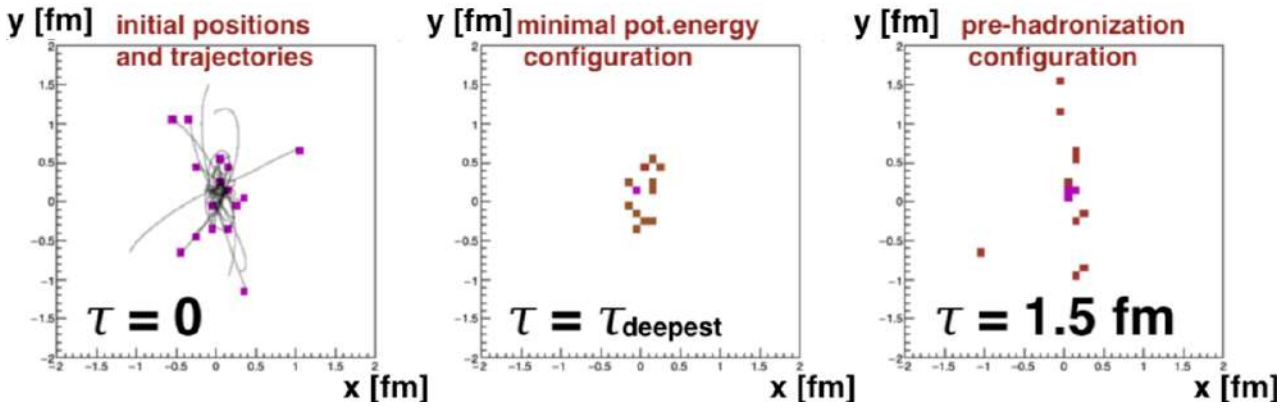

Figure 2.2: Two-dimensional histogram of the string density in the transverse $X-Y$ plane for an event with 16 strings: **Left:** initial positions of string centres (purple squares) and the trajectories of their motion according to Eq. 2.3.1 (grey lines); **Middle:** the configuration of strings after the time $\tau_{\rm deepest}$ that corresponds to the minimal potential energy of the string system; **Right:** the configuration of strings after $\tau = 1.5$ fm that is the conventional time for the string hadronisation.

event-by-event (Fig. 2.2, middle). This is the time it takes for a string transverse configuration to attain the global minimum of the potential energy, evolving according to Eq. (2.3.1). Thus, $\tau_{\rm deepest}$ depends not only on the initial string transverse positions, but also on the number of strings. It is also worth emphasising that, for $\tau = 1.5$ fm, one obtains a more dilute system, while for $\tau_{\rm deepest}$, the string density is highest.

It is important to note that for some configurations of strings the minimum of the potential energy of the system can only be reached at $\tau > 1.5$ fm. In this case, we use $\tau = 1.5$ fm for the transverse evolution of string system to ensure that $\tau_{\rm deepest}$ does not exceed the typical time for string hadronisation [59].

2.4 Longitudinal dynamics of finite in rapidity strings

This realisation of the model accounts for the longitudinal dynamics of finite in rapidity strings, in contrast to the static particle sources considered in Chapter 1.

The problem of finding the momentum of partons, $p_{\rm part}$, (see Sec. 2.1.1) was addressed to find the values of initial positions of string ends in rapidity, $y_{\rm init}^{\rm part}$, as

$$y_{\rm init}^{\rm part} = \sinh^{-1}\left(\frac{p_{\rm part}}{m_{\rm part}}\right), \tag{2.4.1}$$

where $p_{\rm part} = x_i p_{\rm beam}$, $p_{\rm beam} = \sqrt{s/4 - {m_{\rm p}}^2}$ is a proton beam momentum, x_i is the

fraction of proton's momentum carried by i-th parton (see Appendix A), $m_{\rm p} = 0.938$ GeV, $m_{\rm part}$ is the parton mass at the end of the string. For $m_{\rm part}$ we substitute the mass of the gluon cloud, $m_{g\rm cloud}$, (see Appendix A) or the current quark masses: $m_u = 0.0022$ GeV, $m_d = 0.00479$ GeV, $m_s = 0.095$ GeV, and $m_c = 1.275$ GeV for quarks u, d, s, and c, respectively.

However, the string tension, σ_T, slows down the massive partons flying outwards with momentum $p_{\rm part}$ according to

$$dp_{\rm part}/dt = -\sigma_T, \tag{2.4.2}$$

where the Coulombic term of the potential in Eq. (0.0.1) is neglected. As a result, the initial rapidity of the string end, $y^{\rm part}_{\rm init}$, should be decreased [114] by the value

$$y^{\rm part}_{\rm loss} = \cosh^{-1}\left(\frac{\tau^2\sigma_T^2}{2m^2_{\rm part}} + 1\right), \tag{2.4.3}$$

where τ is the time during which the longitudinal evolution of a string takes place.

Let us make an important statement: the value of the evolution time, τ, inserted in Eq. (2.4.3), changes not only the length of the strings, but also strings' positions with respect to midrapidity. This is because $y^{\rm part}_{\rm loss}$ applies to both ends of the string independently and depends on the parton's mass. Therefore, after taking into account the modification of a string length, or, in other words, having subtracted $y^{\rm part}_{\rm loss}$ from $y^{\rm part}_{\rm init}$, some strings may appear lying entirely in one (forward or backward) hemisphere. In this case, it is no longer true that all strings cross $y = 0$ as it was assumed in Chapter 1. Therefore, some results on the rapidity dependence of correlation quantities may change.

At this step in our approach there is some arbitrariness in the choice of τ. The idea is to synchronise the longitudinal string dynamics with the transverse ones. Thus, to substitute $\tau_{\rm deepest}$ or $\tau = 1.5$ fm to Eq. (2.4.3). Note, that in the model, the longitudinal and transverse dynamics are implemented sequentially only to simplify the calculations. It is clear that they must occur simultaneously, since the longitudinal dynamics of a string is determined by the initial momenta of the partons at its' ends and the tension of the gluon field, and is, therefore, inevitable from the very beginning of the formation of a string.

Thus, by considering the evolution of the string system up to some time, we obtain different string configurations that specify the energy density distributions

in $p + p$ collisions.

2.5 String fusion

Changes in strings' lengths and positions relative to mid-rapidity make the string system inhomogeneous in rapidity. Furthermore, due to the attractive motion of strings in the transverse plane (Sec. 2.3), they form clusters of fully or partially overlapped strings (taking into account that they have a finite transverse size caused by the colour confinement). Since the overlaps change with rapidity, one obtains a non-trivial three-dimensional distribution of string density.

To systematically study the fusion of strings, this work considers two modes of the model (similar to investigations in the framework of toy-model, see Chapter 1).

As a reference scenario, we consider the case of free particle sources. In means that the possibility of string fusion is ignored, even when they overlap. Thus, all particle sources are identical and produce particles in the same manner.

The main interest is to consider string–string interaction effects in a form of fusion. It leads to the formation of the new types of particle producing sources (string clusters) with the different degrees of intersections. Therefore, string clusters have various tensions that are higher than the one for a free string.

There have been several proposals made on how to account for string fusion [91]. In Chapter 1, we only briefly described one of the simplified methods (the cellular approach). Let us provide a more detailed description here, especially since the way of accounting for string fusion will be revised and improved in the next model version (see next Chapter).

First, one may assume that the colour field changes only in the region where some number of strings overlaps and stays unmodified in the rest transverse areas of these strings. Another possibility is that, if some number of strings overlap even on an arbitrarily small area, they form a cluster that has the uniformly modified colour field over the entire area of the union of all these strings. However, so far, the attempts were in vain to find the observables sensitive to the type of colour field modification [115].

Therefore, we again follow a cellular approach in the transverse plane developed in Ref. [91]. This means that we only look after strings' centres positions on the

transverse grid with the constant cell size of width $d = 0.3$ fm, which corresponds to the string radius. Thereby, the only strings to interact are the strings whose centres lie in the same transverse cell. This simplification is beneficial from the point of view of computing resources.

As in Chapter 1, the fusion problem is three-dimensional since in the rapidity space there are the fluctuations of both the lengths of strings and the strings' positions with respect to midrapidity. Therefore, for strings whose centres are in the same cell in the transverse plane, one has to search for their overlaps in the rapidity space to perform fusion in these intersections (see Fig. 1.1).

In this model, we also follow the idea [68] of string fusion that changes the string's production characteristics: mean particle multiplicity for a cluster of k fused strings, μ_k, is found according to Eq. (1.1.1). It is smaller than the one for a superposition of k free strings (each characterised by μ_0) that gives in total $\mu_k = k\mu_0$. One can qualitatively explain the relation from Eq. (1.1.1) between μ_0 and μ_k as follows. Given the case of the overlap of a few strings, their colour field vectors could be randomly oriented with respect to each other. To find the resulting colour field inside the cluster of k overlapped strings, one can consider this problem as a random walk in the vector colour space, thus, obtaining not the factor of k, but the factor $\sqrt{k}$ for k overlapping strings compared to a single free string. The first consideration of this behaviour was proposed in Ref. [116] by the analogy with the formation of the colour "rope", while a rigorous comparison of the string percolation approach to the colour–glass condensate model can be found in Ref. [117].

To study the correlations between multiplicity and transverse momentum of particles, the mechanism of p_T generation is introduced in this realisation of the model. In Ref. [70] the mean transverse momentum of particles produced by a cluster of k strings, $\langle p_T \rangle_k$, is related to the average transverse momentum of particles produced by a free colour string, p_0, similarly to Eq. (1.1.1) as

$$\langle p_T \rangle_k = p_0 \sqrt[4]{k}. \tag{2.5.1}$$

Thus, the fusion of strings increases the average momentum of the particles. In the developments of this model, published in Refs. [104, 105, 106], it was this formula, Eq. (2.5.1), that was used to determine the average momentum of particles from the string cluster.

However, in our more complete works, see Refs. [102, 103], we propose an analogy with the β parameter defined in Refs. [109, 118, 119, 120, 121]. In these works, also based on the multi-pomeron exchange scenario, the increase in $\langle p_T \rangle$ is achieved due to the collectivity of the total number of strings, M, in the event. This interplay is taken into account as a power of M^{β}, where the expression for β is found [121] from the fit to the experimental data as

$$\beta = 1.16[1 - (\ln\sqrt{s} - 2.52)^{-0.19}]. \tag{2.5.2}$$

Remarkably, the parameter β is approximately 0.25 at $\sqrt{s} = 900$ GeV and it changes sign at lower collision energies according to the fit in Ref. [121], which makes its usage of special interest in our future studies of $p+p$ interactions in, for example, NICA collider energy domain. In this case, the average transverse momentum will be suppressed by the string fusion according to Eq. (2.5.3). It give us the idea to combine these two approaches and to introduce the factor k^{β} instead of $\sqrt[4]{k}$ (the two approximately coinciding at the LHC energies) to change the average transverse momentum of particles from a string cluster as

$$\langle p_T \rangle_k = p_0 k^{\beta}. \tag{2.5.3}$$

However, let us stress that k here is a number of strings overlapped in some rapidity interval for a string cluster defined in some transverse cell, while M from Refs. [109, 121] is the overall number of particle sources in an event. It is likely that a new data fit will be required to refine the definition of β in our new interpretation of string fusion.

In the current implementation of the model, at this stage of the simulation, the string system is already frozen, and no transverse position is assigned to the clusters of strings, as soon as there is no need of it in the further calculations. However, the understanding where a fused string will be located in the transverse plane (at the centre of gravity, at the arithmetic mean of the centres of the fused strings, or somewhere else) is a serious issue, which also intersects with the problem of determining the thickness of a string cluster. We will return to these issues in the next Chapter as we will move on to the advanced version of the model.

At this step, we determined the effect of string cluster formation on the mean transverse momentum of the particles.

2.6 Effective string hadronisation

We perform the effective string hadronisation in the same manner as in Chapter 1 by dividing a string in the rapidity dimension into units of length ε. To describe the decay of a string, we use the Schwinger fragmentation mechanism [33, 34, 54]: in order to achieve a uniform distribution of produced particles in rapidity, we generate their rapidities according to the Gaussian distribution for each interval of length ε. We do it in the way that the mean for Gauss corresponds to the centre of the interval, and the variance corresponds to its width. We find the charged particle event multiplicity, $N_{\rm ch}$, according to Eqs. (1.1.1), (1.1.2) and (1.1.3). It is important to mention that this ε-division is only a technical solution to approximate the string fragmentation mechanism. Therefore, the procedure is the same for free strings and string clusters.

The transverse momentum of particles, produced by free string or by cluster of k strings, is sampled from the following distribution, corresponding to the Schwinger particle production [33, 34, 54],

$$f(p_T) = \frac{\pi p_T}{2\langle p_T\rangle_k^2}\exp\left(-\frac{\pi p_T^2}{4\langle p_T\rangle_k^2}\right), \tag{2.6.1}$$

with $\langle p_T\rangle_k$ defined in Eq. (2.5.3).

Simultaneously the appearance of particles of a certain type is determined according to Schwinger-like probabilities

$$\sim \exp\bigl(-\pi m_i^2/\sigma_{\rm eff}k^{2\beta}\bigr), \tag{2.6.2}$$

with $\sigma_{\rm eff} = 4p_0^2$ being the modified effective string tension. Traditionally, in the models that rely on the Schwinger mechanism of particle production [118], $\sigma_{\rm eff}$ slightly differs from the conventional string tension, σ_T, appearing in Eq. (2.4.3). It is to effectively take into account the re-scatterings of particles. Our model includes π, K, p and ρ-resonance, with the latter decaying into two charged pions. Their masses from Particle Data Group (PDG) are substituted in Eq. (2.6.2) instead of m_i.

Knowing the particle's mass, transverse momentum, and rapidity, one can find the longitudinal component of its momentum from Eq. (0.0.2), and hence the pseudorapidity, Eq. (0.0.3). Thus, in the approach described in this Chapter, one can calculate particle correlations in pseudorapidity rather than in rapidity (the simpli-

fication used in Chapter 1), which will be in direct correspondence with how it is done in the analysis of experimental data.

2.7 Model formalism

The developed elaborated Model, presented in details in Sec. 2.1 - 2.6, proposes a phenomenological solution to the problem of describing the multi-particle production in proton-proton collisions using the Monte-Carlo approach to the formation and fragmentation of colour strings. At the same time, it seems possible to construct an analytical description of the specific problem of studying forward-backward rapidity correlations in the colour string formation scenario. A comparison of numerical and analytical calculations would serve as a verification of the numerical results obtained in the model.

In this dissertation, this is done [102] by the extension of the analytical description of the model with fragmentation of strings of two types, see Ref. [80], to the model formalism with strings of three types. In the current model, three types of strings appear in the study of the particle production in two separated rapidity intervals due to finiteness of strings in rapidity.

Therefore, two rapidity windows of width δy at some distance Δy, symmetrically placed with respect to midrapidity, define the following classes of strings: (i) fragmenting simultaneously into both forward and backward windows and (ii) fragmenting only into the forward one or (iii) only into the backward one. The probability to have simultaneously $n_{\rm long}$ strings of the first type, $n_{\rm for}$ strings of the second type, and $n_{\rm back}$ of the third type, $q\left(n_{\rm long}, n_{\rm for}, n_{\rm back}\right)$, is such that

$$\sum_{n_{\rm long}, n_{\rm for}, n_{\rm back}} q\left(n_{\rm long}, n_{\rm for}, n_{\rm back}\right) = 1. \tag{2.7.1}$$

Let us introduce the following notations for the first, second and cross-moments of this distribution

$$\sum_{n_{\rm long}, n_{\rm for}, n_{\rm back}} q\left(n_{\rm long}, n_{\rm for}, n_{\rm back}\right) n_i = \overline{n_i}, \tag{2.7.2}$$

$$\sum_{n_{\rm long}, n_{\rm for}, n_{\rm back}} q\left(n_{\rm long}, n_{\rm for}, n_{\rm back}\right) n_i^2 = \overline{n_i^2}, \tag{2.7.3}$$

$$\sum_{n_{\rm long}, n_{\rm for}, n_{\rm back}} q\left(n_{\rm long}, n_{\rm for}, n_{\rm back}\right) n_i \cdot n_j = \overline{n_i \cdot n_j}, \tag{2.7.4}$$

$$D_{n_i} = \overline{n_i^2} - \overline{n_i}^2, \tag{2.7.5}$$

$$\operatorname{cov}(n_i, n_j) = \overline{n_i \cdot n_j} - \overline{n_i} \cdot \overline{n_j}, \tag{2.7.6}$$

where indices i and j lie within "long", "for" and "back" string types.

To calculate the multiplicities, N_F and N_B, in two rapidity windows it is necessary to sum the contributions from strings of different types to these forward and backward acceptances

$$N_F = \sum_{k=1}^{n_{\text{long}}} N_F^{(k)} + \sum_{s=1}^{n_{\text{for}}} N_F^{(s)}, \tag{2.7.7}$$

$$N_B = \sum_{k=1}^{n_{\text{long}}} N_B^{(k)} + \sum_{t=1}^{n_{\text{back}}} N_B^{(t)}. \tag{2.7.8}$$

Thus, for the case of free sources, the joint multiplicity distribution $P(N_F, N_B)$ is given as a convolution of the probability distribution, $q(C)$, to have some string configuration C, and the forward-backward multiplicity distribution for this fixed configuration, $P_C(N_F, N_B)$, as

$$P(N_F, N_B) = \sum_C q(C)\, P_C(N_F, N_B). \tag{2.7.9}$$

The specific form of $P_C(N_F, N_B)$ can be found as convolutions of the corresponding probabilities from single strings of "long", "for" and "back" types

$$\begin{aligned} P(N_F, N_B) = & \sum_{(N_F^{(k)}, N_F^{(s)})} \delta_{N_F, \sum_{k=1}^{n_{\text{long}}} N_F^{(k)} + \sum_{s=1}^{n_{\text{for}}} N_F^{(s)}} \cdot \\ & \sum_{(N_B^{(k)}, N_B^{(t)})} \delta_{N_B, \sum_{k=1}^{n_{\text{long}}} N_B^{(k)} + \sum_{t=1}^{n_{\text{back}}} N_B^{(t)}} \cdot \\ & \cdot \prod_{k=1}^{n_{\text{long}}} P\left(N_F^{(k)}, N_B^{(k)}\right) \prod_{s=1}^{n_{\text{for}}} P\left(N_F^{(s)}\right) \prod_{t=1}^{n_{\text{back}}} P\left(N_B^{(t)}\right). \end{aligned} \tag{2.7.10}$$

We introduce the following notations for the first moments of distributions of single strings

$$\sum_{N_F^{(k)}, N_B^{(k)}} P\left(N_F^{(k)}, N_B^{(k)}\right) N_F^{(k)} = \sum_{N_F^{(s)}} P\left(N_F^{(s)}\right) N_F^{(s)} = \overline{\mu_F}, \tag{2.7.11}$$

$$\sum_{N_F^{(k)}, N_B^{(k)}} P\left(N_F^{(k)}, N_B^{(k)}\right) N_B^{(k)} = \sum_{N_B^{(t)}} P\left(N_B^{(t)}\right) N_B^{(t)} = \overline{\mu_B}, \tag{2.7.12}$$

and by analogy for higher moments. In these formulas, as in Eqs. (2.7.7), (2.7.8) and (2.7.10), subscript k runs over the number of strings in both rapidity windows, $n_{\rm long}$, subscript s runs over the number of strings appearing only in forward rapidity window, $n_{\rm for}$, and subscript t runs over the number of strings appearing only in backward rapidity window, $n_{\rm back}$.

In the case of rapidity windows symmetrically located with respect to midrapidity, the following relation is satisfied

$$\overline{\mu_F} = \overline{\mu_B} \equiv \overline{\mu}. \tag{2.7.13}$$

Using all the aforementioned notations, we find expressions for the components of the correlation coefficient $b_{\rm corr}[N_F, N_B]$, Eq. (0.0.6), and the strongly intensive quantity $\Sigma[N_F, N_B]$, Eq. (0.0.7), as

$$\langle N_F \rangle = \overline{\mu} \cdot (\overline{n_{\rm long}} + \overline{n_{\rm for}}), \tag{2.7.14}$$

$$\langle N_B \rangle = \overline{\mu} \cdot (\overline{n_{\rm long}} + \overline{n_{\rm back}}), \tag{2.7.15}$$

$$D_{N_F} = \overline{\mu}^2 \cdot \left(D_{n_{\rm long}} + 2 \cdot {\rm cov}\,(n_{\rm long}, n_{\rm for}) + D_{n_{\rm for}}\right) + D_\mu \cdot (\overline{n_{\rm long}} + \overline{n_{\rm for}}), \tag{2.7.16}$$

$$D_{N_B} = \overline{\mu}^2 \cdot \left(D_{n_{\rm long}} + 2 \cdot {\rm cov}\,(n_{\rm long}, n_{\rm back}) + D_{n_{\rm back}}\right) + D_\mu \cdot (\overline{n_{\rm long}} + \overline{n_{\rm back}}), \tag{2.7.17}$$

$${\rm cov}\,(N_F, N_B) = \overline{\mu}^2 \cdot \left(D_{n_{\rm long}} + 2 \cdot {\rm cov}\,(n_{\rm long}, n_{\rm for}) + {\rm cov}\,(n_{\rm for}, n_{\rm back})\right). \tag{2.7.18}$$

What slightly simplifies the expressions is that, in the model, the number of particles from one string is generated according to the Poisson distribution, which results in $D_\mu = \overline{\mu}$.

Finally, combining the obtained expressions for the moments of $N_F - N_B$ distribution, one gets the analytical formulas for the correlation coefficient and strongly intensive measure

$$b_{\rm corr}[N_F, N_B] = \frac{\overline{\mu} \cdot \left(D_{n_{\rm long}} + 2 \cdot {\rm cov}\,(n_{\rm long}, n_{\rm for}) + {\rm cov}\,(n_{\rm for}, n_{\rm back})\right)}{\overline{\mu} \cdot \left(D_{n_{\rm long}} + 2 \cdot {\rm cov}\,(n_{\rm long}, n_{\rm for}) + D_{n_{\rm for}}\right) + \overline{n_{\rm long}} + \overline{n_{\rm for}}}, \tag{2.7.19}$$

$$\Sigma[N_F, N_B] = 1 + \overline{\mu} \cdot \frac{D_{n_{\rm back}} - {\rm cov}\,(n_{\rm for}, n_{\rm back})}{\overline{n_{\rm long}} + \overline{n_{\rm for}}}. \tag{2.7.20}$$

On the one hand, it is useful to note that in the limit of the absence of $n_{\rm for}$ and $n_{\rm back}$ strings in the model, these formulas reduce to the following expressions

$$b^0_{\rm corr}[N_F, N_B] = \frac{\overline{\mu} \cdot D_{n_{\rm long}}}{\overline{\mu} \cdot D_{n_{\rm long}} + \overline{n_{\rm long}}}, \tag{2.7.21}$$

$$\Sigma^0[N_F, N_B] = 1, \tag{2.7.22}$$

that are identical to the findings in the model with strings infinite in rapidity that produce particles uncorrelated (see Refs. [122] and [80], respectively).

On the other hand, it is clear that, in our model, $b_{\rm corr}[N_F, N_B] \to b^0_{\rm corr}[N_F, N_B]$ and $\Sigma[N_F, N_B] \to \Sigma^0[N_F, N_B]$ at $\Delta y = 0$ position of the rapidity windows, i.e. when the number of strings that produce particles **only** in the forward or **only** in the backward window, $n_{\rm for}$ or $n_{\rm back}$, is small and the fluctuations of $n_{\rm for}$ and $n_{\rm back}$ are Poissonian. Moreover, the numerator of the second term in Eq. (2.7.20), written down explicitly,

$$D_{n_{\rm back}} - {\rm cov}\,(n_{\rm for}, n_{\rm back}) = \langle n^2_{\rm back}\rangle - \langle n_{\rm for} n_{\rm back}\rangle, \tag{2.7.23}$$

demonstrates that if $n_{\rm for}$ were identically equal to $n_{\rm back}$ in each event, then Eq. (2.7.20) would again reduce to Eq. (2.7.22). However, our calculations show (Fig. 2.4, right) that there are non-zero $\langle n_{\rm for} n_{\rm back}\rangle$ correlations that determine the growth of $\Sigma[N_F, N_B]$ with Δy. In the case of $b_{\rm corr}[N_F, N_B]$, Eq. (2.7.19), the picture is even more complex since one has to additionally consider the cross-terms of $\langle n_{\rm long} n_{\rm for}\rangle$ and $\langle n_{\rm long} n_{\rm back}\rangle$ that result in the decrease of $N_F - N_B$ correlation with Δy (Fig. 2.4, left).

Thus, the obtained formulas enrich our understanding of the impact of non-trivial fluctuations in the number of strings in forward-backward windows on correlation and fluctuation measures.

2.7.1 Analytical and numerical calculations in the model with free strings for inelastic $p + p$ interactions at $\sqrt{s} = 200$ GeV

To use the analytical expressions from Eqs. (2.7.19) and (2.7.20), one has to substitute into them the moments of the distribution of string configurations Eq. (2.7.2)-(2.7.6). They can be determined from the numerical calculations for free particle sources.

In this section, the results are presented for the case when correlations between multiplicities in two rapidity windows of width $\delta y = 0.2$ were studied. Calculations were performed for one million generated events.

Fig. 2.3 shows a good agreement between the full model calculation (empty triangles) and the formula from Eq. (2.7.14) (dashed line) for the mean charged

particle multiplicity, $\langle N_F \rangle$, in the forward rapidity window, when the distance, Δy, between it and the backward rapidity acceptance (same definitions as in Fig. 1.2, right) is increased.

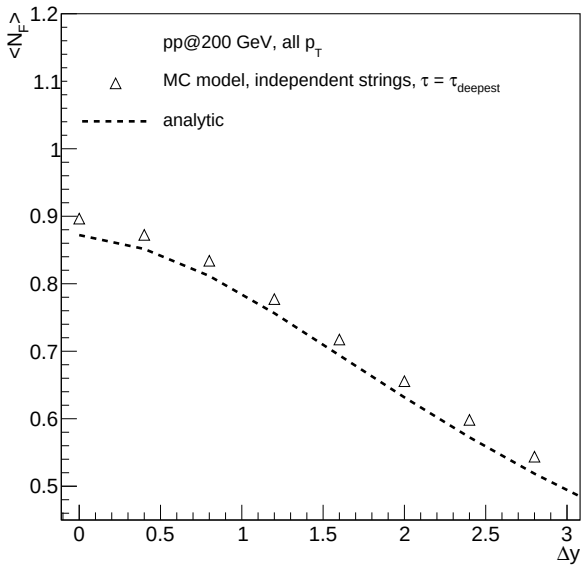

Figure 2.3: Dependence of the mean multiplicity in the forward rapidity window, $\langle N_F \rangle$, on the distance between the rapidity intervals, Δy, for the case of independent (free) sources. The results are presented for analytical (lines) and numerical (triangles) calculations.

It should be noted, that if some p_T cut is applied to the numerical calculations (triangles), one should re-scale the analytical curve by finding the proper value of $\overline{\mu}$. In general, the value of $\langle N_F \rangle$ decreases with the increase of Δy, which is explained by the decrease of the number of strings of $n_{\rm long}$ type and, therefore, the reduction of their contribution with Δy.

Fig. 2.4 shows a comparison of full model calculations (empty triangles) with the analytical expressions from Eqs. (2.7.19) and (2.7.20) (dashed lines) for $b_{\rm corr}[N_F, N_B]$ and $\Sigma[N_F, N_B]$. In Refs. [80, 96, 98], the weakening of $b_{\rm corr}[N_F, N_B]$ and the growth of $\Sigma[N_F, N_B]$ with increasing distance between windows, Δy, is a consequence of a decrease of correlations between particles produced by one source. As it was already mentioned, in this dissertation, correlations from a single source are neglected and the entire effect is reproduced due to fluctuations of the initial states - the choice of string configurations.

One can see (Fig. 2.4) a good agreement between the plots shown with empty

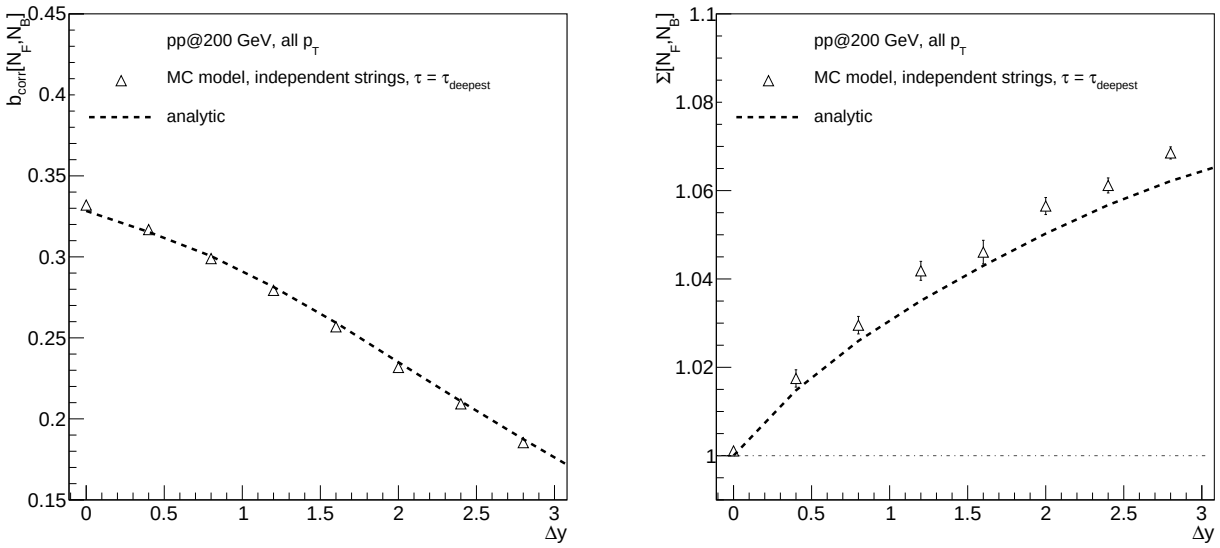

Figure 2.4: Dependence of the quantities $b_{corr}[N_F, N_B]$ (**left**) and $\Sigma[N_F, N_B]$ (**right**) on the distance between the rapidity intervals, Δy, for the case of independent (free) sources. The results are presented for analytical (lines) and numerical (triangles) calculations.

triangles and dashed lines. Thus, the comparison of the Monte-Carlo method with the direct analytical calculations proves the reliability of the application of numerical calculations, which allows us to proceed to the consideration of the results taking into account string fusion. Note that the presented formalism for free strings can be generalised to the case with fusion by introducing new classes of strings (additionally to "long", "for", "back") corresponding to different degrees of strings' overlaps. However, in this work, we restrict ourselves to numerical calculations in the model with string fusion.

2.7.2 Numerical calculations in the model with 3D dynamics of strings and consequent string fusion for p+p interactions at $\sqrt{s} = 200$ GeV

This subsection presents the part of the results [102] obtained in the developed model with string fusion. The full numerical simulation includes: string formation due to colour reconnection between partons, participating in the interaction; strings' transverse attractive dynamics; longitudinal dynamics of strings; cellular fusion of string segments overlapped in rapidity dimension; effective string hadronisation to the final particles. Calculations were performed for one million generated events.

Fig. 2.5 shows results of our calculations for correlation and fluctuation quanti-

ties, Eqs. (2.7.19) and (2.7.20), constructed for charged hadron multiplicities in two rapidity windows. The calculations were carried out both for string clusters (full circles and triangles) and for free (independent) strings (empty circles and triangles). Note, that the plot shown with empty triangles is repeated for consistency from Fig. (2.4). String evolution is considered either up to proper time $\tau = 1.5$ fm (circles), or until the minimum potential energy of the string system at the moment $\tau_{\rm deepest}$ is reached (triangles).

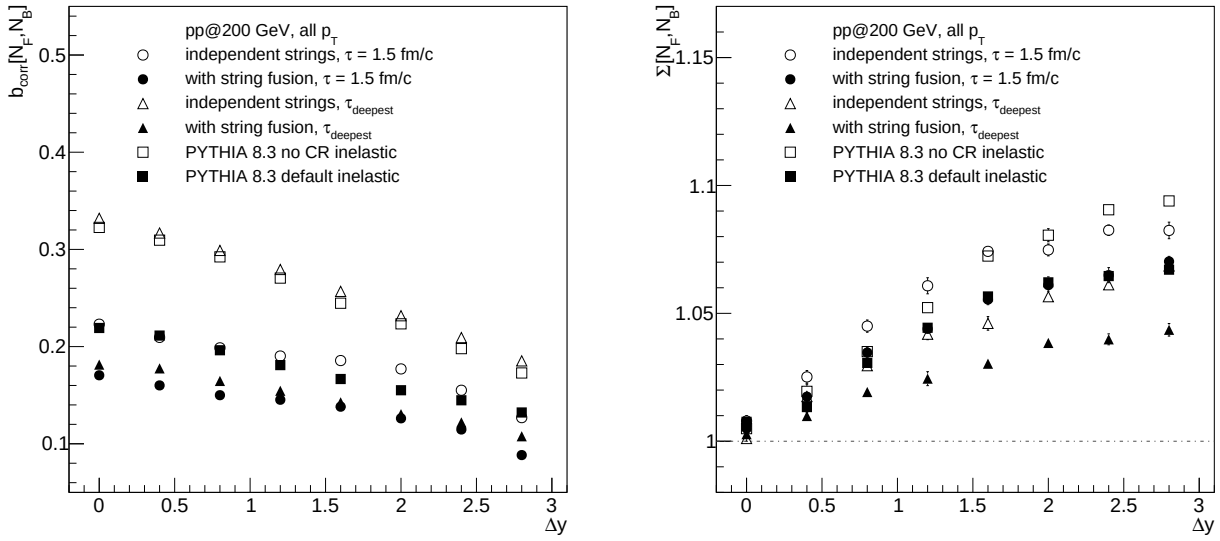

Figure 2.5: Model dependence of the correlation coefficient $b_{\rm corr}[N_F, N_B]$ (**left**) and strongly intensive quantity $\Sigma[N_F, N_B]$ (**right**) on the distance between the rapidity intervals Δy, where forward and backward multiplicities were calculated, for inelastic p+p interactions at $\sqrt{s} = 200$ GeV.

To compare the results of the developed model (Fig. 2.5) with the available Monte-Carlo event generators, we chose PYTHIA8.3 [123, 124] with the standard set of settings (Monash tune [125]). PYTHIA predictions are presented (Fig. 2.5) with two options considered: without (empty squares) and with (full squares) colour reconnection (CR) mechanism [126]. It can be shortly formulated as a re-grouping of colour strings between partons in a way that the total length of the colour strings formed is as short as possible. This mechanism in PYTHIA is also responsible for the increase in the average transverse momentum with increasing multiplicity, i.e. for an effect similar to the one resulting from the fusion of strings.

One can see that the values of $b_{\rm corr}[N_F, N_B]$ monotonically decrease (Fig. 2.5, left) with Δy, while $\Sigma[N_F, N_B]$ values monotonically increase (Fig. 2.5, right). These

dependencies repeat the rough estimates of $b_{\rm corr}[N_F, N_B]$ and $\Sigma[N_F, N_B]$ behaviour with the spacing of F-B windows obtained in the toy-model (see Chapter 1).

The model behaviour of $b_{\rm corr}[N_F, N_B]$ with string fusion is qualitatively consistent with the data on $p+p$ collisions [127]. By comparing full and empty symbols, one observes that the values of $b_{\rm corr}[N_F, N_B]$ and $\Sigma[N_F, N_B]$ decrease with string fusion considered in the model. Similar change in the magnitudes of $b_{\rm corr}[N_F, N_B]$ and $\Sigma[N_F, N_B]$ is seen for PYTHIA results with CR. The key conclusion here is that string fusion significantly modifies the values of both quantities. At the same time, at the moment of reaching the minimum of the potential energy by string system, the degree of string overlaps is the maximum and, as a consequence, this leads to the maximum deviation of the results from the free strings case.

A similar conclusion about the role of string fusion can be made for the joint fluctuations of the multiplicity and the total transverse momentum measured in one rapidity acceptance in terms of strongly intensive quantities, Eq. (0.0.8) and (0.0.9), shown in Fig. 2.6 (same notations as in Fig. 2.5). In addition, both values of $\Delta[P_T, N]$ and $\Sigma[P_T, N]$ are greater than unity (Fig. 2.6), which is consistent with the previous conclusions for this collision energy [120]. Earlier it was shown that as the energy decreases, the values of $\Delta[P_T, N]$ become less than unity. The monotonic growth with increasing window width δy also qualitatively agrees with [120], where the motion of strings in the transverse plane was not taken into account.

Moreover, the values of $\Delta[P_T, N]$ and $\Sigma[P_T, N]$ without string fusion (Fig. 2.6, empty circles and triangles) are consistent with unity for any δy, which corresponds to the definition of these quantities in the case of independent particle production. This is in contrast to PYTHIA event generator results without CR mechanism (empty squares), meaning that PYTHIA has some residual $P_T - N$ fluctuations.

In turn, string fusion makes the model values of $\Delta[P_T, N]$ and $\Sigma[P_T, N]$ dependent on δy and, in addition, on the string density (compare results for $\tau_{\rm deepest}$ (full triangles) and $\tau = 1.5$ fm (full circles)). Thus, they lose the property of strong intensity and start to depend on the formation of string clusters. In the meantime, CR mechanism in PYTHIA (full squares) also enhances the rise of $\Delta[P_T, N]$ and $\Sigma[P_T, N]$ with δy, but in such a way that our model graphs do not reach their level. Therefore, in the next section of this Chapter, the inference of model parameters will be presented to obtain the best possible description of the experimental data.

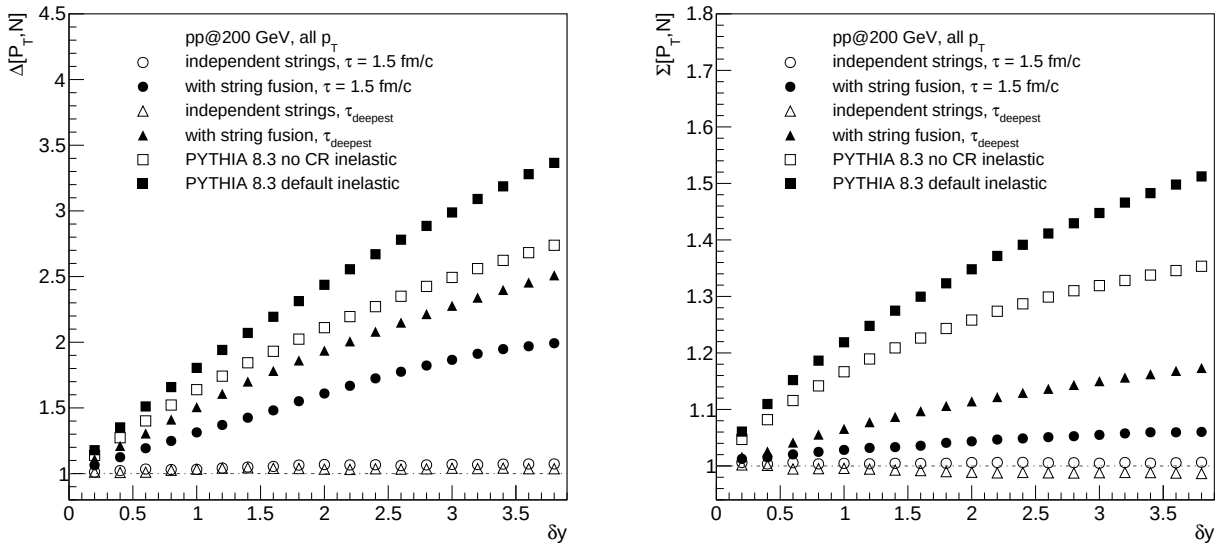

Figure 2.6: Model dependence of the quantities $\Delta[P_T, N]$ (**left**) and $\Sigma[P_T, N]$ (**right**) on the width of the rapidity interval δy, where P_T and N were calculated, for inelastic $p+p$ interactions at $\sqrt{s} = 200$ GeV.

In particular, this is necessary to select the proper time, τ, until which to consider the evolution of the system of strings in the transverse plane (and in the longitudinal dimension).

2.8 Model results for inelastic $p+p$ interactions at $\sqrt{s} = 900$ GeV

This section presents results published in Ref. [103] that are also obtained in the model described in this Chapter. Calculations were performed for one million generated events. We selected ALICE data [128, 129] on inelastic $p+p$ interactions at $\sqrt{s} = 900$ GeV to tune our model on a few distributions of global observables by fixing the values of two free parameters (μ_0 and p_0, see the next subsection). Once it is done, we compare model results with the data on correlations to see whether one can draw a conclusion about the preference of one or another model regime. Moreover, the very possibility of detecting traces of string dynamics or fusion in experimental data is very attractive.

2.8.1 Inference of model parameters

To tune our model, we simultaneously approximate ALICE data on p+p inelastic interactions at $\sqrt{s} = 900$ GeV on the charged particle multiplicity distribution [128], η-spectrum [128], and $\langle p_T \rangle$–N correlation function [129]. Global model parameters are: parameter of the effective string hadronisation, $\varepsilon = 0.1$, and the transverse grid cell size of 0.3 fm. They were fixed from the beginning of simulation, however, in principle, they can be changed, which may require reconfiguring free parameters. The values of the parameters for multi-pomeron distribution and for the transverse dynamics of strings are fixed to those from Sec. 2.1–2.3.

The best correspondence between model results and ALICE data [128, 129] is obtained for the following values of the free model parameters $\mu_0 = 0.87$ and $p_0 = 0.38$ GeV (see next subsection).

2.8.2 Global observables

We decided to tune our model with the fusion of particle-producing sources, evolving in transverse and longitudinal dimensions until proper time $\tau_{\rm deepest}$. First of all, it is because this concept of time for system evolution that depends on particular string configuration and is dynamically defined in each event seems to be more physical than the rough estimate of the time before the onset of hadronisation ($\tau = 1.5$ fm [59]). Moreover, the form of the dependence of mean particle transverse momentum, $\langle p_T \rangle$, on charged particle multiplicity, $N_{\rm ch}$, also makes this choice more legitimate (see next subsection).

The choice of values of the model parameters is made from the comparison of model predictions and experimental results for some of the so-called global observables characterising an event: the multiplicity of charged particles and the pseudorapidity distribution of particles.

Fig. 2.7, right, shows model approximation of ALICE data on η-spectrum at midrapidity [128]. We stress that starting from quite a complicated string structure in the rapidity space, a symmetrical inclusive η-distribution is obtained in the whole available η-range. Thus, the experimentally observed plateau of particle production at midrapidity is seen without the assumption of the boost invariance of particle-producing system [130]. To adjust the model value of $dN_{\rm ch}/d\eta|_{\eta=0}$ the

model parameter μ_0 (mean particle multiplicity per rapidity unit from a free string) was changed.

Having set $\mu_0 = 0.87$, we plot the charged particle multiplicity distribution (Fig. 2.7, left). In the experimental data on inelastic scattering, there are events with low total multiplicity. They are biased by the diffraction processes, which is due to the technical difficulty in recognising such events. Therefore, to describe ALICE data [128], we removed events with $N_{\rm ch} = 0$ since diffraction processes are not considered in the model. Thus, the corrected multiplicity distribution, $P(N_{\rm ch})$, is plotted in Fig. 2.7, left, found as

$$P(N_{\rm ch}) = \frac{P_{\rm full}(N_{\rm ch})}{1 - P_{\rm full}(0)}, \tag{2.8.1}$$

where $N_{\rm ch}$ denotes the charged particle multiplicity and $P_{\rm full}$ is the $N_{\rm ch}$ distribution that includes events without registered particles ($N_{\rm ch} = 0$).

One can see a fairly good agreement between the model result with string fusion and the measured η-spectrum (Fig. 2.7, right, red line and black dots), however, the model slightly deviates in describing the details of the experimental multiplicity distribution (Fig. 2.7, left). One of the possible sources of this discrepancy is the use of parameters for the distribution in the number of pomerons, Eq. (2.1.2), taken from Ref. [108]. What may play a role is the fact that the authors consider a fusion of strings infinite in rapidity and scattered in the transverse plane according to the Gaussian distribution. In this thesis, we additionally take into account the attractive dynamics of strings that significantly modifies the probabilities of string fusion. Moreover, in this work, we consider strings finite in rapidity, thus, our picture of string fusion is different from the one assumed in Ref. [108]. This circumstance shows possibility for further improvement of the fit quality by defining the new set of Regge parameters (see the list after Eq. (2.1.2)).

For comparison, in both Fig. 2.7 left and right, the results for free strings are calculated with the parameters obtained earlier from the data fit by the model in the regime with string fusion. One can see from the multiplicity distribution (Fig. 2.7, left) and pseudorapidity spectrum (Fig. 2.7, right) that the inclusion of the string fusion effect results in the decrease of the average multiplicity.

One should keep in mind that, in the case of the ALICE η-spectrum description (Fig. 2.7, right), the model can be easily re-tuned so that the no-interaction sce-

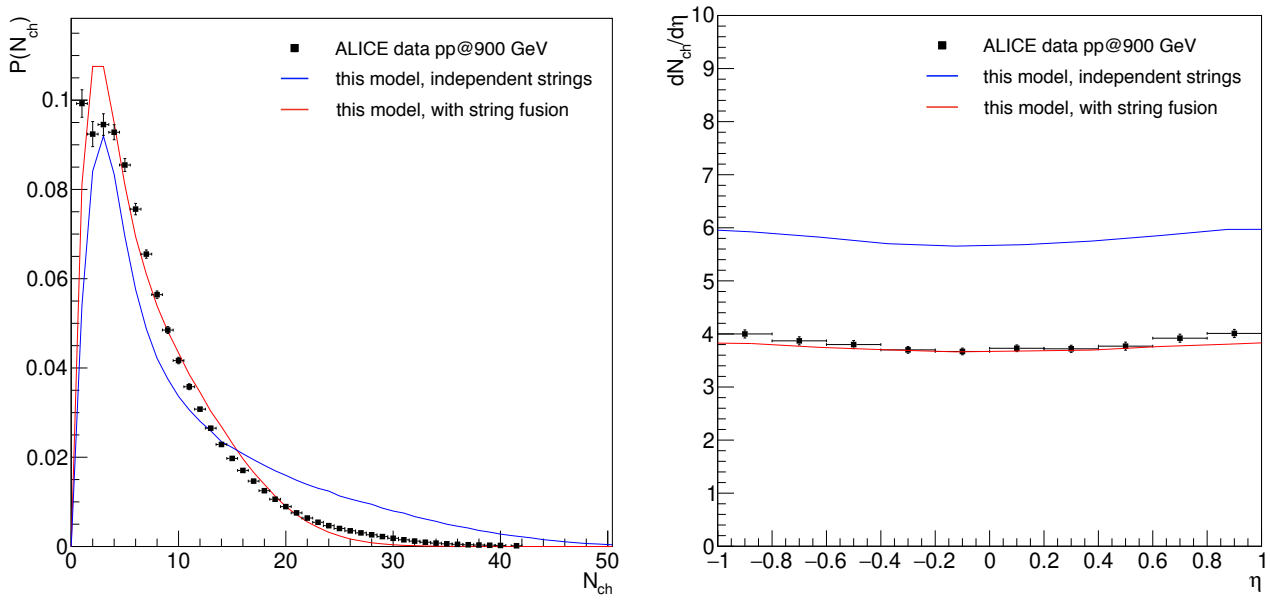

Figure 2.7: Comparison of model results for independent (free) particle-producing sources (blue lines) and for interacting strings (red lines) with the ALICE data [128] (black squares) for inelastic $p+p$ interactions at $\sqrt{s} = 900$ GeV. **Left**: charged particle multiplicity distribution, $P(N_{\rm ch})$, Eq. (2.8.1), defined in the pseudorapidity acceptance $|\eta| < 1$ for the full p_T range of particles; **Right**: η-distribution for the full p_T range.

nario would describe the data. However, already the comparison of the multiplicity distribution (Fig. 2.7, left) shows that the very shape of $P(N_{\rm ch})$ is different for the model without string fusion (although, we repeat, the mean value can be fixed). The importance of taking string fusion into account is even more evident not at the level of global observables, but at the level of correlations, as described in the following subsections.

2.8.3 $\langle p_T \rangle$–N correlation function

We study $\langle p_T \rangle$–N correlations in ALICE acceptance [129] of $|\eta| < 0.8$, $0.15 < p_T < 4$ GeV. Again the model results with interacting particle-producing sources, evolving till $\tau_{\rm deepest}$, were tuned to describe ALICE data [129]. Mean transverse momentum of particles produced by a free string, p_0, is selected as $p_0 = 0.38$ GeV to describe $\langle p_T \rangle = 0.489 \pm 0.001$ GeV measured by ALICE [129] at low $N_{\rm ch}$ (see Fig. 2.8). Results obtained with other model options (but with substitution of parameters determined from the approximation of the data in the model regime with string fusion and $\tau_{\rm deepest}$) are also presented for comparison. Model findings are compared to the PYTHIA event generator predictions.

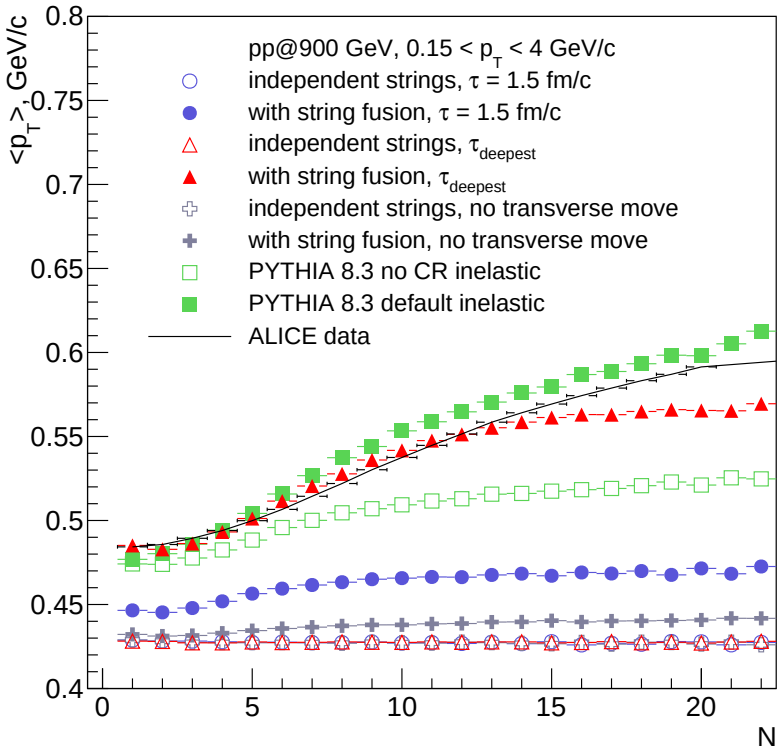

Figure 2.8: $\langle p_T \rangle$–N correlation function calculated in $|\eta| < 0.8$ pseudorapidity acceptance with $0.15 < p_T < 4$ GeV for inelastic $p + p$ interactions at $\sqrt{s} = 900$ GeV. Model results for string system evolving till τ_{deepest}, represented by full red triangles, are tuned to follow ALICE data [129] (the black line: data points are connected to guide the eye). See text for details.

From Fig. 2.8 one can see that the model results for independent (free) strings (empty markers, except the squares) almost coincide for different regimes of transverse strings' dynamics: empty crosses - no transverse dynamics; empty triangles - transverse dynamics until the unified time $\tau = 1.5$ fm; empty circles - transverse dynamics until τ_{deepest} defined for each event. Moreover, in this model regime (free strings) there is no mechanism that provides the increase of $\langle p_T \rangle$ with N, which is clearly demonstrated by the mentioned empty markers in Fig. 2.8.

As regards the interacting particle-producing sources, one can see more significant $\langle p_T \rangle$–N correlations in Fig. 2.8 for the cases with the larger strings' density reached in the event. One could also see that the colour reconnection (CR) mechanism in PYTHIA (full green squares) plays formally a similar role as our string fusion mechanism, increasing the $\langle p_T \rangle - N$ correlation. However, PYTHIA without CR included (empty green squares) still has some background correlations (as for $\Delta[P_T, N]$ and $\Sigma[P_T, N]$, see section 2.7.2).

The important understanding, coming from the current section, is that the ex-

perimentally observed behaviour (Fig. 2.8, black line) that clearly demonstrates remarkable $\langle p_T \rangle - N$ correlation, can be described in the developed model only by taking into account the fusion of strings into clusters. Moreover, only the simulation with string fusion and their transverse evolution till $\tau_{\rm deepest}$, i.e. till the maximum string density in an event is reached, gives the desired slope of the correlation function $\langle p_T \rangle - N$. In other modes of the model with string fusion, it is possible to choose the value of the model parameter p_0 to adjust $\langle p_T \rangle$ at low $N_{\rm ch}$, but the slope of $\langle p_T \rangle - N$ is not steep enough.

In brief, even though one may try to tune global observables without taking into account the collective effects of some sort, it is not possible to explain the growth of $\langle p_T \rangle$ with N. Thus, in the following we focus on the consideration of the developed model with the evolution of the string density up to time $\tau_{\rm deepest}$, which corresponds to the maximum possible string overlaps, and their subsequent fusion, while other options obtained with the parameters for the mode of interest will be shown just for comparison.

2.8.4 Multiplicity correlations

In this section, the multiplicity correlations in pseudorapidity in terms of the correlation coefficient $b_{\rm corr}[N_F, N_B]$, Eq. (0.0.6), are presented. We again study this quantity since we hope that in the more complex model we will be able to access the information about particle sources and their distribution. The obtained result slightly differs from the ones presented in Chapter 1 (toy-model, Fig. 1.2) and the ones shown in the previous section (this model, $p + p$ at $\sqrt{s} = 200$ GeV, no tuning on data, Fig. 2.5), therefore, we will spend some time presenting it.

Fig. 2.9 shows our model calculations of $b_{\rm corr}[N_F, N_B]$ as a function of the distance $\Delta\eta$ between forward and backward pseudorapidity acceptances of width $\delta\eta = 0.2$.

We stress that in a model with boost invariance in rapidity, i.e. when the string longitudinal dynamics is ignored and infinite strings are considered, the fluctuations in the number of strings would provide the constant input to the long-range correlations at all positions of forward and backward rapidity windows. However, this is not the case in our model, as with the loss of translational invariance, one obtains different "volume" fluctuations (fluctuating number of strings acting as particle-emitting

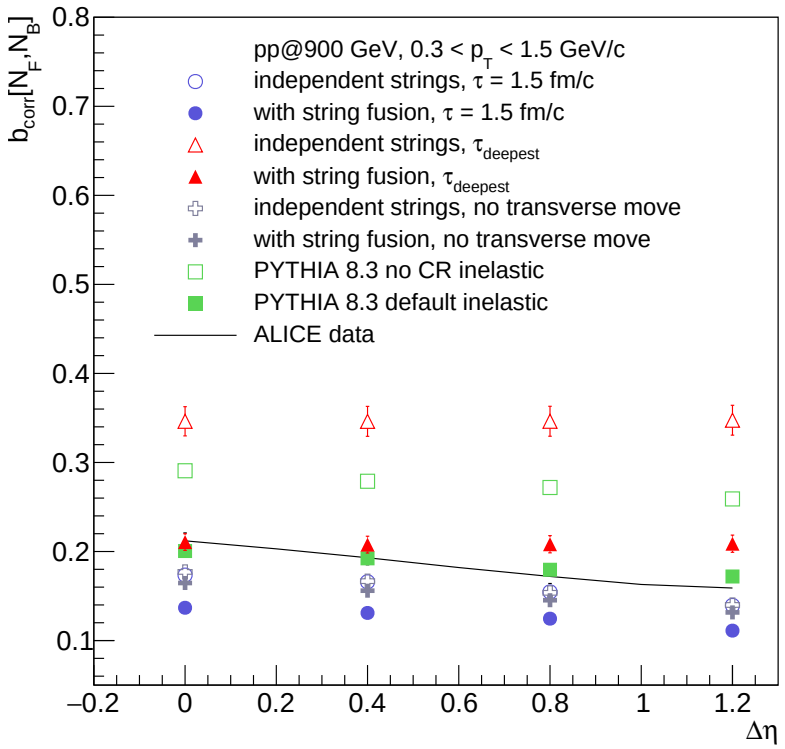

Figure 2.9: Model results for $b_{\rm corr}[N_F, N_B]$, Eq. (0.0.6), as a function of the distance, $\Delta\eta$, between forward and backward pseudorapidity acceptance intervals, where the forward, N_F, and backward, N_B, multiplicities, are calculated for inelastic $p+p$ interactions at $\sqrt{s} = 900$ GeV (see text for details). Particles are selected with 0.3 GeV $< p_T <$ 1.5 GeV. The black line is drawn to guide the eye trough the ALICE data [129].

sources) at different $\Delta\eta$.

Remarkably, the values of $b_{\rm corr}[N_F, N_B]$ split and Fig. 2.9 shows two groups of results. The first group is a set of plots for $b_{\rm corr}[N_F, N_B]$ that exhibit almost no dependence on $\Delta\eta$ both with (full red triangles) and without (empty red triangles) string fusion for system of strings evolving till $\tau_{\rm deepest}$. It happens this way because $\tau_{\rm deepest}$ is appeared to be not large: for the used model parameters, the average $\tau_{\rm deepest}$ at $\sqrt{s} = 900$ GeV is about 0.73 fm. Therefore, the colour strings stay long enough to produce particles into both forward and backward η-windows. This is why one sees a strong correlation which does not weaken with $\Delta\eta$ (empty and full red triangles). The values of $b_{\rm corr}[N_F, N_B]$ differ for model regimes: the results for $\tau_{\rm deepest}$ with string fusion (red triangles) are the closest to the experimental values (black line), since this model mode was used to fix the parameters based on data (see two previous subsections).

The second group of plots represents $b_{\rm corr}[N_F, N_B]$ decreasing with $\Delta\eta$, which

resembles the results in Chapter 1 (toy-model, Fig. 1.2) and the ones shown in the previous section (this model, $p+p$ at $\sqrt{s} = 200$ GeV, no tuning on data, Fig. 2.5). The values of $b_{\rm corr}[N_F, N_B]$ fall down with the increase of $\Delta\eta$ since the colour strings are significantly shrunk by the value of $y_{\rm loss}^{\rm part}$, Eq. (2.4.3), with $\tau = 1.5$ fm evolution time. Therefore, the number of strings that produce particles in both forward and backward pseudorapidity windows strongly decreases with the separation of these windows, which leads to the weakening of the correlation. As a cross-check, one can notice that the results for $\tau = 1.5$ fm and for the case without transverse string dynamics almost coincide for independent strings (open circles and crosses). This is because, in these both cases, we used $\tau = 1.5$ fm for the longitudinal dynamics.

In general, the results for interacting strings lie below the corresponding plots for independent strings because of the lower multiplicity caused by string fusion in the former case. The same prediction on the suppression of $b_{\rm corr}[N_F, N_B]$ values was obtained earlier for strings that are infinite in rapidity [56].

In Fig. 2.9, the reduction of $b_{\rm corr}[N_F, N_B]$ for the model with string fusion (full triangles or full circles) compared to the results in the model with free strings (empty triangles or empty circles, respectively) has the same magnitude at all considered $\Delta\eta$. This means that string fusion occurs with approximately the same frequency at these $\Delta\eta$. It is not the case for $b_{\rm corr}[N_F, N_B]$ presented in Chapter 1 (toy-model, Fig. 1.2) and for the one shown in the previous section (this model, $p+p$ at $\sqrt{s} = 200$ GeV, no tuning on data, Fig. 2.5). The new result seems to be more reliable since this model is more developed than the toy-model from Chapter 1. Moreover, the selection of its parameters is data-driven, contrary to the results for $\sqrt{s} = 200$ GeV. Moreover, a comparable behaviour is observed for PYTHIA simulations: colour reconnection gives an effect similar to that for the string fusion mechanism - an overall decrease of multiplicity and that of $b_{\rm corr}[N_F, N_B]$, constant with $\Delta\eta$. Note, that PYTHIA with colour reconnection (full green squares) almost perfectly follows the experimental $b_{\rm corr}[N_F, N_B]$ (black line).

Concerning the comparison of ALICE data [99] and model results (Fig. 2.5): the simultaneous fit to the experimental $dN_{\rm ch}/d\eta$ and $P(N_{\rm ch})$ distributions allows us to reproduce the experimental value of $b_{\rm corr}[N_F, N_B]$ only at midrapidity ($\Delta\eta = 0$, interacting strings evolving till $\tau_{\rm deepest}$, full red triangles). However, for the moment, the model does not follow the steady decrease of the $b_{\rm corr}[N_F, N_B]$ values in data

(the full red triangles versus the black line).

Thus, since we have chosen (and tuned) the model with the fusion of strings that have evolved until $\tau_{\rm deepest}$, from comparing the results for $b_{\rm corr}[N_F, N_B]$ with ALICE data [99], we can say:

1. The resulting background of multiplicity correlations, arising from fluctuations in the number of strings producing particles in forward and backward pseudorapidity windows, cannot describe the experimental data that contains the contribution of short-range correlations. However, it provides a non-trivial "reference" level that varies depending on the evolution time τ of the string density.

2. There are no short-range correlations introduced to the model (no correlations between the produced particles from a string). We assume that taking them into account, for example, in analogy with Ref. [95], together with the long-range ones (this model) can give the correct behaviour of $b_{\rm corr}[N_F, N_B]$.

To conclude here, we note that the evolution time and the relevant string density are found playing the major role in defining how large the correlation coefficient is and how it behaves with the distance, $\Delta\eta$, separating forward and backward pseudorapidity acceptance intervals.

2.8.5 Multiplicity fluctuations with strongly intensive observable

To avoid the dependence of the results on the system "volume" (number of strings and string clusters), it is reasonable to study joint multiplicity fluctuations in forward and backward pseudorapidity intervals in terms of the aforementioned fluctuation measure, $\Sigma[N_F, N_B]$, [80], Eq. (0.0.7).

Let us remind the reader that the strongly intensive quantities [79] by construction do not depend nor on the system volume, nor on its event-by-event fluctuations in the simple models. They are normalised to be equal to zero in the absence of fluctuations and to be equal to unity in the case of the models with independent particle production [97].

Fig. 2.10 demonstrates an increase from the unity of $\Sigma[N_F, N_B]$ values with the distance between forward and backward η-acceptances. One can argue that

the results for free and interacting strings split, which makes $\Sigma[N_F, N_B]$ dependent on the types of particle-producing sources. This result is in agreement with the conclusions made in Ref. [96]: string fusion makes $\Sigma[N_F, N_B]$ being equal to the weighted average of Σ values for strings of different types, thus, depending on the characteristics of particle-producing sources.

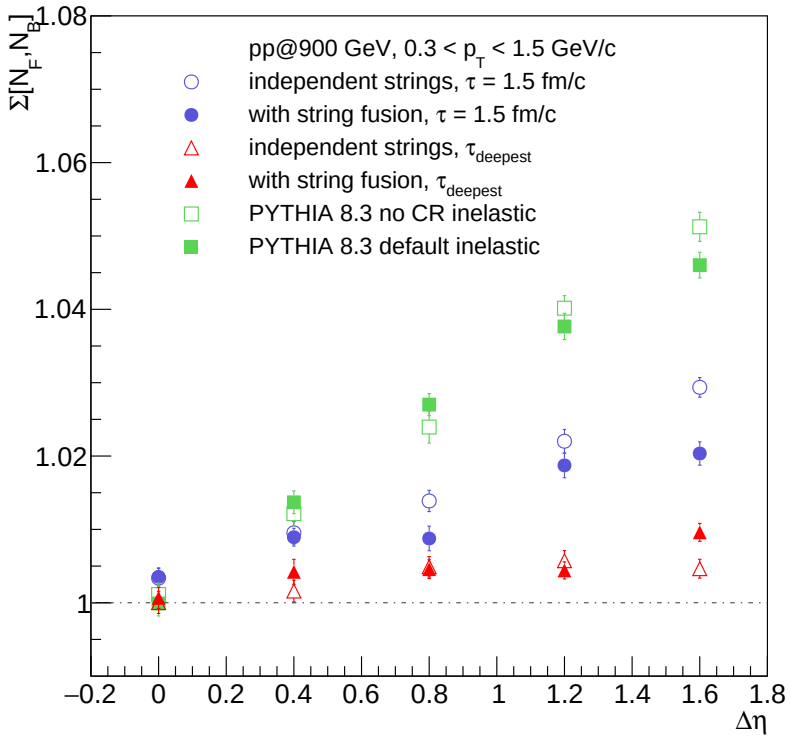

Figure 2.10: Model results for $\Sigma[N_F, N_B]$, Eq. (0.0.7), as a function of the distance, $\Delta\eta$, between forward and backward pseudorapidity acceptance intervals, where N_F and N_B multiplicities are calculated for inelastic $p + p$ interactions at $\sqrt{s} = 900$ GeV (see text for details). Particles are selected with: 0.3 GeV $< p_T <$ 1.5 GeV.

The values of $\Sigma[N_F, N_B]$ for $\tau = 1.5$ fm (blue circles) at the largest $\Delta\eta$ are smaller for the case of the formation of string clusters (full blue circles) than for free strings (empty blue circles). This difference resembles also the splitting for the PYTHIA plots with (full green squares) and without (empty green squares) colour reconnection. Model results for τ_{deepest} lie even lower (red triangles), although it is complicated to distinguish the two model regimes here.

The $\Delta\eta$ behaviour of $\Sigma[N_F, N_B]$ (Fig. 2.10) is similar to the one obtained in the presented simplified calculation (see Chapter 1) and for this model without the fixation of parameters (at $\sqrt{s} = 200$ GeV, see section 2.7.2). However, in Fig. 2.10, there is no rapid decline of $\Sigma[N_F, N_B]$ to the level of unity at large $\Delta\eta$ since this study is performed in ALICE acceptance and such large $\Delta\eta$ as in Fig. 1.3, are not

available for analysis. A considerable difference with the PYTHIA predictions can be explained by the absence of short-range effects in our model that was currently aimed at the study of long-range correlation effects.

One has to mention that the same qualitative behaviour of $\Sigma[N_F, N_B]$ with $\Delta\eta$ was obtained in Ref. [95], where the authors considered only strings infinite in rapidity, but included the effects of short-range correlations. Thus, one may argue that both the absence of short-range correlations and the presence of "short" strings in our model give the same results for $\Sigma[N_F, N_B]$, which indicates the importance of the coherent application of the two approaches.

Thus, the intermediate conclusion for $\Sigma[N_F, N_B]$ behaviour broadly repeats the one made in Chapter 1, however, it is now based on the results in the advanced model [103] that has been tuned to the experimental data. This correspondence confirms the correctness of the model and makes the conclusions drawn more significant.

2.8.6 Forward multiplicity studies

In the analysis of the experimental data, along with the choice of some stable variables, such as $\Sigma[N_F, N_B]$, another possibility to control an event's initial conditions is to select for analysis some sort of similar events. This is crucial in the study of fluctuations since the influence of trivial fluctuations may spoil the studied signal and, thus, should be eliminated.

In the context of the present study, it is necessary to make an important remark. We follow the picture of multi-pomeron exchange, with each cut pomeron resulting in the formation of two colour strings. In this model, the events differ by the number of created colour strings that form the event-by-event fluctuating effective "volume" of the system that produces particles. In this sense, one can group the $p + p$ events in some classes with more or less similar number of strings created, which can be related with the centrality determination in $A + A$ collisions. In this study [103], we repeat the procedure used in the ALICE experiment to define multiplicity-based classes of events in proton–proton collisions following Ref. [101].

Knowing pseudorapidity value, η, for each particle, we plot the multiplicity of particles that would fly into the V0-detector of ALICE [131], whose acceptance covers $2.8 < \eta < 5.1$ and $-3.7 < \eta < -1.7$ regions. This is to avoid auto-correlations

with the TPC (Time-Projection Chamber) data. We divide the distribution into five classes, each of which containing 20% of the events. For the analysis, the 0–20%, 20–40%, and 40–60% classes are taken and the strongly intensive quantity $\Sigma[N_F, N_B]$, Eq. (0.0.7), is calculated for events from each class.

It is important to mention that the acceptance of the ALICE V0-detector covers the region where quasi-diffractive processes play a role. Furthermore, in this region, it is crucial to properly model the string fragmentation close to the string endpoints, e.g. to take into account the possibility to have a diquark as an endpoint, which can produce additional baryon yields, etc. Finally, these detectors have non-ideal resolution, and hence, this factor has to be included in the simulations as well. All these effects are not taken into account in this version of the model. Because of this, we do not perform any direct comparison with the available experimental data [101] obtained in very narrow multiplicity-based event classes. Instead, we study whether $\Sigma[N_F, N_B]$ depends on an event "type" and whether the property of strong intensity is violated for $\Sigma[N_F, N_B]$ under the assumption of string fusion.

In Fig. 2.11, one can see that, for all multiplicity-based event classes, $\Sigma[N_F, N_B]$, Eq. (0.0.7), exhibits the same behaviour: an increase with $\Delta\eta$. The main result is that in the model, for more "central" events, the obtained value of $\Sigma[N_F, N_B]$ is systematically larger than the one for more "peripheral" events, although with the limited statistical accuracy this deviation does not exceed $1-2$ standard deviations. The same behaviour was observed by ALICE in $p+p$ data [101].

This is another manifestation of the string fusion effect because, for more "central" events, i.e. events with the higher forward multiplicity, one has a larger number of strings. This means that one has a higher probability of strings interaction and that one could possibly produce string clusters of higher string tension. A similar analysis with the same conclusion was performed recently in Ref. [95] for interacting strings that are infinite in rapidity. Again, let us emphasise the importance of taking into account both the short-range correlations that were modelled in Ref. [95] and the initial conditions that are considered in this model, e.g. strings of short length in rapidity and/or their shifts with respect to midrapidity, as these two effects give similar results and cannot be easily disentangled by analysing $\Sigma[N_F, N_B]$ only.

At first sight, this result is the exact opposite of the one obtained in the toy-model (see Chapter 1). In Fig. 1.3, the values of $\Sigma[N_F, N_B]$ exhibit a strong decrease with

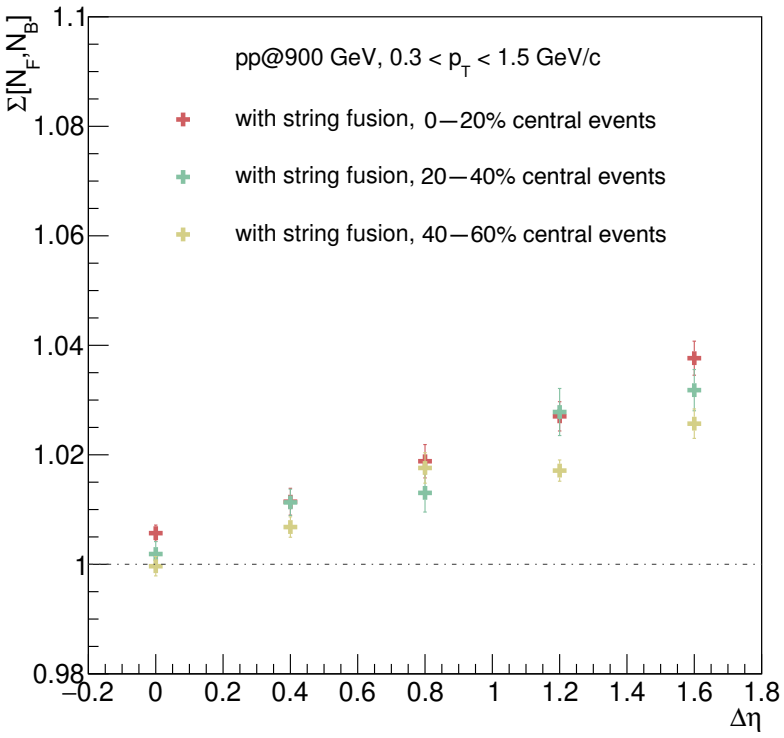

Figure 2.11: Model "centrality" dependence of $\Sigma[N_F, N_B]$, Eq. (0.0.7), for 0–20%, 20–40%, and 40–60% multiplicity-based event classes as a function of the distance $\Delta\eta$ between forward and backward pseudorapidity acceptance intervals, where N_F and N_B multiplicities are calculated for inelastic $p + p$ interactions at $\sqrt{s} = 900$ GeV in the model configuration for interacting strings without transverse dynamics. Particles are selected with 0.3 GeV $< p_T <$ 1.5 GeV.

the density of strings for model regime with string fusion. The string density can be indirectly compared with the "centrality" of events: this measure corresponds to the number of pomerons formed and, in our model, can be related with the number of parton interactions. In turn, in the current section, the "centrality" of $p + p$ collisions is determined in the same way as in the experimental analysis: by percentiles of the multiplicity distribution in the acceptance of the ALICE V0 detector. Thus, the two proxies of the geometrical centrality definition may well give two different results. Another remark is that, to obtain the results presented in Fig. 1.3, we used significantly different average values for the number of strings in an event ($\langle n_{\rm str}\rangle = 8$, 30, 50). In turn, the analysis, presented in this Chapter, is carried in the broad centrality classes of 20% due to the low available statistics as the simulation procedure is too CPU-demanding at the moment. Thus, the effect in Fig. 2.11 of $\Sigma[N_F, N_B]$ dependence on string density, i.e. "centrality" of events, is not so striking and, to some extent, it is even difficult to judge its direction. But the main conclusion is still valid: string fusion decreases the values of $\Sigma[N_F, N_B]$ in

the way similar to the simplified calculation in Chapter 1.

2.8.7 Connection of $\Sigma[N_F, N_B]$ with cumulants and factorial cumulants

To illustrate the beauty of the mathematics standing behind the observable $\Sigma[N_F, N_B]$, Eq. (0.0.7), let us briefly discuss its connection with the other often used objects, namely the cumulants and factorial cumulants.

Following the notations from [132] we note that the moments $\mu_{\nu_1,...,\nu_N}$ of the distribution of random variables $X_1, ..., X_N$ can be found from $M(\xi_1, ..., \xi_N)$ - the moment generating function,

$$M(\xi_1, ..., \xi_N) \equiv \left\langle e^{\sum_{i=1}^{N} \xi_i X_i} \right\rangle, \tag{2.8.2}$$

by taking the corresponding derivatives

$$\mu_{\nu_1,...,\nu_N} = \frac{\partial^{\nu_1}}{\partial \xi_1^{\nu_1}} ... \frac{\partial^{\nu_N}}{\partial \xi_N^{\nu_N}} M(\xi_1, ..., \xi_N) \Big|_{\xi_1=...=\xi_N=0}. \tag{2.8.3}$$

Then the cumulants $\kappa_{\nu_1,...,\nu_N}$ of the distribution of random variables $X_1, ..., X_N$ can be found from the cumulant generating function, i.e. the logarithm of the moment generating function,

$$K(\xi_1, ..., \xi_N) \equiv \ln M(\xi_1, ..., \xi_N) = \ln \left\langle e^{\sum_{i=1}^{N} \xi_i X_i} \right\rangle, \tag{2.8.4}$$

also by taking the corresponding derivatives

$$\kappa_{\nu_1,...,\nu_N} = \frac{\partial^{\nu_1}}{\partial \xi_1^{\nu_1}} ... \frac{\partial^{\nu_N}}{\partial \xi_N^{\nu_N}} K(\xi_1 ... \xi_N) \Big|_{\xi_1=...=\xi_N=0}. \tag{2.8.5}$$

In other words, the cumulants $\kappa_{\nu_1,...,\nu_N}$ are the coefficients of the Taylor series expansion around zero of the cumulant generating function:

$$K(\xi_1, ..., \xi_N) = {\sum}'_{\nu_1,...,\nu_N} \left(\prod_j \frac{\xi_j^{\nu_j}}{\nu_j!} \right) \kappa_{\nu_1,...,\nu_N}, \tag{2.8.6}$$

where $\sum'$ does not contain the term with $\nu_1 = ... = \nu_N = 0$.

The meaning of the definition of cumulants can be presented as follows [133]: any k-particle distribution,

$$\frac{dN}{d\mathbf{p}_1 ... d\mathbf{p}_k} \equiv f(\mathbf{p}_1, ..., \mathbf{p}_k), \tag{2.8.7}$$

can be divided into the sum of its correlated, f_c, and uncorrelated, f, contributions. For $k = 2$, it becomes

$$f(\mathbf{p}_1, \mathbf{p}_2) = f(\mathbf{p}_1)f(\mathbf{p}_2) + f_c(\mathbf{p}_1, \mathbf{p}_2), \tag{2.8.8}$$

where the second term represents the genuine contribution of two-particle correlations to the measured two-particle distribution. For $k = 3$, the expression becomes more complex, since in addition to the genuine three-particle correlation, one has to take into account all combinations of two-particle correlations:

$$\begin{aligned} f(\mathbf{p}_1, \mathbf{p}_2, \mathbf{p}_3) = {} & f(\mathbf{p}_1)f(\mathbf{p}_2)f(\mathbf{p}_3) \\ & + f_c(\mathbf{p}_1, \mathbf{p}_2)f(\mathbf{p}_3) + f(\mathbf{p}_1)f_c(\mathbf{p}_2, \mathbf{p}_3) + f(\mathbf{p}_2)f_c(\mathbf{p}_1, \mathbf{p}_3) \\ & + f_c(\mathbf{p}_1, \mathbf{p}_2, \mathbf{p}_3). \end{aligned} \tag{2.8.9}$$

In this case, $f_c(\mathbf{p}_1, \mathbf{p}_2, \mathbf{p}_3)$ is a three-particle cumulant,

$$\begin{aligned} f_c(\mathbf{p}_1, \mathbf{p}_2, \mathbf{p}_3) = {} & f(\mathbf{p}_1, \mathbf{p}_2, \mathbf{p}_3) - f(\mathbf{p}_1)f(\mathbf{p}_2)f(\mathbf{p}_3) \\ & - f_c(\mathbf{p}_1, \mathbf{p}_2)f(\mathbf{p}_3) + f(\mathbf{p}_1)f_c(\mathbf{p}_2, \mathbf{p}_3) + f(\mathbf{p}_2)f_c(\mathbf{p}_1, \mathbf{p}_3), \end{aligned} \tag{2.8.10}$$

and this procedure can be generalised for cumulants of higher orders. Thus, the k-particle cumulant is obtained from the k-particle distribution after subtracting l-particle correlations of lower orders ($l < k$).

Here, for completeness, we provide the relations [132] between the first few cumulants, Eq. (2.8.5), and the moments, Eq. (2.8.3):

$$\kappa_1 = \mu_1, \tag{2.8.11}$$

$$\kappa_2 = \mu_2 - \mu_1^2, \tag{2.8.12}$$

$$\kappa_{1,1} = \mu_{1,1} - \mu_{0,1}\mu_{1,0}, \tag{2.8.13}$$

$$\kappa_{2,1} = 2\mu_{0,1}\mu_{1,0}^2 - 2\mu_{1,1}\mu_{1,0} - \mu_{0,1}\mu_{2,0} + \mu_{2,1}, \tag{2.8.14}$$

$$\kappa_{1,2} = 2\mu_{1,0}\mu_{0,1}^2 - 2\mu_{1,1}\mu_{0,1} - \mu_{0,2}\mu_{1,0} + \mu_{1,2}, \tag{2.8.15}$$

$$\begin{aligned} \kappa_{1,1,1} = {} & 2\mu_{0,0,1}\mu_{0,1,0}\mu_{1,0,0} - \mu_{0,1,1}\mu_{1,0,0} \\ & - \mu_{0,1,0}\mu_{1,0,1} - \mu_{0,0,1}\mu_{1,1,0} + \mu_{1,1,1}. \end{aligned} \tag{2.8.16}$$

Another characteristic of the distribution is the factorial moments, $\mu^f_{\nu_1,\ldots,\nu_N}$, that can be found from $F(\xi_1, ..., \xi_N)$ - the factorial moment generating function,

$$F(\xi_1, ..., \xi_N) \equiv \left\langle \prod_{i=1}^{N} (1 + \xi_i)^{X_i} \right\rangle, \tag{2.8.17}$$

by taking the corresponding derivatives

$$\mu^f_{\nu_1,...,\nu_N} = \frac{\partial^{\nu_1}}{\partial\xi_1^{\nu_1}}...\frac{\partial^{\nu_N}}{\partial\xi_N^{\nu_N}}F(\xi_1,...,\xi_N)\Big|_{\xi_1=...=\xi_N=0}. \tag{2.8.18}$$

Then the factorial cumulants, $\kappa^f_{\nu_1,...,\nu_N}$, can be found from the factorial cumulant generating function, i.e. the logarithm of the factorial moment generating function,

$$K^f(\xi_1,...,\xi_N) \equiv \ln F(\xi_1,...,\xi_N) = \ln\left\langle\prod_{i=1}^{N}(1+\xi_i)^{X_i}\right\rangle, \tag{2.8.19}$$

also by taking the corresponding derivatives

$$\kappa^f_{\nu_1,...,\nu_N} = \frac{\partial^{\nu_1}}{\partial\xi_1^{\nu_1}}...\frac{\partial^{\nu_N}}{\partial\xi_N^{\nu_N}}K^f(\xi_1,...,\xi_N)\Big|_{\xi_1=...=\xi_N=0}. \tag{2.8.20}$$

Let us provide the relations between several first cumulants and factorial cumulants:

$$\kappa_1 = \kappa_1^f, \tag{2.8.21}$$
$$\kappa_2 = \kappa_1^f + \kappa_2^f, \tag{2.8.22}$$
$$\kappa_3 = \kappa_1^f + 3\kappa_2^f + \kappa_3^f, \tag{2.8.23}$$
$$\kappa_4 = \kappa_1^f + 7\kappa_2^f + 6\kappa_3^f + \kappa_4^f, \tag{2.8.24}$$
$$\kappa_5 = \kappa_1^f + 15\kappa_2^f + 25\kappa_3^f + 10\kappa_4^f + \kappa_5^f, \tag{2.8.25}$$
$$\kappa_6 = \kappa_1^f + 31\kappa_2^f + 90\kappa_3^f + 65\kappa_4^f + 15\kappa_5^f + \kappa_6^f. \tag{2.8.26}$$

These formulas show that the n-order cumulant is determined by factorial cumulants of $n' \leq n$ orders. It also follows that if the factorial cumulant of n order is zero (i.e. there are no n-particle correlations in the model), then there is no point in studying cumulants of higher order than n, since they will not carry any additional information compared to the cumulants of lower orders [134].

Now we consider the joint distribution $P(N_F, N_B)$ of probabilities of multiplicities of charged particles, N_F and N_B, in pseudorapidity windows in the forward and backward hemispheres. One can introduce cumulants and factorial cumulants for any linear combination of N_F and N_B. Following the notations from Ref. [135], let us define a selected linear combination as a q-vector

$$q_{(x)} = x_1 \cdot N_F + x_2 \cdot N_B. \tag{2.8.27}$$

Let us consider these two specific q-vectors

$$q_{(a)} = N_F + N_B, \tag{2.8.28}$$

$$q_{(b)} = N_F - N_B, \tag{2.8.29}$$

where $a = (1, 1)$ and $b = (1, -1)$. The auxiliary q-vectors that one needs in order to calculate cumulants and factorial cumulants are

$$q_{(a^2)} = q_{(a)}, \tag{2.8.30}$$

$$q_{(b^2)} = q_{(a)}, \tag{2.8.31}$$

$$q_{(ab)} = q_{(b)}. \tag{2.8.32}$$

Then, following Ref. [135], one can immediately express the first-order and second-order cumulants for the joint probability distribution, $P\left(N_F, N_B\right)$, in terms of the moments of the same distribution:

$$\langle q_{(a)} \rangle_{\mathrm{c}} = \langle N_F \rangle + \langle N_B \rangle, \tag{2.8.33}$$

$$\langle q_{(b)} \rangle_{\mathrm{c}} = \langle N_F \rangle - \langle N_B \rangle, \tag{2.8.34}$$

$$\langle q_{(a)}^2 \rangle_{\mathrm{c}} = \langle N_F^2 \rangle - \langle N_F \rangle^2 + \langle N_B^2 \rangle - \langle N_B \rangle^2 + 2 \cdot \mathrm{cov}(N_F, N_B), \tag{2.8.35}$$

$$\langle q_{(b)}^2 \rangle_{\mathrm{c}} = \langle N_F^2 \rangle - \langle N_F \rangle^2 + \langle N_B^2 \rangle - \langle N_B \rangle^2 - 2 \cdot \mathrm{cov}(N_F, N_B), \tag{2.8.36}$$

$$\langle q_{(a)} \cdot q_{(b)} \rangle_{\mathrm{c}} = \langle N_F^2 \rangle - \langle N_F \rangle^2 - \langle N_B^2 \rangle + \langle N_B \rangle^2, \tag{2.8.37}$$

where $\mathrm{cov}(N_F, N_B) = \langle N_F N_B \rangle - \langle N_F \rangle \langle N_B \rangle$. In turn, the factorial cumulants can be straightforwardly expressed in terms of the cumulants:

$$\langle q_{(a)} \rangle_{\mathrm{fc}} = \langle q_{(a)} \rangle_{\mathrm{c}}\,, \tag{2.8.38}$$

$$\langle q_{(b)} \rangle_{\mathrm{fc}} = \langle q_{(b)} \rangle_{\mathrm{c}}\,, \tag{2.8.39}$$

$$\langle q_{(a)}^2 \rangle_{\mathrm{fc}} = \langle q_{(a)}^2 \rangle_{\mathrm{c}} - \langle q_{(a^2)} \rangle_{\mathrm{c}} = \langle q_{(a)}^2 \rangle_{\mathrm{c}} - \langle q_{(a)} \rangle_{\mathrm{c}}\,, \tag{2.8.40}$$

$$\langle q_{(b)}^2 \rangle_{\mathrm{fc}} = \langle q_{(b)}^2 \rangle_{\mathrm{c}} - \langle q_{(b^2)} \rangle_{\mathrm{c}} = \langle q_{(b)}^2 \rangle_{\mathrm{c}} - \langle q_{(a)} \rangle_{\mathrm{c}}\,, \tag{2.8.41}$$

$$\langle q_{(a)} \cdot q_{(b)} \rangle_{\mathrm{fc}} = \langle q_{(a)} \cdot q_{(b)} \rangle_{\mathrm{c}} - \langle q_{(ab)} \rangle_{\mathrm{c}} = \langle q_{(a)} \cdot q_{(b)} \rangle_{\mathrm{c}} - \langle q_{(b)} \rangle_{\mathrm{c}}\,. \tag{2.8.42}$$

One could immediately notice the connection of the presented cumulants and factorial cumulants with the strongly intensive quantity in the case of symmetrical pseudorapidity intervals, i.e. when $\langle N_F \rangle = \langle N_B \rangle$:

$$\Sigma[N_F, N_B] = \frac{\langle q_{(b)}^2 \rangle_{\mathrm{c}}}{\langle q_{(a)} \rangle_{\mathrm{c}}} = 1 + \frac{\langle q_{(b)}^2 \rangle_{\mathrm{fc}}}{\langle q_{(a)} \rangle_{\mathrm{fc}}}\,. \tag{2.8.43}$$

This connection is not surprising as soon as the goal of the construction of these special observables (or ratios of observables) is to suppress trivial statistical fluctuations. Therefore, we have derived [103] the connection between $\Sigma[N_F, N_B]$ and (factorial) cumulants, which is another way to see the property of strong intensity of $\Sigma[N_F, N_B]$.

2.8.8 Connection of $\Sigma[N_F, N_B]$ with the asymmetry coefficient

The main difference between the model results shown in Fig. 2.10 for $\tau = 1.5$ fm and τ_{deepest} comes from the geometry of the system of strings in an event (considering the transverse dynamics and longitudinal compression of strings, as well as the formation of string clusters via fusion). Indeed, as it was already mentioned in section 2.8.4, the average τ_{deepest} is less than $\tau = 1.5$ fm. It results in the event-by-event formation of different sets of strings and/or string clusters that asymmetrically produce particles in the forward and backward η-acceptances. Thus, another way to look at event-by-event multiplicity fluctuations is to construct an event observable,

$$C = \frac{N_F - N_B}{\sqrt{N_F + N_B}}, \tag{2.8.44}$$

that measures an event asymmetry in pseudorapidity [136] and to study the variance, σ^2_C, of its distribution over a set of events.

Let us consider the analytical form of σ^2_C:

$$\sigma^2_C = D_C \equiv \text{Var}(C) = \left\langle \frac{(N_F - N_B)^2}{N_F + N_B} \right\rangle - \left\langle \frac{N_F - N_B}{\sqrt{N_F + N_B}} \right\rangle^2, \tag{2.8.45}$$

where, for convenience, we have redefined the notation of the variance D_A of the distribution of some quantity A as $\text{Var}(A)$.

The observable σ^2_C has been extensively studied in different models [137, 138, 139], e.g. in the cluster model of particle production, this observable helped to extract the average cluster size or, in other words, effective cluster multiplicity. Moreover, the extracted value both from $p + p$ and $Au + Au$ reactions was larger than the one predicted for the hadron-resonance gas model, indicating that correlations cannot be explained purely by the hadronic degrees of freedom considered in some statistical ensembles. In most of these studies, the two-stage scenario was adopted in one way or the other: some of the models take into account string interaction,

while others provide a non-trivial and non-uniform in rapidity fragmentation function of particle-emitting sources. However, none of them consider simultaneously longitudinal dynamics and collectivity as we do in our approach [103].

Let us show that σ_C^2 is closely related to the strongly intensive quantity, $\Sigma[N_F, N_B]$. Using the assumptions,

$$\left\langle \frac{(N_F - N_B)^2}{N_F + N_B} \right\rangle = \frac{\left\langle (N_F - N_B)^2 \right\rangle}{\langle N_F + N_B \rangle}, \tag{2.8.46}$$

$$\left\langle \frac{N_F - N_B}{\sqrt{N_F + N_B}} \right\rangle^2 = \frac{\left\langle (N_F - N_B)^2 \right\rangle}{\langle N_F + N_B \rangle}, \tag{2.8.47}$$

for the first and the second term of σ_C^2 in Eq. (2.8.45), respectively, one arrives at

$$\begin{aligned} \sigma_C^2 &= \frac{\mathrm{Var}(N_F - N_B)}{\langle N_F + N_B \rangle} \\ &= \frac{\langle N_F^2 \rangle - 2\langle N_F N_B \rangle + \langle N_B^2 \rangle - \langle N_F \rangle^2 + 2\langle N_F \rangle \langle N_B \rangle - \langle N_B \rangle^2}{\langle N_F + N_B \rangle} \\ &= \frac{\mathrm{Var}(N_F) + \mathrm{Var}(N_B) - 2\mathrm{cov}(N_F, N_B)}{\langle N_F + N_B \rangle} \\ &= \frac{\langle N_F \rangle \omega[N_B] + \langle N_B \rangle \omega[N_F] - 2\mathrm{cov}(N_F, N_B)}{\langle N_F \rangle + \langle N_B \rangle}, \end{aligned} \tag{2.8.48}$$

where the last equality holds under the assumption of $\langle N_F \rangle = \langle N_B \rangle$. Thus,

$$\sigma_C^2 \approx \Sigma[N_F, N_B]. \tag{2.8.49}$$

The assumptions made, Eqs. (2.8.46) and (2.8.47), are in accordance with the approximate calculations of Ref. [139], where deviations of N_F and N_B from $\langle N_F \rangle$ and $\langle N_B \rangle$ are considered to be small enough.

An important remark concerning σ_C^2 needs to be made. Despite the demonstrated connection with $\Sigma[N_F, N_B]$, strictly speaking, σ_C^2 is not a strongly intensive observable and may receive additional contributions coming from the "volume" fluctuations, as the latter are, in general, not cancelled out without the assumptions in Eqs. (2.8.46) and (2.8.47). Nevertheless, σ_C^2 is considered as an important quantity since it shows the magnitude of the fluctuations in terms of event asymmetry in the longitudinal dimension, i.e. σ_C^2 indirectly provides us with some information about the initial state.

Fig. 2.12, left, shows that σ^2_C, calculated from the model distribution of the asymmetry coefficient C, Eq. (2.8.44), indeed exhibits a behaviour similar to $\Sigma[N_F, N_B]$ (see Fig. 2.10). Although both quantities gradually rise with $\Delta\eta$, σ^2_C is not reaching the unity for the close η-acceptances ($\Delta\eta = 0$). As seen, in this region, there are the largest fluctuations of $N_{F,B}$, and respectively, the assumption of small deviations of event-by-event multiplicities from their average values does not hold.

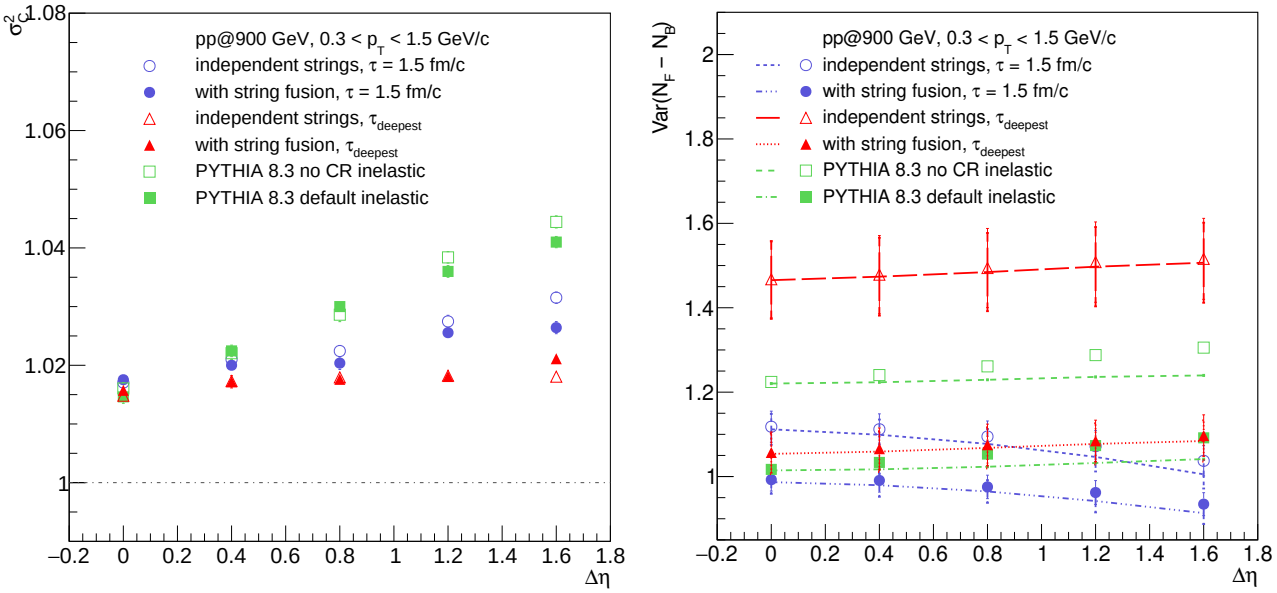

Figure 2.12: Left: σ^2_C of the asymmetry coefficient, C, Eq. (2.8.44), distribution; **Right**: the $\mathrm{Var}(N_F - N_B)$ versus its Skellam baseline, as functions of the distance, $\Delta\eta$, between forward and backward pseudorapidity acceptance intervals, where N_F and N_B multiplicities are calculated event-by-event for inelastic $p + p$ interactions at $\sqrt{s} = 900$ GeV (see text for details). Particles are selected with 0.3 GeV $< p_T <$ 1.5 GeV.

Fig. 2.12, right, explains why the values of σ^2_C are slightly above unity in a more detailed way. The point is that the difference of two quantities, that follow the Poissonian distribution, would follow the Skellam distribution (typically, the Skellam function is considered as a baseline in the studies of net-charge fluctuations). In our case, the numerator of σ^2_C can be treated as a net-hadronic charge in rapidity. Thus, the values of the model results of $\mathrm{Var}(N_F - N_B)$, in Fig. 2.12, right (symbols of different colours), lie slightly above the corresponding Skellam baselines calculated as $\langle N_F \rangle + \langle N_B \rangle$ (dashed lines of the corresponding colours). Therefore, the ratios of those model values over the lines are equal to σ^2_C that is slightly above the unity (Fig. 2.12, left).

Following Ref. [136], we suggest that at $\Delta\eta = 0$ it is the contribution of

strings and/or string clusters, producing particles in both forward and backward η-acceptances, that suppresses the value of $\Sigma[N_F, N_B]$ and σ^2_C. With the increase of $\Delta\eta$, one expects more and more rare impact of such sources. Instead, the "short" quark–gluon strings appear that produce particles only in the forward or in the backward η-intervals.

To summarise the last two subsections, it should be emphasised that the obtained relations demonstrate the strict correspondence of $\Sigma[N_F, N_B]$ and (factorial) cumulants, and the conditional similarity of $\Sigma[N_F, N_B]$ and the asymmetry coefficient of $N_F - N_B$ distribution. This allows one to combine these quantities into a family of measures robust against the trivial multiplicity fluctuations and to choose the most convenient one for study. However, as it is also shown in Eq. (2.7.19), the correlation coefficient $b_{\rm corr}[N_F, N_B]$ provides some additional information on correlated particle production, thus, its study should accompany the use of strongly intensive variables.

2.9 Discussion

This Chapter presents the elaborated model of multi-particle production that is based on the ideas that were for the first time proposed and tested in the toy-model (see Chapter 1). The full chain of an event simulation in the developed more complex model includes:

1. determination of the parton composition of protons with the given number of partons,

2. formation of the number of colour strings in an event that corresponds to the double number of exchanged pomerons,

3. the transverse dynamics of the string system in an event, which is determined by the attractive potential between strings and leads to their clustering,

4. longitudinal dynamics of massive strings' ends that results in the loss of boost invariance in the model,

5. fusion of the fragments of strings whose centres lie in the same transverse cell and that overlap in the rapidity dimension,

6. effective string hadronisation.

In this Monte-Carlo model, we have obtained results on multiplicity and transverse momentum correlations and fluctuations for inelastic $p + p$ interactions at $\sqrt{s} = 200$ GeV [102] and $\sqrt{s} = 900$ GeV [103]. In the current Chapter of the dissertation, long-range correlations are naturally introduced to the model due to the formation of strings finite in rapidity and appear from the fluctuations in the number of strings that produce particles in the pseudorapidity windows in forward and backward hemispheres.

The obtained results are in trend with the conclusions of the toy-model (see Chapter 1), however, they provide more information on particle producing sources and their interactions, thanks to the development of the model and its adjustment to experimental data.

The main conclusions of this Chapter, derived from the comparison of model results with world experimental data and studies in other string-based models, are:

1. The good correspondence between the analytical and numerical calculations in the model without string fusion, but with the longitudinal dynamics was shown for $b_{\rm corr}[N_F, N_B]$ and $\Sigma[N_F, N_B]$ quantities. This fact confirms the numerical correctness of the model and allows us to move on to more complex calculations: consider the fusion of strings in the Monte-Carlo regime.

2. The obtained model results for $b_{\rm corr}[N_F, N_B]$ in inelastic $p + p$ interactions at $\sqrt{s} = 200$ GeV (without specific model tuning) in general repeat the first evaluation results in the toy-model (Chapter 1) and qualitatively resemble the experimental results: the decrease of $b_{\rm corr}[N_F, N_B]$ with Δy. The difference between $b_{\rm corr}[N_F, N_B]$ values with and without string fusion grows with the average string density: the splitting for system evolution till $\tau_{\rm deepest}$ is approximately two times larger than the one for string dynamics till $\tau = 1.5$ fm (to remind the reader: at $\tau_{\rm deepest}$ the string system is in the minimum of potential energy, thus, it is the most dense state). For both cases string fusion decreases the values of $b_{\rm corr}[N_F, N_B]$. It is in agreement with the results of the toy-model in Chapter 1. The behaviour of this difference is the same for two models: the largest gap of the values of $b_{\rm corr}[N_F, N_B]$ with string fusion vs its values for free strings is at low Δy and it gradually decreases with increasing Δy. It is because the majority of strings lie closer to mid-rapidity and, therefore, the

string fusion occurs more often in this region. The same behaviour is seen for PYTHIA event generator data: decrease of $b_{\rm corr}[N_F, N_B]$ with Δy; splitting of results with and without colour reconnection option; the decrease of this splitting from the largest values at $\Delta y = 0$ with the increase of Δy.

3. In the developed model, the obtained grows of $\Sigma[N_F, N_B]$ with Δy above unity corresponds to the previous findings (Chapter 1) and experimental results. The splitting of $\Sigma[N_F, N_B]$ with and without string fusion is approximately the same for $\tau_{\rm deepest}$ and $\tau = 1.5$ fm and matches the one for PYTHIA with and without colour reconnection option. Plots for all model regimes coincide at $\Delta y = 0$ since the covariance in the definition of $\Sigma[N_F, N_B]$, Eq. (0.0.7), is the largest for close rapidity windows. At larger Δy one obtains different values of $\Sigma[N_F, N_B]$ for $\tau = 1.5$ fm and $\tau_{\rm deepest}$ even for free strings due to very different η configurations of string density in an event.

4. The obtained values for strongly intensive quantities $\Sigma[P_T, N]$ and $\Delta[P_T, N]$ as functions of the rapidity acceptance width (P_T and N are measured in the same rapidity window) are greater than unity, which is consistent with the earlier conclusions [120] for such a collision energy, and grow with δy. Model results for free strings coincide, while with string fusion the $P_T - N$ fluctuations grow with the average string density. The results of PYTHIA lie even higher, moreover, PYTHIA without colour reconnection still exhibits the level of $P_T - N$ fluctuations higher than the model result.

5. The further tests showed that the developed model can be tuned to experimental data by selecting just two parameters: the average multiplicity per rapidity unit from a free string, μ_0, and the average transverse momentum of particles from a free string, p_0. The obtained results of the model approximation of ALICE data for inelastic $p + p$ interactions at $\sqrt{s} = 900$ GeV adequately describe not only the distributions of one-dimensional quantities, such as the rapidity spectrum and charged particle multiplicity, but also the correlations between average transverse momentum and multiplicity.

6. In the model with parameters determined from the approximation of the experimental data (see previous point), the result for $\langle p_T \rangle - N$ correlation function

restricts the model regime to be used in the following calculations: the proper time of the evolution of string density in the transverse dimension should be set to $\tau_{\rm deepest}$ (and, consequently, the same for the longitudinal dynamics) and string fusion should be taken into account. Other combinations of the model options do not provide the correct slope of the $\langle p_T \rangle - N$ correlation function observed in the experiment.

7. The results for $b_{\rm corr}[N_F, N_B]$ obtained in the tuned model show a lack of contribution from short-range correlations (whose mechanisms are missing in the model): the model (in the chosen configuration, see the previous list item) values of $b_{\rm corr}[N_F, N_B]$ are almost constant with $\Delta\eta$, whereas the data and PYTHIA show a slow decrease. Thus, we can conclude that the results obtained in the toy-model (Chapter 1) and in this model without parameter fixation (section 2.7.2) overestimate the contribution of long-range correlations (from string number fluctuations in the forward-backward windows) to $b_{\rm corr}[N_F, N_B]$. Hence, to describe the behaviour of $b_{\rm corr}[N_F, N_B]$ with $\Delta\eta$ one has to take into account the correlations of particles produced by a single string. However, in the thesis, we show the importance of taking into account the contribution from long-range correlations, which is defined in our model by finite in rapidity strings.

8. The behaviour of $\Sigma[N_F, N_B]$ in the elaborated tuned model is similar to that obtained in the toy-model (Chapter 1) and in this model without parameter fixation (section 2.7.2). The main conclusion is that accounting for string fusion reduces the values of $\Sigma[N_F, N_B]$, which makes it interesting to further develop the model to describe ion-ion collisions. As mentioned above, the idea is to use the developed model with strings finite in rapidity (in which string fusion reduces $\Sigma[N_F, N_B]$), taking into account short-range correlations (that increase $\Sigma[N_F, N_B]$ with fusion) to describe the general reduction of $\Sigma[N_F, N_B]$ for more central $A + A$ collisions (increasing string density leads to an increase of string fusion).

9. The thesis shows the relation between $\Sigma[N_F, N_B]$ and the widely used quantity, the variance of the asymmetry coefficient, $\sigma^2(C)$, under the assumption of not very large multiplicity fluctuations in forward-backward windows. We also

demonstrate a strict correspondence between $\Sigma[N_F, N_B]$ and the (factorial) cumulants of the $N_F - N_B$ multiplicity distribution.

10. The obtained results of $\Sigma[N_F, N_B]$ dependence on "centrality" are rather of an evaluative nature. In the selected wide (due to the limitation of the available statistics) classes of events, based on forward multiplicity, it was not possible to see such a clear effect of the dependence of $\Sigma[N_F, N_B]$ on the classes of events as in the toy-model with the significantly increasing string density.

To summarise the results of this Chapter, it should be noted that, firstly, the model has shown its power to describe forward-backward multiplicity correlations and fluctuations, as well as those of multiplicity and transverse momentum in a common rapidity acceptance. In this study, the time of 3D strings' evolution and the corresponding string densities are found to play a major role in defining the magnitude of the long-range contribution to the correlation coefficient and in affecting its slope with $\Delta\eta$.

Secondly, the obtained influence of string fusion on the strongly intensive quantity $\Sigma[N_F, N_B]$ confirms the possibility of using the model to describe nucleus-nucleus collisions. In this thesis, we have also shown that the introduction of the string fusion mechanism in the model results in the enhanced $\langle p_T \rangle$–N correlation as the fused strings, on average, decay to the smaller number of particles with higher p_T. In general, model results are found in trend with PYTHIA8.3 event generator simulations, where the Colour Reconnection option plays a formally similar role as the string fusion implemented into our model, although the underlying physics of PYTHIA 8.3 is different.

In the experimental studies of azimuthal particle flows, the main difficulty lies in the procedure of getting rid of non-flow contributions due to all sorts of short-range correlations. Since our model does not contain short-range correlations yet, we use it to study the azimuthal anisotropies of the produced particles in our approach (see next Chapter).

CHAPTER 3

Advanced model of interacting strings and particle boosts

This Chapter presents a substantial extension of the developed (see Chapter 2) model of interacting colour strings, of finite length in rapidity. We propose to abandon the simplistic account of string fusion on a rough lattice and move to a fine division of the transverse plane into sufficiently small pixels. In addition, we introduce the collective behaviour of particles in the string model without hydro phase by considering two interaction mechanisms: "string-string" and "particle-string", following ideas from the papers [71] and [74]. The new procedure is applied to the description of the azimuthal anisotropy observed in inelastic $p + p$ interactions at $\sqrt{s} = 13$ TeV, since the interpretation of these experimental results [23, 24] provokes some tension in the flow-community. The methods and results presented in this Chapter were published in Ref. [140].

3.1 Conceptual improvements of the first model stages

In this section, only those parts of the model are presented that have been improved or newly developed compared to the previous model version (see Chapter 2).

3.1.1 Parton composition of protons

The new model is also based on the simplification that all partons of one colliding proton form strings with all partons of another colliding proton. Therefore, in the model, we call an event the creation of $n_{\rm str}$ between two protons, each containing $n_{\rm part}$ that is equal to the number of strings in an event, $n_{\rm part} = n_{\rm str}$.

To fulfil this requirement, we again prepare an extensive set of protons with all the possible even numbers of partons, $n_{\rm part}$. However, in this version of the model,

we monitor the parton composition of the proton more precisely. Namely, we include also valence diquark (see Appendix B.1). Thus, the parton composition of a proton with n_{part} is presented by one valence quark, one valence diquark, and $(n_{\text{part}} - 2)$ sea quarks (see Appendix B.2). The new algorithm to take into account the law of energy-momentum conservation for partons is provided in Appendix B.3. It is more time- and CPU-efficient than the permutations of partons between two selected protons that were presented in Appendix A and used in the previous model version (Chapter 2).

3.1.2 Event simulation

To remind the reader, the first step of the simulation of an event is to sample the number of exchanged pomerons, n_{pom}, from Eq. (2.1.2). Thus, the number of strings that should be formed in an event, $n_{\text{str}} = 2n_{\text{pom}}$. By creating the event, we mean searching for two protons, with the same number of partons, $n_{\text{part}} = n_{\text{str}}$, so that all their partons can form strings under certain conditions (see subsections 3.1.3 and 3.1.4).

First, we select two random protons from the prepared set (section 3.1.1) with the certain n_{part}. Second, we permute partons in one of the two protons by performing n_{part} replacements and checking whether this leads to the formation of n_{part} good parton pairs (see the requirements in the next two subsections). If not, we select another pair of protons.

3.1.3 String formation: electric charge

In this study, we take into account the electric charge of partons at the ends of each string: their sum, that determines the electric charge of the string, must be equal to one of the following integer numbers: -1, 0, $+1$, $+2$. Consequently, this condition restricts our selection of parton pairs that are the candidates to form a string.

3.1.4 String formation: masses of decay products

We calculate the string energy, $E_{\rm str}$, by summing the energies of partons at the ends of the string, $E_{\rm part1}$ and $E_{\rm part2}$, as

$$E_{\rm str} = \sqrt{m_{\rm part1}^2 + p_{\rm part1}^2} + \sqrt{m_{\rm part2}^2 + p_{\rm part2}^2}, \tag{3.1.1}$$

where $p_{\rm part}$ is the initial momentum of a parton and $m_{\rm part}$ is a dynamically defined parton mass (for details of their definitions, see Appendix B.3).

We accept a string candidate if its energy $E_{\rm str}$ is enough to decay at least in two hadrons at rest, with masses $M_{\rm daughter1}$ and $M_{\rm daughter2}$, i.e. $E_{\rm str} \geq M_{\rm daughter1} + M_{\rm daughter2}$.

In order to test this condition, it is necessary to identify the species of the pair of daughter particles based on the flavours of the partons at string's ends, e.g. the quark-diquark string should decay at least to a baryon and a meson. For completeness, we provide the list of minimum permitted combinations of daughter products, based on the flavours of quarks that we consider in the model: $m_{\rm nucleon} + m_\pi$, $m_{\rm nucleon} + m_K$, $m_{\rm nucleon} + m_D$, $2 \cdot m_\pi$, $2 \cdot m_K$, $2 \cdot m_D$, $m_\pi + m_K$, $m_\pi + m_D$ and $m_K + m_D$. We use $m_{\rm nucleon} = 0.9396$ GeV, $m_\pi = 0.1396$ GeV, $m_K = 0.4977$ GeV, $m_D = 1.8696$ GeV.

3.2 3D grid in the configuration-momentum space

The approach described in Chapter 2 and in Ref. [103] would not work for the description of particle flows in $A + A$ collisions. This is due to the fact that after transverse dynamics, caused by the attraction of strings, the centers of most of the strings will be in the same transverse cell. This would lead to the replacement of all the variety of the degrees of strings' overlaps by a single string with the enhanced tension. In this scenario, it would be impossible to create the anisotropy of produced particles since the information about matter density fluctuations would be lost. This is, however, not an issue in the models without attractive string dynamics in the transverse plane since an event string density is more diluted.

In the new version of our model [140], presented in this Chapter, we propose to introduce the fine 3D cells of the considered configuration-momentum space (much smaller 2D pixels in the transverse plane and the division into slices of the same

size in the rapidity dimension) to study the effects of fluctuating string density in details.

Let us denote the area of the 2D pixel as $S_{\rm bin}$. In order to have a fine grid, one has to select $S_{\rm bin}$ in a way that it is much smaller than the string transverse area, S_0. In the current implementation, we use a string diameter, $d_{\rm str}$, of 0.5 fm and a pixel width, $d_{\rm bin}$, of 0.05 fm, which we believe is sufficient to fulfil this condition.

The resembling procedure is done for the rapidity space with a slice size of $\varepsilon_{\rm rap} = 0.1$. In the previous studies (see Chapters 1 and 2), we placed a longitudinal grid with $\varepsilon = 0.1$ on each string separately. In this approach, we use a uniform splitting for the entire longitudinal dimension.

Finally, we can calculate the number of strings that occupy (cover) each 3D cell in the mixed configuration-momentum space. Thus, in a sense, we move away from the concept of particle-producing strings towards the concept of particle-producing 3D cells enclosing some fraction of the colour flux.

It is important to note that the running time of the program depends significantly on the number of 3D cells, since the algorithm must iterate over all of them to find the number of strings that cover each cell. Thus, it is necessary to restrict the volume of the configuration-momentum space permitted for simulations. In fact, the collision energy determines the longitudinal (in rapidity) size of the defined space, as the beam rapidity rises with $\sqrt{s}$. In its turn, the required transverse area depends on the initial distribution of strings and their final positions after the transverse dynamics. Since, in this investigation, we focus on the transverse evolution of the system until it reaches the global minimum of the potential energy, after the motion according to Eq. (2.3.1) the system becomes even more compact.

3.3 Time of the evolution of string density

In this section, we will spend some time commenting on the visual representation of the 3D evolution of string density. This became possible in the new model, since we split the transverse plane into small pixels and as to the longitudinal space of rapidity it remains the same granularity ε that was used in Chapters 1 and 2. Thus, it is now possible to explicitly depict the positions of strings in the configuration-momentum space.

3.3.1 Influence of the transverse evolution of string system

As it was discussed in the previous Chapter, the transverse evolution of the system of strings in an event, governed by Eq. (2.3.1), can be terminated at some proper time, $\tau_{\rm stop}$, which will affect the final string density and will determine the string configuration before hadronisation.

In Chapter 2, it was shown that the largest number of overlaps between strings occurs after the time that we called $\tau_{\rm deepest}$. This is the time it takes for a string transverse configuration to attain, evolving according to Eq. (2.3.1), the global minimum of the potential energy. There we considered other model regimes, including no transverse evolution and transverse evolution until the conventional time $\tau_{\rm stop} = 1.5$ fm [60], that poorly described the data (especially the $\langle p_T \rangle - N$ correlation). Thus, in the present study, we consider $\tau_{\rm stop} = \tau_{\rm deepest}$ that varies event-by-event.

Fig. 3.1 shows how a few events (one event for each row) with different numbers of strings (shown in different rows) look before and after the transverse evolution of string density. One should note that Z axis, shown in colours, is not to scale between the different plots. It is because the red areas on each histogram correspond to the largest string density independently of other plots. Thus, on the top left plot, presenting an event with just two strings, each string is shown with red. And the same red colour corresponds to the overlap of around 60 strings on the bottom left plot. It is possible to scale all histograms to the same Z axis, however, this will degrade the visual perception of events with a small number of strings.

The first and second columns in Fig. 3.1 demonstrate the event projections to the transverse plane, $X - Y$, before and after the transverse dynamics of strings, respectively. The third and fourth columns present the projections to the X-rapidity plane before and after the transverse evolution, respectively. The time of the transverse motion, $\tau_{\rm transv} = \tau_{\rm deepest}$, is indicated on each plot since it depends on the initial number of strings in an event (and on their initial positions).

One can clearly see that after the considered transverse evolution the string system is highly compressed and the 2D distribution (Fig. 3.1, second column) approaches a more round shape in comparison to the initial positions of the strings (Fig. 3.1, first column). In the rapidity dimension, we obtain fairly uniform distribution up to large rapidities (Fig. 3.1, fourth column).

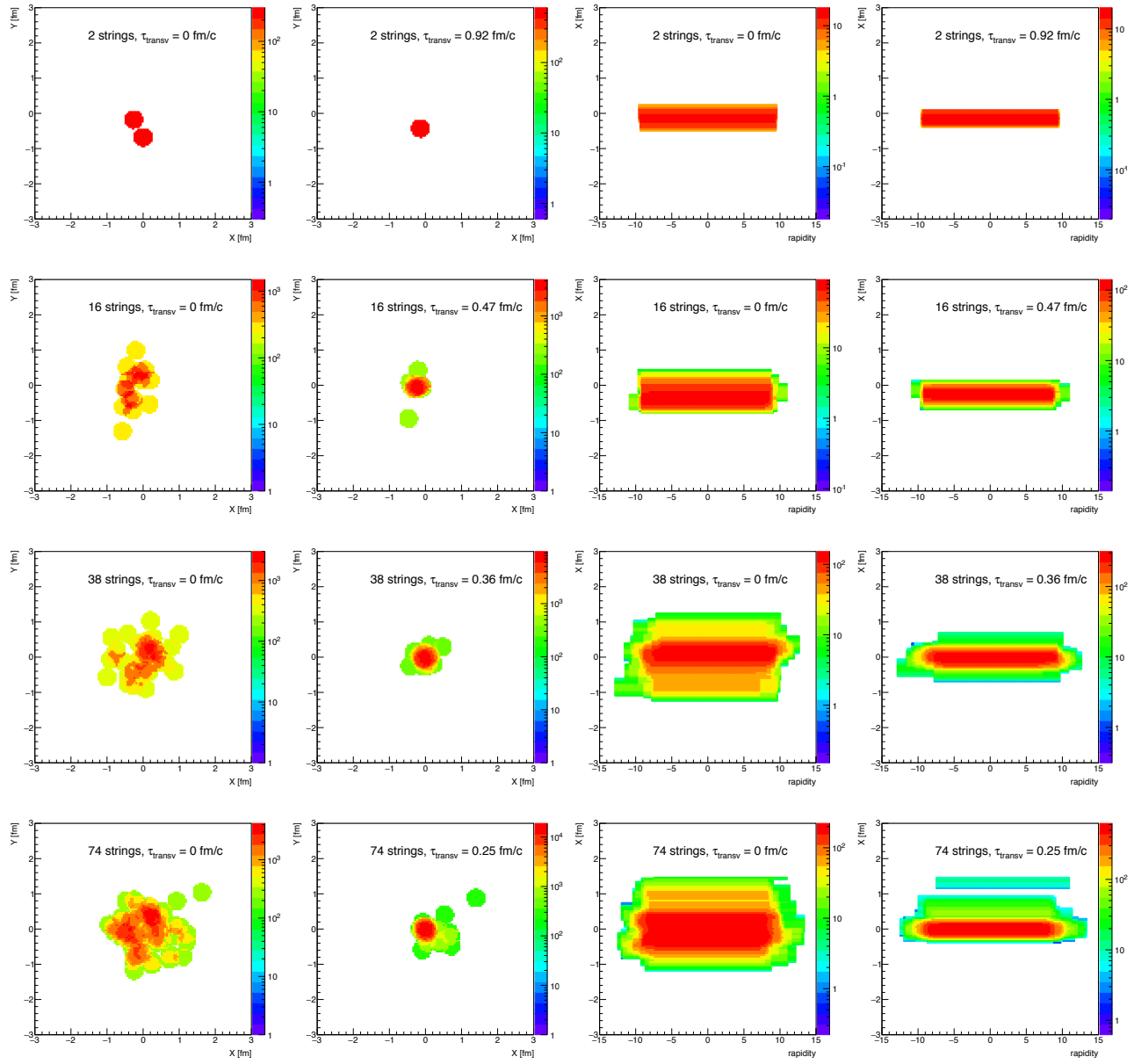

Figure 3.1: The simulated events with 2 strings (first row), 16 strings (second row), 38 strings (third row) and 74 strings (fourth row). The figure shows the projections of 3D string density in these events to the transverse plane, $X-Y$, before (first column) and after (second column) the transverse evolution; event projection to the $X-$rapidity plane before (third column) and after (fourth column) the transverse evolution. The time of the transverse evolution, τ_{transv}, is indicated on the plots. For the second and fourth columns $\tau_{\text{transv}} = \tau_{\text{deepest}}$. Z axis not to scale.

3.3.2 The time of movement for the ends of the strings

In this model version, we still hold the idea of the correspondence between the time for transverse and longitudinal dynamics of the string system in an event. Thus, we relate the proper time τ from Eq. (2.4.3) with the time for the transverse evolution, τ_{transv}, to synchronise the dynamics of the string system in rapidity and

$X - Y$ dimensions.

However, one has to take into account that the compressions and stretchings of a string are periodic (yo-yo solution [49]) and are followed one by another. Moreover, the movement of end points with different masses, m_{part1} and m_{part2}, in our case is not symmetrical (we denote by 1 or 2 one of the string ends). Therefore, we define the maximum proper time for each string end, $\tau_{\text{max}}^{\text{part1,2}}$, after which it will fully stop to begin the deceleration (acceleration) after acceleration (deceleration) as

$$\tau_{\text{max}}^{\text{part1,2}} = \frac{m_{\text{part1,2}}}{\sigma_T}\sqrt{2(\cosh\left(\tilde{y}_{\text{init}}^{\text{part1,2}}\right) - 1)}, \tag{3.3.1}$$

where $\tilde{y}_{\text{init}}^{\text{part1,2}}$ are the initial rapidities of the string ends converted to the string rest frame, m_{part} is dynamically defined parton masses (for details of their definitions, see Appendix B.3).

To convert the rapidity of a string end from the laboratory frame, $y_{\text{init}}^{\text{part}}$, to the string rest frame, $\tilde{y}_{\text{init}}^{\text{part}}$, one has to know the rapidity of the string in the laboratory frame, y_{str}. It is calculated as follows. First, we define strings' momentum, $p_{\text{str}} = p_{\text{part1}} - p_{\text{part2}}$, and energy, E_{str}, from Eq. (3.1.1). Thus, the rapidity of a string, y_{str}, is

$$y_{\text{str}} = \frac{1}{2}\ln\left(\frac{E_{\text{str}} + p_{\text{str}}}{E_{\text{str}} - p_{\text{str}}}\right). \tag{3.3.2}$$

Once it is known one can recalculate the rapidities of the string ends in its rest frame as

$$\tilde{y}_{\text{init}}^{\text{part1,2}} = y_{\text{init}}^{\text{part1,2}} - y_{\text{str}}, \tag{3.3.3}$$

and substitute them into Eq. (3.3.1).

It is necessary to account for the periodicity of string motion. Namely, after the time $2 \cdot \tau_{\text{max}}^{\text{part1,2}}$ from Eq. (3.3.1), the sign of $dp_{\text{part1,2}}/dt$ flips. Therefore, it is crucial to correctly connect the τ_{deepest}, that is found from the transverse dynamics for the whole event, with $\tau_{\text{max}}^{\text{part1,2}}$, that varies for two ends of the string and for each individual string in the event. To summarise, the time of the movement of a string end only during the last period should be used in Eq. (2.4.3). The rapidities of the string ends after such loss, $y_{\text{fin}}^{\text{part1,2}}$, are found by subtraction of $y_{\text{loss}}^{\text{part1,2}}$ from $y_{\text{init}}^{\text{part1,2}}$ with the correct signs.

Fig. 3.2 presents how the string density of the model events from Fig. 3.1 (already after the transverse evolution) changes after we take into account the longitudinal

losses of strings' lengths. The first column in Fig. 3.2 is repeated from Fig. 3.1 (last column) for clarity.

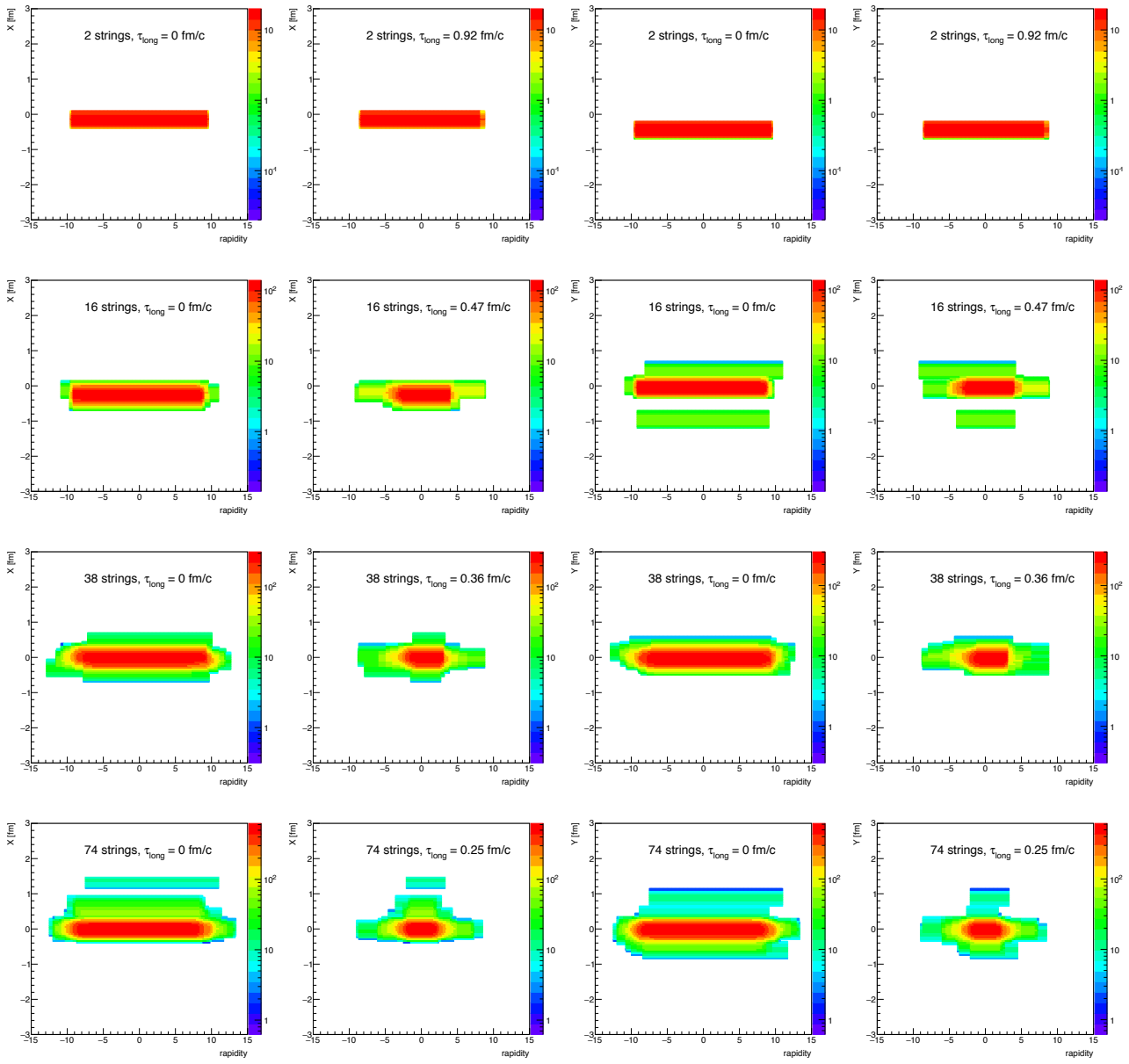

Figure 3.2: The simulated events with 2 strings (first row), 16 strings (second row), 38 strings (third row) and 74 strings (fourth row). The figure shows an event projection to the $X-$rapidity plane before (first column) and after (second column) the longitudinal evolution; event projection to the $Y-$rapidity plane before (third column) and after (fourth column) the longitudinal evolution. The time of the longitudinal evolution, τ_{long}, is indicated on the plots. For the second and fourth columns $\tau_{\text{long}} = \tau_{\text{deepest}}$. Z axis not to scale.

In Fig. 3.2, one can see the event projections on the X-rapidity plane before (first column) and after (second column) the longitudinal dynamics. The third and fourth column show the Y-rapidity plane projections also before and after the longitudinal

dynamics, respectively. Again Z axis should not be scaled (see the explanation in the previous subsection).

It can be seen that the string system in the final state (Fig. 3.2, second and fourth columns) has a significant compression in the longitudinal direction. The cloud of a high density of strings is no longer infinitely extended as it is often assumed in the string models [56], thus, our model loses the translational invariance in rapidity. This statement was made already in Chapters 1 and 2, but here this is clearly shown in the graphs. The transverse evolution of the strings, as described in the previous subsection, also leads to varying string density, which makes an event strongly heterogeneous.

Thus, in the model, the obtained string configurations provide a characteristic form of particle distribution in rapidity: a plateau at mid-rapidity and a decline of the distribution at high rapidities.

3.4 Fusion and the kinetic energy of strings

In this section, we propose to consider additional effects [71] of string interactions that arise from their fusion.

Since the total energy of the system of strings in an event should be conserved, we assume that when strings overlap, a redistribution of their potential, U, and kinetic, T, energy occurs. It is because the overlap of colour strings modifies the strength of the colour field inside them, which affects the string tension. Therefore, the partial overlap of a few strings leads to a decrease in the potential energy of each of them in this region. This modification causes an opposite change in their kinetic energies, pulling them towards each other as in Ref. [71]. The consequent formation of a string cluster increases the string tension in comparison to a free string. The alternative option that is also mentioned in Ref. [71] causes the decrease in the effective string tension and, therefore, should lead to the string repulsion (see an example of its implementation in Ref. [72]).

As a result, we need to parameterise the gain of kinetic energy, $\Delta T_{i,j}$, that the i-th string in an event obtains from the overlap with the j-th one. Its functional form should reflect the fact that the full overlap of two strings would mean that their fusion is completed and they stop. On the other hand, $\Delta T_{i,j}$ should fade with

the distance between strings' centres. Thus, the following dependence on $d_{i,j}$, the 2D distance between the i-th and j-th strings, is proposed

$$\Delta T_{i,j} = \chi d_{i,j} \exp\left(\frac{-d_{i,j}^2}{4r_0^2}\right), \tag{3.4.1}$$

where $d_{i,j} \leq 2r_0$, $r_0 = 0.25$ fm is the string radius, while χ is a dimensional constant measured in GeV/fm that is a free model parameter.

To find $\Delta T_{i,j}$ for i-th string we iterate over its neighbouring overlapping strings in every rapidity slice, ε_{rap}. To find the gained momentum of a string, we neglect the final momentum of strings after the transverse dynamics since the string motion according to Eq. (2.3.1) is non-relativistic. Thus, the i-th string's energy, m^i_{str}, will be increased by the proposed gain $\Delta T_{i,j}$ and the string will gain the transverse momentum from the j-th string according to

$$\Delta p_T^{i,j} = \sqrt{(\Delta T_{i,j} + m^i_{\text{str}})^2 - (m^i_{\text{str}})^2}, \tag{3.4.2}$$

where m^i_{str} is the mass of the i-th string.

To find the direction of the obtained momentum, $\Delta p_T^{i,j}$, one should take the azimuthal direction of the vector from the centre of the i-th string to the centre of the j-th string, $\phi_{i,j}$. It is determined by the distances on X and Y axes between their centres, $\Delta X_{i,j}$ and $\Delta Y_{i,j}$. The projections Δp^i_X and Δp^i_Y of the transverse momentum, Δp^i_T, that the i-th string gains from the intersections with all its neighbours are found by summing the projections of $\Delta p_T^{i,j}$ between overlapping pairs as

$$\Delta p^i_X = \sum_{j \neq i}^{n_{\text{str}}-1} \Delta p_T^{i,j} \cos(\phi_{i,j}), \;\; \Delta p^i_Y = \sum_{j \neq i}^{n_{\text{str}}-1} \Delta p_T^{i,j} \sin(\phi_{i,j}). \tag{3.4.3}$$

Thus, the 2D vector of the string's transverse momentum, $\overrightarrow{\Delta p^i_T}$, is determined by its overlaps with other strings in each rapidity slice, ε_{rap}. It is this extra momentum that boosts particles produced by the string (see subsection 3.5.1).

3.4.1 Particle production from 3D cells

In this study, we define string hadronisation in each 3D cell defined as 2D pixel in the transverse plane and ε_{rap} slice in the rapidity dimension. The colour field inside a 3D cell determines the average number of charged particles produced, their average

transverse momentum and type. Particles' rapidities are found from the uniform distribution in each rapidity slice. Thus, we assume that particles propagate in the given ε_{rap} and do not leave it.

In this model, we move away from the rough cellular fusion of strings in order to take into account more accurately the string overlaps. The introduced fine binning of the configuration-momentum space (see Sec. 3.2) is exactly what it is needed for.

3.4.2 Mean multiplicity with string fusion

Let us consider a rapidity slice of a free single string. The colour field inside it, $\mathcal{E}_0$, can be represented as a sum of colour fields inside all transverse (2D) pixels that tessellate the area of this string

$$\mathcal{E}_0 = \sum_{\text{bins}} \mathcal{E}_{\text{bin}} = \frac{\mathcal{E}_0}{S_0} \sum_{\text{bins}} S_{\text{bin}}. \tag{3.4.4}$$

Thus, the field inside a 2D pixel, $\mathcal{E}_{\text{bin}}$, is proportional to the ratio of its area, S_{bin}, to the area of a string, S_0.

Let us now consider a random 3D cell in the configuration-momentum space that is populated with k strings. The resulting colour field inside it, $\mathcal{E}_{\text{tot}}$, will be the square root of the sum of squares of the fields from k strings, $\mathcal{E}_i$, that cover this cell

$$\mathcal{E}_{\text{tot}} = \sqrt{\sum_{i=1}^{k} \mathcal{E}_i^2} = \sqrt{\sum_{i=1}^{k} (\frac{S_{\text{bin}}}{S_0^i} \mathcal{E}_0^i)^2}. \tag{3.4.5}$$

For simplicity, the present study considers all strings to have the same transverse area, S_0^i, that is not varying along the rapidity direction, albeit the picture may be more complex [67]. The colour field of a free string, $\mathcal{E}_0^i$, is assumed to be constant and is defined by the confinement properties [61]. Therefore, in our case, the Eq. (3.4.5) can be simplified to

$$\mathcal{E}_{\text{tot}} = \sqrt{k} \frac{S_{\text{bin}}}{S_0} \mathcal{E}_0. \tag{3.4.6}$$

The average multiplicity from a free string, ν_0, is proportional to the field of a string, $\mathcal{E}_0$. Thus, by transitivity, for the k strings that overlap in a 3D cell one obtains $\nu_{\text{tot}} \propto \mathcal{E}_{\text{tot}}$.

Typically, the average multiplicity of a unit of rapidity, ε_{rap}, of a free string is denoted as μ_0. Therefore, one can define an average multiplicity from a 3D cell with

length $\varepsilon_{\rm rap}$ and transverse area $S_{\rm bin}$ as

$$\mu_{\rm bin} = \mu_0 \varepsilon_{\rm rap} \sqrt{k} \frac{S_{\rm bin}}{S_0}, \tag{3.4.7}$$

with μ_0 being a free model parameter and $S_0 = \pi r_0^2$. For comparison, in the previous Chapter, we calculated the mean multiplicity from the cluster of k strings (without division in the transverse plane), $\mu_{\rm clust}$, as $\mu_{\rm clust} = \mu_0 \varepsilon_{\rm rap} \sqrt{k}$, following [68].

The actual charged particle multiplicity produced by the 3D cell, $N_{\rm bin}$, is sampled from the Poisson distribution with a given mean $\mu_{\rm bin}$. The multiplicity of charged particles in the event, $N_{\rm ch}$, is a sum over all 3D cells of the numbers of particles in each cell. Thus, the procedure of effective hadronisation is now applied at the level of particle-producing 3D cells instead of particle-producing strings. It allows us to explicitly take into account density fluctuations of string medium.

3.4.3 Mean transverse momentum of particles with string fusion

The mean transverse momentum of the particles produced by a free string, p_0, does not depend on the string's length in rapidity or its transverse area. Thus, we assume that it will remain unchanged despite the division of the cross-sectional area of strings into 2D pixels. Therefore, we keep the modification of p_0 for the cluster of k fused strings, $\langle p_T \rangle_k$, used in the previous Chapter (see Eq. (2.5.3)). However, now we find the degree of overlap, k, in each 3D cell. Particles' transverse momenta and masses are sampled from the Schwinger distribution, Eqs. (2.6.1) and (2.6.2).

We should mention another variant of the particle production mechanism, the thermal model [52, 141] that better describes the p_T spectrum. The thermal model is derived from the Schwinger approach assuming fluctuations in string tension from event to event and from string to string in each event. The problem is that its implementation in the Monte-Carlo algorithm is much more complicated than using Schwinger probabilities. This is because the joint $p_T - m$ distribution used in $\exp\Big(-\sqrt{p_T^2 + m^2}/\sigma_{\rm eff}\Big)$ for the thermal model must be obtained. In turn, for the Schwinger mechanism, it is possible to factorize the $p_T - m$ distribution for independent substitution into $\exp\big(-(p_T^2 + m^2)/\sigma_{\rm eff}\big)$. Thus, in the current version of our model, we again follow the Schwinger approach, Eqs. (2.6.1) and (2.6.2).

3.5 The origin of azimuthal particle correlations in the model

In addition to a more accurate account of string fusion, the purpose of introducing a fine grid in the transverse plane is to consider azimuthal correlations of particles in our model. It is worth noting that in the previous Chapters we did not introduce such a particle characteristic as the azimuthal angle, ϕ, at all, since we restricted ourselves to the consideration of rapidity correlations. In a naive approach, one could uniformly assign angles $\phi \in [-\pi, \pi]$ to the particles, which would determine their independent propagation in the transverse plane. However, in this Chapter we follow the ideas from Refs. [71, 74] on how to introduce the correlated azimuthal behaviour of particles into the colour string model without hydrodynamic phase. There are three main ingredients here.

First, in models of this type, the strings in the event must form some clusters [31] distributed anisotropically. Note that our approach differs from hybrid models [142] in which the formed colour strings are the initial condition for hydro. In them, the spatial asymmetry of the strings would already lead to azimuthal particle flows. In contrast, we study a very possibility: whether the azimuthal correlations observed in $p+p$ data can be described without hydro phase. In such a case, only fluctuations of the string density will not cause any azimuthal particle flows. However, in our model, this initial state anisotropy is crucial for the two mechanisms described further as it controls the strength of their effect.

Second, we consider the change in the strings' kinetic energy that occurs when they overlap in 3D space. As a result, the boost from a string is transferred to the particles that it is fragmented to [71]. It creates correlations in p_T and ϕ between particles produced from strings that interact with each other. What is important is that we consider string hadronisation at the moment of reaching the minimum of the potential energy of the system of strings (at τ_{deepest}). This results in the high similarity of the geometry of events with the close number of strings, which leads to nearly identical picture of particle boosts. For instance, Fig. 3.1, second column, second row shows a typical event with 16 strings. We argue that all events with this n_{str} resemble each other up to the event rotation and some statistical fluctuations. It means that these events have non-zero flow of comparable magnitude, therefore, the signal survives after averaging over this group of events.

Third, particles passing through single strings or string clusters lose some part of their energy due to gluon radiation in the medium [74]. When a particle loses all its momentum, it means that it failed to escape the string environment. Consequently, there arise azimuthal directions at which particles with such momentum cannot leave the system of strings for the given string geometry. Thus, particle distribution in ϕ ceases to be uniform and there appears some correlations of particle motion in the transverse plane. Moreover, the complex geometry of the string medium leads to different path lengths in different azimuthal directions and to different losses of transverse momentum.

The first mentioned mechanism was naturally introduced into our model already in its previous version: considered transverse dynamics of strings results in the formation of string clusters of different degrees of overlap. Longitudinal dynamics makes the fluctuations of string density dependent on the rapidity coordinate.

The latter two are the new features implemented in the model, described in the following subsections. Note that different degrees of string overlaps cause variations in the magnitude of energy loss and particle boosts cell-by-cell in the transverse plane-rapidity space. As a result, the particle production in a given event becomes highly asymmetric in azimuthal angle and pseudorapidity.

3.5.1 Particles' boosts in the transverse plane

The particle's transverse momentum sampled from Eq. (2.6.1) gets a Lorenz boost if it originates from the string piece that was boosted due to string fusion [71] (see section 3.4).

To define the boost vector, we loop over all 3D cells and find the strings that cover each of them. The 3D cell is assigned the momentum projections, $\Delta p_X^{\mathrm{bin},i}$ and $\Delta p_Y^{\mathrm{bin},i}$, that are found as fractions of the momentum projections of the i-th string that covers it, Δp_X^{i} and Δp_Y^{i}, from Eq. (3.4.3) as

$$\Delta p_{X,Y}^{\mathrm{bin},i} = \Delta p_{X,Y}^{i} \frac{d_{\mathrm{bin}}^2}{S_0} \frac{\varepsilon_{\mathrm{rap}}}{\delta y^i}, \tag{3.5.1}$$

where $d_{\mathrm{bin}} = 0.05$ fm is the 2D pixel size in X and Y in the transverse plane, $\delta y^i = |y_{\mathrm{fin}}^{\mathrm{part1}} - y_{\mathrm{fin}}^{\mathrm{part2}}|$ is the length of i-th string in rapidity that highly fluctuates and is calculated as the difference between the rapidities of the ends of the string, $y_{\mathrm{fin}}^{\mathrm{part1}}$ and $y_{\mathrm{fin}}^{\mathrm{part2}}$.

Similarly, we find $m^{\mathrm{bin},i}$ - the part of the mass of the i-th string, m^i_{str}, that corresponds to this 3D cell

$$m^{\mathrm{bin},i} = m^i_{\mathrm{str}} \frac{d^2_{\mathrm{bin}}}{S_0} \frac{\varepsilon_{\mathrm{rap}}}{\delta y^i}. \tag{3.5.2}$$

Using Eq. (3.5.1) and (3.5.2), we can find the energy of i-th string contained in the 3D cell, $\Delta E^{\mathrm{bin},i}$, as

$$\Delta E^{\mathrm{bin},i} = \sqrt{(m^{\mathrm{bin},i})^2 + (\Delta p_X^{\mathrm{bin},i})^2 + (\Delta p_Y^{\mathrm{bin},i})^2}. \tag{3.5.3}$$

If this 3D cell is covered by k strings in an event, their $\Delta p^{\mathrm{bin},i}_{X,Y}$ from Eq. (3.5.1) and $\Delta E^{\mathrm{bin},i}$ from Eq. (3.5.3) should be included in its total momentum, $p^{\mathrm{bin,total}}_{X,Y}$, and the total energy inside it, $E^{\mathrm{bin,total}}$, as

$$p^{\mathrm{bin,total}}_{X,Y} = \sum_{i=1}^{k} \Delta p^{\mathrm{bin},i}_{X,Y}, \tag{3.5.4}$$

$$E^{\mathrm{bin,total}} = \sum_{i=1}^{k} \Delta E^{\mathrm{bin},i}. \tag{3.5.5}$$

We perform particle production from each 3D cell in the cell's rest frame as described in Sec. 3.4.1. In this frame, particle's azimuthal angle, ϕ, is sampled from the uniform distribution from $-\pi$ to π. To get to the laboratory reference frame one boosts the four-momenta of the produced particles using the boost vector with $p_X^{\mathrm{bin,total}}$, $p_Y^{\mathrm{bin,total}}$ and $E^{\mathrm{bin,total}}$.

Thus, we obtain the correlated transverse motion of particles produced by 3D cells that strongly depends on the degrees of strings' overlaps inside them.

3.5.2 Transverse momentum loss

In this model, we assume that once produced within some rapidity slice $\varepsilon_{\mathrm{rap}}$, a particle does not leave it flying away from the string in the transverse plane. When the particle traverses a 2D pixel with a certain density of strings, it loses some part of its initial momentum, p_{init}, due to gluon radiation (Fig. 3.3), reaching the value, p_{fin}. In an analogy with the QED process of photon radiation by charged particle moving in the external electromagnetic field, it can be expressed in the following way [74]

$$p_{\mathrm{fin}} = (p_{\mathrm{init}}^{1/3} - \varkappa \sigma_{\mathrm{eff}}^{2/3} l)^3, \tag{3.5.6}$$

where $\varkappa$ is a quenching coefficient that is a free model parameter. It is necessary to apply the Eq. (3.5.6) iteratively since $\sigma_{\text{eff}} = 4p_0^2 k^{2\beta}$ varies pixel-by-pixel based on the number of overlapped strings, k, inside it. Thus, the length of one 2D step, l, can be approximated by $d_{\text{bin}}\sqrt{2}$ (the length of the 2D pixel's diagonal). To find the trajectory of a particle in the transverse plane, we apply the Bresenham's line algorithm [143, 144] separately in each rapidity slice. Since the density of strings fluctuates with rapidity, l and σ_{eff} differ not only at different azimuthal angles, ϕ, but also within different rapidity slices, ε_{rap}.

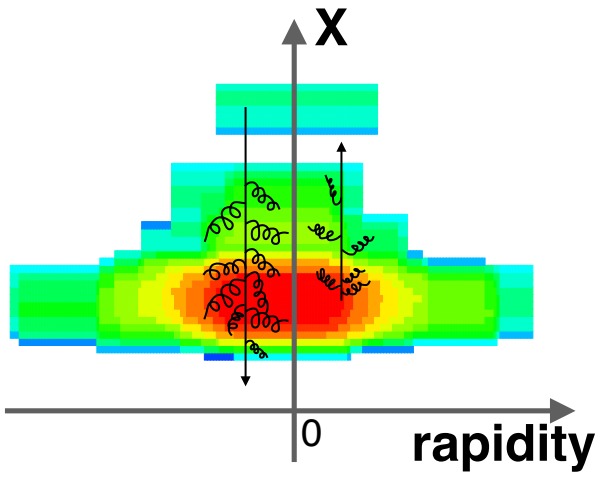

Figure 3.3: Schematic picture of the gluon radiation (curly lines) that particles experience when passing (straight lines) through the inhomogeneous string medium (colourful areas with the density from the highest (red) to the lowest (cyan) in X-rapidity plane (see text for details).

Another important remark is that in general, the value of p_{fin} can be equal to zero after a number of iterations of Eq. (3.5.6). We interpret this as the inability of the particle to escape in a given azimuthal direction, thus it is absorbed by the string environment. In this case, the energy of the particle is spent on producing another particle to try to replace it. For the new particle, we regenerate its transverse momentum and azimuthal angle, thus, it has a chance to escape in a new direction. Since we know the required number of particles to be emitted from each three-dimensional cell (from the Poisson distribution with mean from Eq. (3.4.7)), we will have to generate a particle until the combination of its transverse momentum and azimuthal direction allows it, having been emitted by a given three-dimensional cell, to leave the string medium.

We have to mention that the proper way to take into account the loss of momenta due to gluon radiation would be to apply it at the quark level. Thus, the resulting

momentum loss for a particle should be summed after the coalescence of quarks into a colourless hadron is performed. However, this procedure would significantly complicate the model. Thus, we assume that all this is included in the quenching coefficient $\varkappa$. However, it would be interesting to make the quenching coefficient different for baryons and mesons, which would effectively take into account the different number of quarks in them and, thus, the influence of a string medium.

In general, this mechanism of azimuthal correlations arising from the momentum loss of particles in the string medium can be compared with studies of azimuthal parton escape in transport models [145].

3.6 Inference of the model parameters

Having introduced the new mechanisms and also having improved the basics of event generation, we have to re-tune the model. At the moment, the transverse flow signal in proton-proton collisions has been measured only at high energies and high multiplicities. Thus, we selected ATLAS data on inelastic proton-proton interactions at $\sqrt{s} = 13$ TeV [146] to fix model parameters and to compare model results for azimuthal correlations with it.

Fig. 3.4 represents the comparison of the model (lines) and experimental (dots) distributions. Calculations were performed for ten million generated events. We aim to describe not only the global observables such as charged particle multiplicity distribution (Fig. 3.4, second row, left), transverse momentum (Fig. 3.4, first row, right) and pseudorapidity spectra (Fig. 3.4, first row, left), but also the $\langle p_T \rangle - N_{\rm ch}$ correlation function (Fig. 3.4, second row, right).

As it was stated above, in this Chapter, we consider only the model regime with the transverse evolution of string density up to time $\tau_{\rm deepest}$, which corresponds to the maximum frequency of string overlaps in the minimum of the potential energy of the system, and, hence, to the maximum degree of their fusion. The choice of such a model configuration was justified in the previous Chapter.

The value of $dN_{\rm ch}/d\eta|_{\eta=0}$ (Fig. 3.4, first row, left) is adjusted by finding the appropriate value of the mean particle multiplicity from a 3D cell of a free string, μ_0. In turn, the width of the $dN_{\rm ch}/d\eta$ distribution is controlled by the value of the string tension, σ_T, that defines the longitudinal dynamics of strings, Eq. (2.4.3).

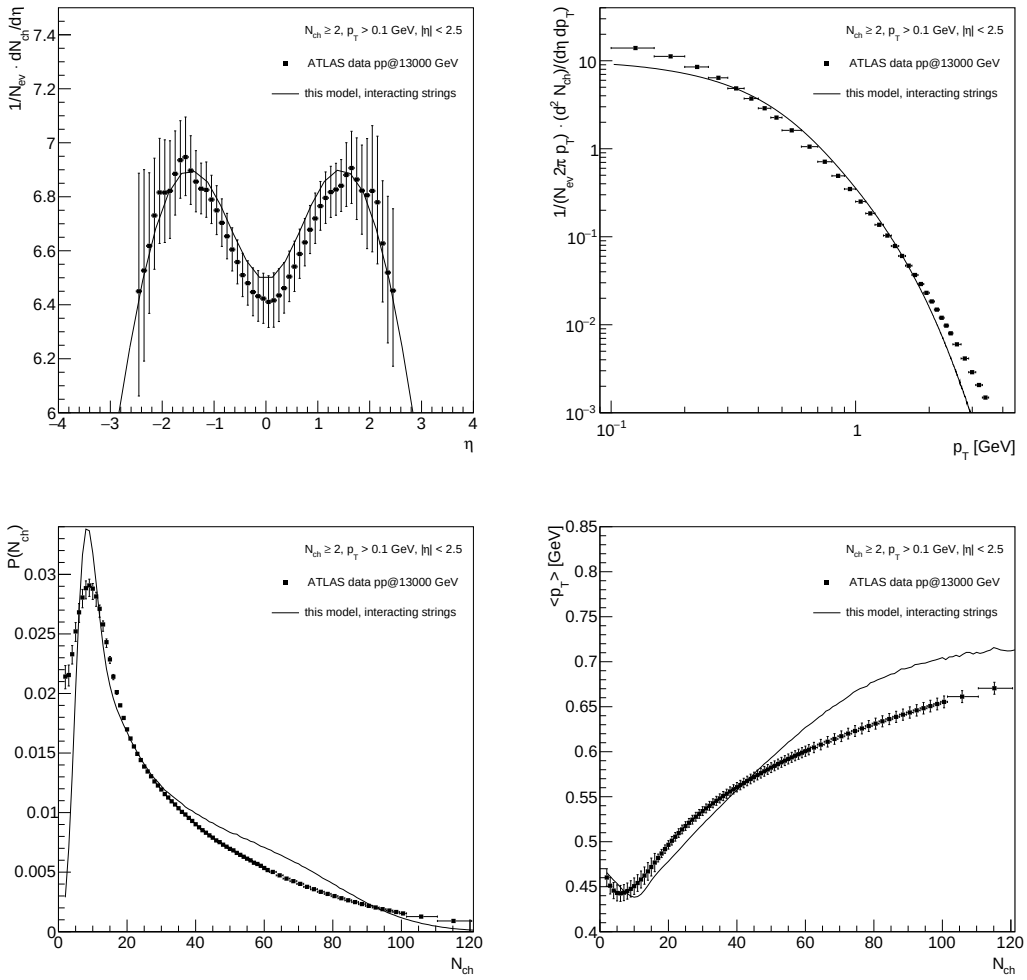

Figure 3.4: Model results (lines) compared with the ATLAS data [146] (squares) for inelastic $p+p$ interactions at $\sqrt{s} = 13$ TeV. **First row**: $dN_{\rm ch}/d\eta$ distribution **(left)** within limited to experimental measurements η range and charged particles' p_T spectrum **(right)**. **Second row**: Charged particle multiplicity distribution, $P(N_{\rm ch})$, **(left)** and $\langle p_T \rangle - N_{\rm ch}$ correlation function **(right)**. Particles selection $p_T > 0.1$ GeV and $|\eta| < 2.5$, event selection: $N_{\rm ch} \geq 2$. See text for model parameters.

By tuning the mean transverse momentum of particles produced by a free string, p_0, we settle the $\langle p_T \rangle$ at low $N_{\rm ch}$ (Fig. 3.4, second row, right). With the proper selection of the quenching coefficient, $\varkappa$, Eq. (3.5.6), we are able to modify the slope of the $\langle p_T \rangle - N_{\rm ch}$ correlation function at moderate and high $N_{\rm ch}$. At high $N_{\rm ch}$ (when string fusion is most significant) the $\langle p_T \rangle$ is influenced by the value of χ constant, Eq. (3.4.1).

In the charged particle multiplicity distribution (Fig. 3.4, second row, left) the events with $N_{\rm ch} < 2$ are removed as in data, thus, we plot $P(N_{\rm ch}) = P_{\rm full}(N_{\rm ch})/(1 - P_{\rm full}(0) - P_{\rm full}(1))$, where $P_{\rm full}$ is the $N_{\rm ch}$ distribution that includes events without

registered particles ($N_{\rm ch} = 0$). These events are highly influenced by diffractive processes that are not considered in the model. Moreover, even with the $N_{\rm ch} \geq 2$ selection the experimental results at low $N_{\rm ch}$ and low p_T are affected by diffraction. Therefore, our predictions should not be directly compared in this region, but we are mostly interested in high $N_{\rm ch}$ events as they are more relevant in the studies of collective behaviour. The resulting p_T spectrum is presented in Fig. 3.4, first row, right.

The following values of the free model parameters were simultaneously selected to fit at once the mentioned ATLAS data [146]: $\mu_0 = 1.14$, $\sigma_T = 0.55$ GeV/fm, $p_0 = 0.37$ GeV, $\varkappa = 0.1$, $\chi = 0.00001$ GeV/fm. The found value of $\varkappa$ appeared to be rather low in comparison with the one used in, for example, Refs. [147, 148], but in our study, the $\langle p_T \rangle - N$ correlation function acted as a strict condition for $\varkappa$.

3.7 Study of azimuthal correlations in the model description of inelastic $p + p$ interactions at $\sqrt{s} = 13$ TeV

In this Chapter, we study whether the interplay of the two newly introduced mechanisms generating particle azimuthal anisotropy in the presented string model could describe the transverse flow measured in $p + p$ collisions.

3.7.1 Motivation for choosing quantities to study

To quantify the transverse flow signal, one can perform [19] in each event the Fourier expansion of the single-particle distribution in the azimuthal angle, ϕ. However, it is necessary to take into account the intrinsic symmetry of particle production in every event, which is determined by its reaction plane, Ψ_{RP}. It is formed by the direction of the beam and the impact parameter and creates a preferred azimuthal orientation in an event. Thus, the relative particle azimuthal angles, $\phi - \Psi_{RP}$, should be used in the calculations. Therefore, in a given part of phase-space, one can expand the $\phi - \Psi_{RP}$ distribution into Fourier series as

$$E\frac{d^3N_{\rm ch}}{d^3p} = \frac{1}{2\pi}\frac{d^2N_{\rm ch}}{p_T dp_T dy}\left(1 + 2\sum_{n=1}^{\infty} v_n \cos(n(\phi - \Psi_{RP}))\right), \tag{3.7.1}$$

with the set of Fourier coefficients, v_n, that describes the amplitudes of particle distribution asymmetry in the transverse plane averaged over particles in one event.

One should note that both v_n and Ψ_{RP} fluctuate event-by-event and, typically, only the moments of the corresponding distributions are measured experimentally.

The validity of the Fourier expansion in the real case of finite event multiplicity (especially in $p+p$ collisions) is questionable. Moreover, the reaction plane, Ψ_{RP}, cannot be directly measured, so one may substitute it by proxy [149] called the event plane, Ψ_{EP}. However, there is no unique event plane in an event, instead, one determines a set of event planes, Ψ_n, depending on the Fourier harmonic number n as

$$\Psi_n = \frac{1}{n}\tan^{-1}\left(\frac{\sum_i \sin(n\phi_i)}{\sum_i \cos(n\phi_i)}\right), \tag{3.7.2}$$

where the numerator and denominator are calculated from the distributions of the particles in ϕ in an event.

More recent studies have shown [150] that imprecise estimation of the event plane significantly spoils the azimuthal flow signal in this approach. Therefore, one has to use more sophisticated measures, such as two-particle correlations that, under certain assumptions, naturally exclude the dependence on Ψ_{RP} in $\Delta\phi = \phi_1 - \phi_2$. Using the multi-particle cumulants [87] of different orders, n, that correlate m particles, $c_n\{m\}$ (see, for example, Eq. (0.0.11)), will be even better, especially in sub-event method [88], since they are supposed to truly suppress the non-flow effects. In the described reaction plane method, this confidence level of particle flow results can only be achieved through the summation over the infinite number of particles in an event.

3.7.2 Event classification

In the studies of $A+A$ collisions, it was demonstrated that the emergent flow signal strongly depends on the centrality of events selected for the analysis: the largest azimuthal asymmetries of produced particles were observed for the semi-peripheral reactions [151, 152]. The current understanding suggests that the initial spacial event anisotropy is transferred by the thermalised viscous hydro-phase of the collision into the momentum asymmetry of the final hadrons. The application of this mechanism is questionable for $p+p$ collisions [27], however, the intriguing results on azimuthal correlations in proton-proton data were observed only for high-multiplicity events [23, 24]. Therefore, also for $p+p$-interactions it is necessary to

make the event classification based on some quantity that will serve as an indirect indicator of the energy density reached in the interaction region.

In this study, we repeat ATLAS procedure for event classification from Ref. [153] based on charged-particle multiplicity in a certain acceptance. Thus, the $N_{\rm ch}^{\rm sel}$ distributions were obtained for particles with $|\eta| < 2.5$ and one of the following p_T intervals: $0.3 < p_T < 3.0$ GeV, $p_T > 0.2$ GeV, $p_T > 0.4$ GeV or $p_T > 0.6$ GeV. These distributions were split up into percentiles to find to which event class based on $N_{\rm ch}^{\rm sel}$ a given event belongs. The purpose of this grouping of events is [153] to study the dependence of the azimuthal flows on the centrality classes in events of different "types": with more or less soft particles. In this way, we can compare the magnitude of the signal in "central" events with a different fraction of particles with large p_T.

To plot the results in a unified way for event classifications with different p_T selections, we correlate $N_{\rm ch}^{\rm sel}$ with the charged particle multiplicity $N_{\rm ch}$ calculated for particles with $|\eta| < 2.5$ and $p_T > 0.4$ GeV. We find the mean $\langle N_{\rm ch} \rangle$ for every event class based on $N_{\rm ch}^{\rm sel}$ and plot it along the X-axis to represent the results for cumulants. Thus, the results for each event class will be grouped in correspondence with the class defined by some value of $\langle N_{\rm ch} \rangle$. It means that, for example, 4 different values of $\langle N_{\rm ch} \rangle$ will correspond to 5% of the most central events defined by 4 different methods of grouping events by p_T.

3.7.3 Model results with momentum loss, but without particle boosts

In this subsection, we verify whether the introduced momentum loss of particles in the string medium (Sec. 3.5.2) will provide us with the sufficient effect of azimuthal anisotropy of particles. Calculations were performed for one million generated events.

In Fig. 3.5, the model result for the two-particle angular correlation function, $C(\Delta\eta, \Delta\phi)$, Eq. (0.0.10), calculated for particles with $|\eta| < 2.5$ and $0.3 < p_T < 3.0$ GeV, is presented for the $0 - 10\%$ event class based on the multiplicity $N_{\rm ch}^{\rm sel}$ of particles with $|\eta| < 2.5$ and $p_T > 0.2$ GeV. One can see the prominent peak at $\Delta\phi \approx 0$, $\Delta\eta \approx 0$, and the extended structure along $\Delta\eta \approx 0$ that come from the decays of the ρ-resonances [154]. However, there is no near-side ridge structure visible in the presented $C(\Delta\eta, \Delta\phi)$.

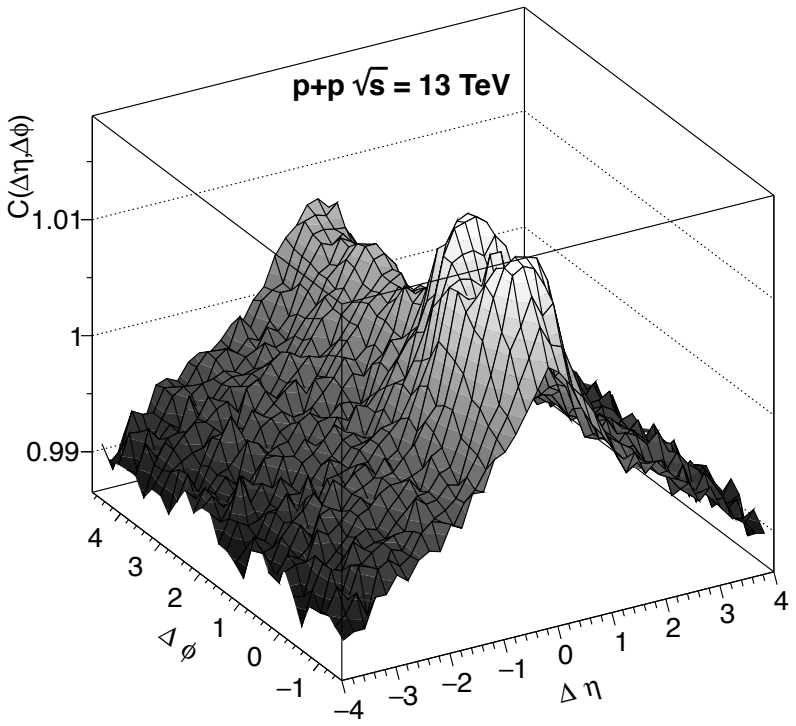

Figure 3.5: Model results for the two-particle correlation function, $C(\Delta\eta, \Delta\phi)$, calculated for particles with $|\eta| < 2.5$ and $0.3 < p_T < 3.0$ GeV and presented for event class with particle selection $p_T^{\rm cent} > 0.2$ GeV and $\langle N_{\rm ch}\rangle \approx 53$ for inelastic $p+p$ interactions at $\sqrt{s} = 13$ TeV.

Fig. 3.6, shows $c_2\{2\}$ (first row, left) and $c_2\{2\}_{(2\text{subs})}$ (second row, left), calculated for the particles with $|\eta| < 2.5$ and $0.3 < p_T < 3.0$ GeV, as functions of $\langle N_{\rm ch}\rangle$ (see the legend for the definition of $N_{\rm ch}^{\rm sel}$ that was correlated with $N_{\rm ch}$).

We remind the reader that to find $v_2\{2\}$ from $c_2\{2\}$ the latter must be positive. Thus, $v_2\{2\}$, Eq. (0.0.12), is a proxy for the elliptic flow harmonic that will coincide with the true v_2 from Eq. (3.7.1) at $n = 2$ in the absence of non-flow contributions. That is why there are so few extracted values of $v_2\{2\}$ (Fig. 3.6, first row, right) and that is why it is impossible to draw any meaningful conclusion even about $v_2\{2\}$ dependence on $\langle N_{\rm ch}\rangle$, except for the absolute values. Model results with negative $c_2\{2\}$ at low $\langle N_{\rm ch}\rangle$ (Fig. 3.6, first row, left) coincide with the observed change in sign from positive to negative for $c_2\{4\}$ in Ref. [153]. This behaviour, in general, demonstrates that contributions from non-flow correlations remain in $c_2\{2\}$. To get rid of them, it was proposed [88] to study cumulants in subevents separated in rapidity. Thus, by introducing a pseudorapidity gap, $\Delta\eta$, between particles with ϕ_1 and ϕ_2, one can eliminate the short-range correlations (coming, for instance, from resonance decays, jets, and momentum conservation laws) and measure $c_2\{2\}_{(2\text{subs})}$ and the corresponding $v_2\{2\}_{(2\text{subs})}$.

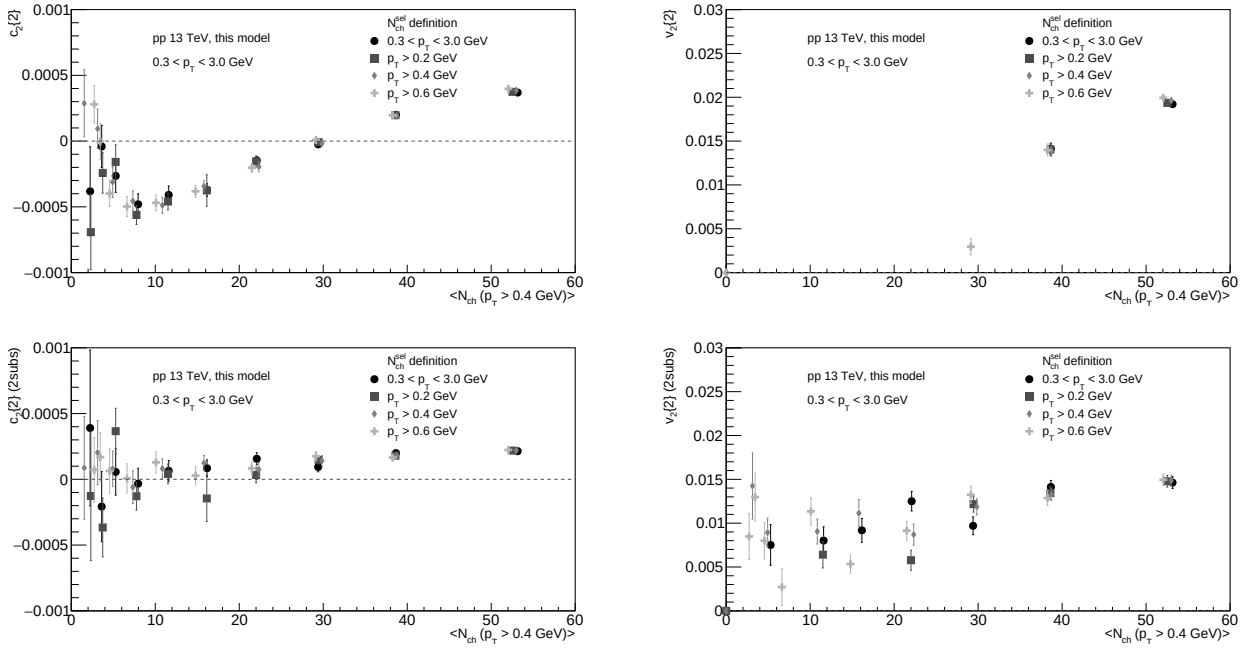

Figure 3.6: Model results for 2-particle cumulants $c_2\{2\}$ (**first row, left**) and $c_2\{2\}_{(2\text{subs})}$ (**second row, left**) and second flow harmonics $v_2\{2\}$ (**first row, right**) and $v_2\{2\}_{(2\text{subs})}$ (**second row, right**) calculated for particles with $0.3 < p_T < 3.0$ GeV and presented as functions of $\langle N_{\text{ch}} \rangle$ estimated for different event selection based on particles' p_T^{cent} for inelastic $p + p$ interactions at $\sqrt{s} = 13$ TeV.

Model values of $c_2\{2\}_{(2\text{subs})}$ (Fig. 3.6, second row, left) are much closer to the positive once, which can be interpreted as the partial suppression of the correlations from ρ decay [154]. Here, the two-subevent method shows its advantage although the statistical uncertainties increase. However, the comparison of model plot in Fig. 3.6, second row, left with the ATLAS result for $c_2\{2\}$ with η-gap (see Ref. [153], Fig.4, upper right plot) reveals that the magnitude of the model transverse flow is too low. Moreover, all plots in Fig. 3.6 show no dependence on p_T^{cent} within the statistical errors in contrast to the experimental results [155] meaning that the model lacks the p_T dependence of particles' flows. In addition, the experimentally obtained values of $v_2\{2\}_{(2\text{subs})} \approx 0.05$ shown in Ref. [155] are larger than the model results (Fig. 3.6, second row, right). We note that the main point of the ATLAS paper [155] is that $c_2\{4\}_{(2,3\text{subs})}$ should be measured instead of $c_2\{2\}$, however, in our current model implementation the values of $c_2\{4\}_{(2,3\text{subs})}$ are consistent with zero.

The result obtained in the developed model at this stage suggests that although accounting for momentum loss in the string medium is important in the study of azimuthal anisotropies of produced particles, it is insufficient to describe the ob-

served phenomena. This statement somewhat contradicts the results of the original approach, Refs. [147, 148], and an interesting analogy with the azimuthal "escape" of partons in transport models [145]. A natural candidate for increasing the signal of azimuthal correlations is to introduce additional particle boosts from the motion of overlapping strings that was described in Sec. 3.5.1. The next section presents model results with these two mechanism simultaneously switched on.

3.7.4 Model results for $C(\Delta\eta, \Delta\phi)$ with both momentum loss and particle boosts.

In this subsection, the results are presented for the full configuration of the most recent model version: it includes particles' boosts from the fused strings and the loss of particle momentum in the string medium. Calculations were performed for ten million generated events.

In Fig. 3.7, the result for the two-particle angular correlation function, $C(\Delta\eta, \Delta\phi)$, Eq. (0.0.10), calculated for particles with $|\eta| < 2.5$ and $0.3 < p_T < 3.0$ GeV, is presented for the $0 - 10\%$ event class based on the multiplicity $N_{\rm ch}^{\rm sel}$ of particles with $|\eta| < 2.5$ and $p_T > 0.6$ GeV.

Remarkably, the shape of $C(\Delta\eta, \Delta\phi)$ in Fig. 3.7, left contains a near-side ridge at $\Delta\phi \approx 0$ extended over the entire presented $\Delta\eta$ range in contrast to the result without particle boosts in Fig. 3.5. This structure indicates emission of particles in narrowly collimated azimuthal directions in wide $\Delta\eta$ range. In the model framework, this structure is created by particles produced from the boosted string cluster that is of elongated shape in rapidity.

The right-hand side of the Fig. 3.7 contains the schematic explanations of the correlation structures in $C(\Delta\eta, \Delta\phi)$. The bottom picture (Fig. 3.7, right) corresponds to the particle emission at $\Delta\eta \approx 0$, $\Delta\phi \approx 0$. The prominent peak at $\Delta\phi \approx 0$, $\Delta\eta \approx 0$, and the extended structure along $\Delta\eta \approx 0$ (Fig. 3.7, left) are similar to those obtained in the model without particle boosts (Fig. 3.5). These structures again come from the decays of the ρ-resonances [154]. However, the relative height of $\Delta\phi \approx 0$, $\Delta\eta \approx 0$ peak is greater because of the possible higher boost of ρ in Fig. 3.7. In other words, if ρ-resonances were greatly boosted by the cluster of strings, then the decay products (two charged pions) will give contribution to $\Delta\phi \approx 0$, $\Delta\eta \approx 0$ resulting in the enhanced peak. Otherwise, if ρ was "slow", then

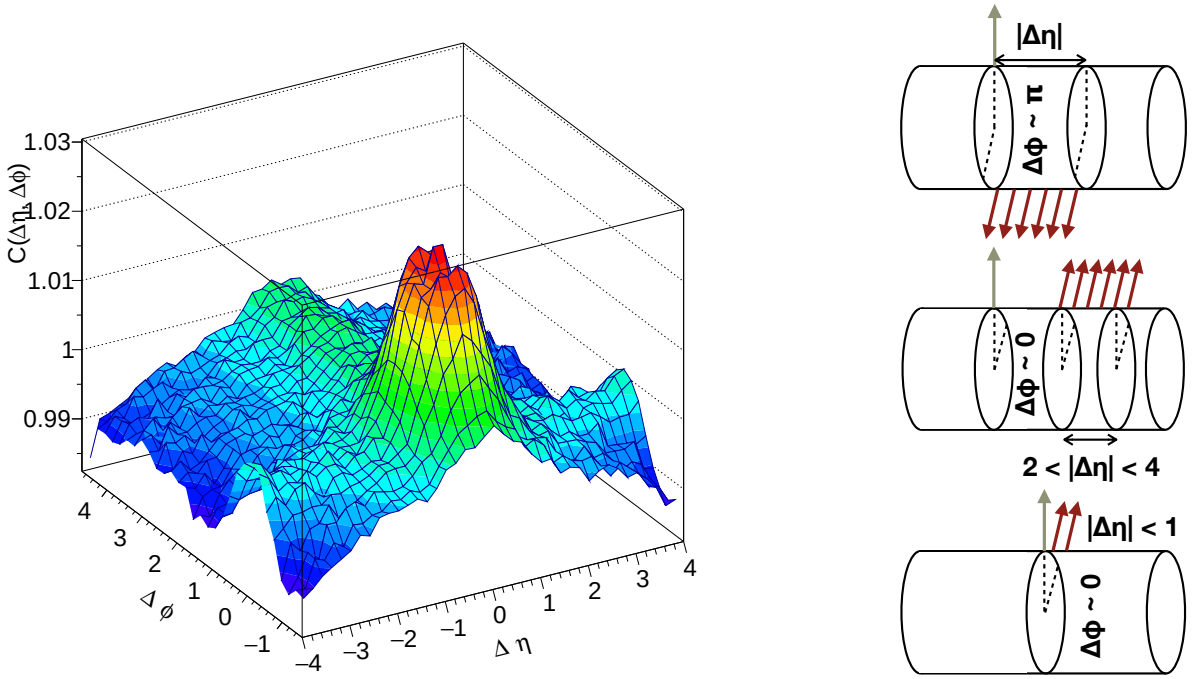

Figure 3.7: Left: Model result for the two-particle correlation function, $C(\Delta\eta, \Delta\phi)$, calculated for particles with $|\eta| < 2.5$ and $0.3 < p_T < 3.0$ GeV and presented for event class $0 - 10\%$ based on charged particles multiplicity $N_{\rm ch}^{\rm sel}$ within particle selection $|\eta| < 2.5$ and $p_T > 0.6$ GeV for inelastic $p + p$ interactions at $\sqrt{s} = 13$ TeV. **Right:** a schematic explanation of the observed $\Delta\eta - \Delta\phi$ correlations.

pions will fly apart at any larger azimuthal angles (all available $\Delta\phi$ is covered by this structure, $\Delta\phi = \pi$ as a limit for the decay products of ρ at rest).

The middle picture on the right-hand side of the Fig. 3.7 explains the near-side ($\Delta\phi = 0$, $\Delta\eta > 2$) ridge (Fig. 3.7, left). The observation of this structure means that there is a production of particles with close ϕ at very different η. This fits well with the picture of the creation of particles by extended in rapidity segments of colour strings that were boosted due to string fusion. Thus, the particles produced inside some rapidity interval fly in the transverse direction defined by the 2D momentum vector of this string segment. It means that the larger the string overlap in some region is, the larger the boost that particles will obtain from it is, the larger the contribution to the near-side ridge it will give. As it was stated above, the transverse dynamics of strings considered till $\tau_{\rm deepest}$ results in the creation of the compact "hot-spot" (Fig. 3.1, second column) in each event (regardless the number of strings), different up to some statistical fluctuations, which enhances the azimuthal correlations of particles.

It must be added that in the data [23, 24, 156], there is another structure in the two-particle angular correlation function, called the away-side ridge. It corresponds to the enhanced back-to-back particle production ($\Delta\phi \approx \pi$) at all possible $\Delta\eta$ and contains contributions from both particles' flow and conservation laws. The upper picture on the right-hand side of the Fig. 3.7 gives the graphical interpretation of this structure. However, Fig. 3.7, left, shows that the away-side ridge is absent in our current model result.

The obtained model topology of the two-particle angular correlation function (Fig. 3.7, left) can be explained as follows. First, it is the formation of very dense particle-producing string cluster that appears due to the active strings overlaps and fusion (see the red hot-spot for all rows in the second column in Fig. 3.1). This cluster of many fused strings produces particles in the single preferred direction resulting in $\Delta\phi \approx 0$. In the meantime, the peripheral area of events (is shown in green and surrounds the red hot-spot, second column in Fig. 3.1) seems to be to scarce to produce enough particles in the multi-directions and to form the away-side ridge. The obtained transverse distributions of the strings density in an event (Fig. 3.1, second column) resemble the characteristic core-corona picture [157]. In the model language, it is the time of the string system evolution in the transverse plane that tightly controls a degree of core-corona separation.

3.7.5 Model results for cumulants with both momentum loss and particle boosts.

Fig. 3.8 shows the new model results for $c_2\{2\}$ (first row), Eq. (0.0.11), and $v_2\{2\}$ (second row), Eq. (0.0.12), calculated for particles with $|\eta| < 2.5$ and $0.3 < p_T < 3.0$ GeV, as functions of $\langle N_{\rm ch}\rangle$. Calculations were performed for ten million generated events. This gives us access to event classes of smaller width than in section 3.7.3, thus, we can eliminate the admixture of events with other multiplicities and get more "pure" results. In Fig. 3.8, the results are presented for event classes of a 0.5% width of the $N_{\rm ch}^{\rm sel}$ distribution calculated for different event classifications based on p_T (the same procedure as in Figs. 3.6).

Since the fluctuations are too large for classes of 0.5% width at low $\langle N_{\rm ch}\rangle$, we limit $\langle N_{\rm ch}\rangle$ to start from ~ 40. Here, the values of $c_2\{2\}$ are positive and show an increase towards high-multiplicity collisions. One can see that the values of $c_2\{2\}$

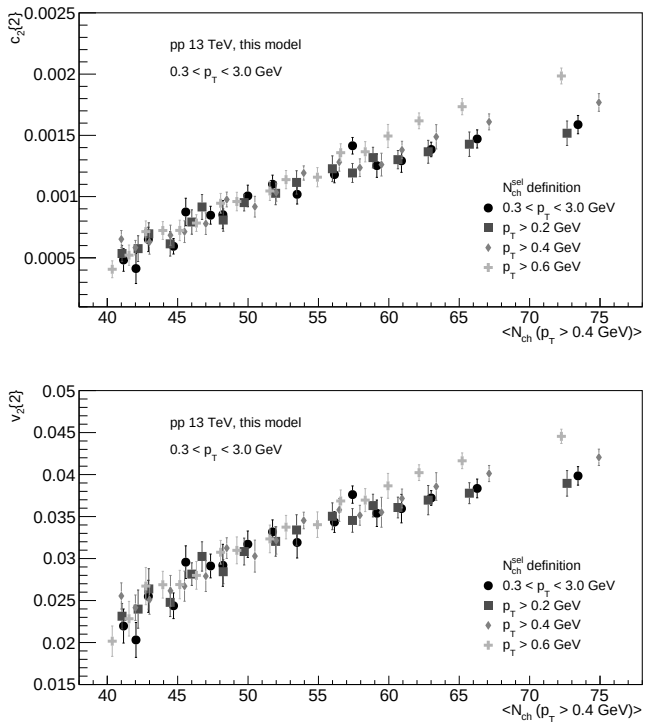

Figure 3.8: Model results for two-particle cumulant, $c_2\{2\}$, (**first row**) and the corresponding second flow harmonic, $v_2\{2\}$, (**second row**) calculated for particles with $0.3 < p_T < 3.0$ GeV and $|\eta| < 2.5$ and presented as a function of $\langle N_{\rm ch} \rangle$ estimated for different event selections of 0.5% width of $N_{\rm ch}^{\rm sel}$ distribution calculated for particles with different p_T (indicated in the legend) and $|\eta| < 2.5$ for inelastic $p + p$ interactions at $\sqrt{s} = 13$ TeV.

with particle boosts (Fig. 3.8, first row) are approximately four-times larger at high $\langle N_{\rm ch} \rangle$ than the values of $c_2\{2\}$ obtained without particle boosts (Fig. 3.6, first row, left). The associated second flow harmonic, $v_2\{2\}$, (Figs. 3.8, second row) repeats this behaviour. We interpret it as follows.

The transverse motion of strings, considered up to time $\tau_{\rm deepest}$, which corresponds to the maximum degree of their overlaps and fusion, results in the formation of special event geometry: for a fixed number of strings events look similar but may be rotated. Therefore, the magnitudes of particle boosts are very close since they are defined by the degree of strings' overlaps. As the number of strings increases, the average boost becomes stronger since the degree of overlap is higher in the "hot-spot" of an event. Thus, the string fusion plays a more significant role with the increased string density and both momentum quenching and boosting of particles lead to a greater signal of azimuthal flow at large $\langle N_{\rm ch} \rangle$. Finally, each event is characterised by the finite v_2 but, since their configurations are very similar, even after averaging

over events v_2 is not zero.

It is important to note that model results can be compared only with the experimental data in which the non-flow contributions (that are much richer than the ρ resonance decay introduced to the model) were suppressed. It is, for example, the measured $c_2\{2\}$ with η-gap (see Ref. [153], Fig.4, upper right plot). To suppress the possible remaining contributions from ρ decays in the model (as the only source of the non-flow correlations) we apply the aforementioned procedure [88] and calculate $c_2\{2\}_{(2\text{subs})}$ and corresponding $v_2\{2\}_{(2\text{subs})}$ in two-subevents separated in pseudorapidity (see Fig. 3.9).

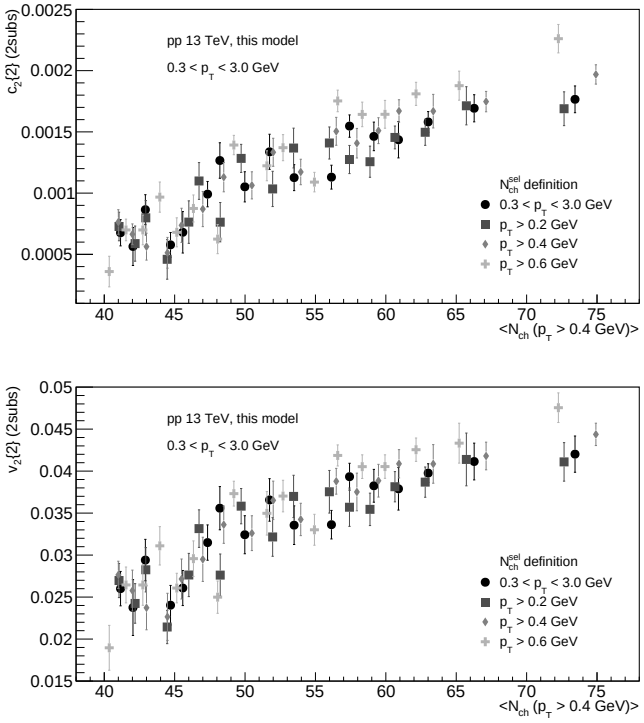

Figure 3.9: Model results for two-particle cumulant, $c_2\{2\}_{(2\text{subs})}$, (**first row**) and the corresponding second flow harmonic, $v_2\{2\}_{(2\text{subs})}$, (**second row**) calculated by two-subevent method for particles with $0.3 < p_T < 3.0$ GeV and $-2.5 < \eta < -0.83$ or $0.83 < \eta < 2.5$ and presented as functions of $\langle N_{\text{ch}} \rangle$ estimated for different event selections of 0.5% width of $N_{\text{ch}}^{\text{sel}}$ distribution calculated for particles with different p_T (indicated in the legend) and $|\eta| < 2.5$ for inelastic $p+p$ interactions at $\sqrt{s} = 13$ TeV.

Fig. 3.9 presents $c_2\{2\}_{(2\text{subs})}$ (first row) and $v_2\{2\}_{(2\text{subs})}$ (second row) calculated in the two-subevent method [88] for particles with $0.3 < p_T < 3.0$ GeV and $-2.5 < \eta < -0.8$ or $0.8 < \eta < 2.5$. One can see that $c_2\{2\}_{(2\text{subs})}$ and $v_2\{2\}_{(2\text{subs})}$ repeat the behaviour of $c_2\{2\}$ and $v_2\{2\}$ from Fig. 3.8 reaching the slightly higher values. Thus,

we assume that the two-subevent method indeed eliminated some of the remaining impact of the ρ-resonance decays, even though its usage requires larger statistics of simulated events.

ATLAS results for $c_2\{2\}$ with η-gap (see Ref. [153], Fig.4, upper right plot) show almost constant value of ≈ 0.003 for $\langle N_{\rm ch}\rangle$ from 0 till 180. The largest model values reaches $c_2\{2\}_{(2\rm subs)} \approx 0.002$ for events with the highest $\langle N_{\rm ch}\rangle \approx 75$ in the considered event classes of 0.5% width. The available statistics of our model (~ 10 mln events) stops us from analysing cumulants in narrower event classes (0.1% or 0.05%), which does not allow us to perform one-to-one comparison with the ATLAS data [153]. However, if one extrapolates model result to the event classes with higher $\langle N_{\rm ch}\rangle$ it is very likely that ATLAS limit will be reached.

On the scale presented in Ref. [153], Fig.4, upper right plot, it is difficult to estimate the growth of $c_2\{2, |\Delta\eta| > 2\}$ with $\langle N_{\rm ch}\rangle$ measured by ATLAS. However, a dependence similar to our model findings was presented by ALICE (see preliminary results in Ref. [158]). It is the two-particle correlation, $\Upsilon(\Delta\phi)$, integrated over rapidity, that grows with the event multiplicity. The results of ALICE are also presented for the near-side ridge, but they differ in particle selection, which also does not allow a direct numerical comparison with our model results, but only a qualitative comparison.

At large $\langle N_{\rm ch}\rangle$ in Fig. 3.8 and Fig. 3.9, one can see a slight splitting of the results with different $N_{\rm ch}^{\rm sel}$ definitions. The primary goal of the analysis with the different p_T selections is to test the sensitivity of the azimuthal flow to particles' transverse momenta. To see it more clearly, we plot (Fig. 3.10) the p_T dependence of two-particle cumulants, $c_2\{2\}$ and $c_2\{2\}_{(2\rm subs)}$, for $0-5\%$ event class of $N_{\rm ch}^{\rm sel}$ distribution based on particles with $0.3 < p_T < 3.0$ GeV and $|\eta| < 2.5$. To achieve a similar number of particles for all model points, we perform the calculation of cumulants in p_T intervals of the varying sizes.

Fig. 3.10 shows that $c_2\{2\}$ and $c_2\{2\}_{(2\rm subs)}$ values gradually increase as the functions of the momentum of particles that are used in their calculations. This is in qualitative agreement with the ATLAS results [153] showing a similar behaviour. An important remark is that the model results without particle boosts showed no dependence on p_T (Fig. 3.6, no dependence on the p_T selection for $N_{\rm ch}^{\rm sel}$).

In the full model workflow, the p_T-behaviour of $c_2\{2\}$ and $c_2\{2\}_{(2\rm subs)}$ (Fig. 3.10)

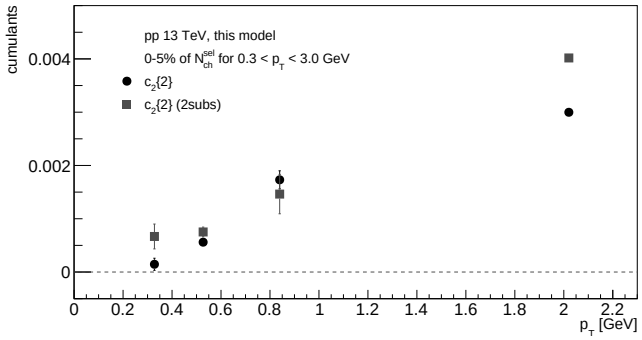

Figure 3.10: Model results for two-particle cumulants, $c_2\{2\}$ and $c_2\{2\}_{(2\text{subs})}$, as functions of p_T of particles used in their calculations presented for $0-5\%$ event class based on $N_{\text{ch}}^{\text{sel}}$ distribution calculated for particles with $0.3 < p_T < 3.0$ GeV, $|\eta| < 2.5$ for inelastic $p+p$ interactions at $\sqrt{s} = 13$ TeV.

can be explained as follows. First of all, the introduced mechanism of momentum quenching of particles in the string medium produces larger anisotropy for particles with higher p_T. It is because it becomes increasingly more difficult for particle to escape the string matter while saving sufficiently large transverse momentum. In turn, string-string interaction and their consequent boosts in the transverse plane increase the p_T of correlated particles, leading to larger anisotropy from these boosts.

To summarise, the model results obtained for the second order two-particle cumulants are in qualitative agreement with ALICE and ATLAS data for inelastic $p+p$ interactions at $\sqrt{s} = 13$ TeV.

3.8 Discussion

In this Chapter, we extended the developed model of interacting colour strings finite in rapidity with the advanced mechanisms of "string-string" and "string-particle" interactions to address the challenging question of the origin of the collective azimuthal particles' flows observed in inelastic proton-proton interactions.

In the developed model, an event picture prior to hadronisation looks like a highly inhomogeneous string medium (see Fig. 3.1, second column and Fig. 3.2, second and fourth columns). Originating from the multi-pomeron exchange, the system of particle-producing strings is disordered by the longitudinal and transverse dynamics of the system. For clarity, we repeat below the transverse plane projection of the rare event with 74 strings (Fig. 3.11).

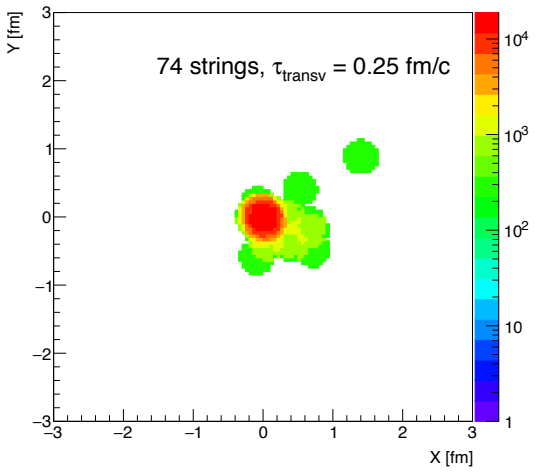

Figure 3.11: A simulated event with 74 strings. The figure shows the projection of the 3D string density to the transverse plane, $X - Y$ after the transverse evolution during $\tau_{\text{transv}} = \tau_{\text{deepest}}$, indicated on the plot.

One observes (Fig. 3.11 as well as Fig. 3.1, second column and Fig. 3.2, second and fourth columns) the peculiar grouping of strings in the mixed configuration-momentum space. Some of them are isolated forming the debris of $p+p$ interaction. Others partially overlap, while the most "lucky" ones form a dense cluster of strings, overlapping to the highest degree (red hot-spot). It is the presence of such a core that determines the crucial collective features of the soft particle production in $p+p$ collisions. In particular, in the model, the particle anisotropy appears due to this complex configuration of strings and string clusters in an event, and additionally due to the effect of particle momentum quenching.

Thus, we observe a recognisable core-corona picture of the string system [157]. It is the interplay of these two characteristic event regions that defines the properties of azimuthal correlations in the model. Namely, in the corona region it is only the loss of particle's momentum that plays a role. On the other hand, the impact of the complex core structure is more difficult to deduce. Its low occupancy regions create correlated multi-directional particle boosts, while the "hottest" region determines a single dominant direction and, therefore, strongly boosts particles with $\Delta\phi \approx 0$.

The model result for the angular correlation function, $C(\Delta\eta, \Delta\phi)$, reveals the characteristic near-side ridge that is formed by the collimated emission of particles, boosted by the clusters of strings.

On the other hand, the away-side ridge is missing from the model results. We

interpret that as due to an excessive approach of strings at the τ_{deepest} moment, which results in the formation of the over-condensed string region. In this case, the production of particles with $\Delta\phi \approx \pi$ separation in the model framework with p_T boost should come from the peripheral, low-occupancy parts of the core. It seems that, in the current implementation, this area is too scarce to create the away-side ridge. A similar observation was made in Ref. [159], where the absence of the away-side ridge was caused by the difficulties in defining the cutoff between the core and corona.

The model results for the second order two-particle cumulants are in qualitative agreement with ALICE and ATLAS data for inelastic $p+p$ interactions at $\sqrt{s} = 13$ TeV. In future studies, the higher statistics (about 1000 times more than it is now) will be needed to calculate multi-particle cumulants and to access high-multiplicity events. The azimuthal flow signal obtained in the model grows with the transverse momentum of particles in high-multiplicity events. This reflects its origin from the azimuthal correlations between particles produced by the interacting strings.

Conclusion

This dissertation presents a step-by-step development of the Monte-Carlo model of interacting colour strings of finite length in rapidity aimed to describe particle correlations at the LHC energies.

The development and application of the non-perturbative approaches in high-energy physics is dictated by the inability to use the QCD methods to describe the multi-particle production in the soft part of the spectrum in hadron collisions. One of the successful approaches is based on the concept of formation of colour strings between colliding partons that fragment into observable hadrons. This approach appeared to be effective both in phenomenological calculations and as the basis of many Monte-Carlo event generators.

This thesis proposes to extend the colour string approach by taking into account in detail the initial stages of collisions, that is, the formation of finite and inhomogeneous string density in configuration-momentum space. This enriches the structure of the particle-emitting medium, but it ceases to be translationally invariant [130]. Nevertheless, the developed model reproduces the experimentally observed plateau of the distribution of the number of particles at midrapidity, which emphasises the importance of the study of correlations, differentially in rapidity, to reveal the intrinsic structure of the system of particle sources.

The additional novelty of the present work is in the simultaneous consideration of the fusion of overlapping colour strings, which not only changes the characteristics of particle production for string clusters, but also creates azimuthally correlated particle yields. This study is motivated by the unexpected experimental evidence of the collectivity observed in proton-proton collisions at the LHC, which challenges the accepted paradigm of "triviality" of proton-proton interactions compared to nucleus-nucleus ones.

It is interesting to draw parallels between the latest, most complete, version of

our model and the event generators also based on colour string fragmentation such as EPOS4 [35] and PYTHIA [36]. The core concept of our model is the description of $p + p$ inelastic interaction via the multi-pomeron exchange, which resembles the parallel scatterings of partons that occur in EPOS4. The way we find momenta of string end-points combines ideas of energy-momentum sharing and saturation implemented in EPOS4. All this is strikingly different from the idea of hard scattering that is a starting point of multi-parton interactions in PYTHIA. The concept that has not been realized in any existing event generator is the transverse dynamics of strings [59] caused by their attraction is introduced in our model. It changes the three-dimensional string density in the event and leads to the clustering of particle sources. Taking into account the fusion of overlapped strings forms a string hot-spot in an event, which is analogous to the formation of core in EPOS4. Also the idea of formation of the fused particle source with higher tension is realised in PYTHIA by the rope-mechanism. Finally, in EPOS4 evolution of the core is considered in hydro-regime, which results in azimuthal flow signal. In the presented model, the sources of azimuthal anisotropy of the produced particles are particle boosts from partially overlaped and fused strings (similar to the effect of the string shoving mechanism in PYTHIA) and particle momentum losses in the string medium.

The main results that were obtained in the developed approach and presented in this dissertation:

1. In the simplified model without short-range correlations introduced, taking into account the finiteness of strings in rapidity leads to the decrease of the correlation coefficient $b_{\rm corr}[N_F, N_B]$ and increase of the strongly intensive quantity $\Sigma[N_F, N_B]$ with increasing rapidity distance, Δy, between rapidity acceptances, where multiplicities N_F and N_B are calculated. This behaviour competes with the possible contribution from the short-range correlations, earlier shown in other authors' string models, that also decreases $b_{\rm corr}[N_F, N_B]$ and increases $\Sigma[N_F, N_B]$ with Δy. As it is shown, by considering both mechanisms separately, one can obtain a fair description of the experimental data, which makes an arbitrary selection of one of these scenarios illegitimate. Thus, this thesis proves that the rapidity dependent background of long-range correlations, determined solely by fluctuations in the number of strings in forward and backward rapidity acceptances, is an important ingredient of the proper

representation of correlations to be performed in future studies.

2. In the simplified model without short-range correlations introduced, taking into account both the finiteness of strings in rapidity and fusion of strings overlapped in 3D configuration-momentum space leads to the decrease of strongly intensive quantity $\Sigma[N_F, N_B]$ in comparison to its values calculated for free strings. On the one hand, this contradicts the results earlier obtained in other authors' models with infinite strings and short-range correlations. On the other hand, this is consistent with the experimental observations of the decrease of $\Sigma[N_F, N_B]$ for more central nucleus-nucleus collisions, thus, for more dense string states. Based on the comparison of results of this dissertation and of the mentioned models, it can be assumed that simultaneously taking into account both the finiteness of strings in rapidity and short-range correlations will give a resulting decrease in $\Sigma[N_F, N_B]$ with string fusion in $A + A$ collisions. Moreover, it is anticipated that in $p + p$ data the leading contribution will be still defined by the short-range correlations that provide the increase of $\Sigma[N_F, N_B]$ with string fusion for more "central" events, as in data. However, taking into account the contribution from the finiteness of strings in rapidity will modify it. Thus, this point supports the previous statement and speaks in favour of the possibility to develop a model that simultaneously takes into account these two mechanisms.

3. In the elaborated model with finite in rapidity strings, taking into account the transverse dynamics of strings, caused by their attraction, and formation of string clusters due to their fusion leads to the proper description of the behaviour of $\langle p_T \rangle - N$ correlation function observed in $p + p$ interactions at high energies. The thesis shows that it is the regime with the highest degree of strings' overlap, reached at τ_{deepest}, that describes the slope of $\langle p_T \rangle - N$.

4. The analytical relation of strongly intensive quantity $\Sigma[N_F, N_B]$ to cumulants, factorial cumulants and asymmetry coefficient of $N_F - N_B$ distribution is shown in this dissertation. This finding enriches the understanding of the property of strong intensity by expanding the class of observables that are robust to trivial volume fluctuations. The thesis demonstrates that to probe the forward-backward correlations and fluctuations, it is sufficient to study

only one of the indicated quantities. However, adding the correlation coefficient to the analysis is beneficial as it provides complementary information on $\langle N_B(N_F)\rangle$.

5. In the elaborated model with limited in rapidity strings, taking into account the 3D dynamics of string density, the effect of string fusion is shown to modify the values of the correlation coefficient $b_{\rm corr}[N_F, N_B]$ and strongly intensive quantities $\Sigma[N_F, N_B]$, $\Sigma[P_T, N]$ and $\Delta[P_T, N]$ in the same manner as the Colour Reconnection mechanism used in PYTHIA event generator. The observed consistency of both approaches, that are based on different ideas but either addresses the transition of a string system to an energetically more favourable state, with experimental behaviour makes them strong alternatives.

6. In the advanced model with limited in rapidity strings, taking into account the 3D dynamics of string density and string fusion that additionally boosts produced particles in the transverse dimension and affects their losses of momenta in the inhomogeneous string environment, the results on the azimuthal anisotropies of particle production are obtained. The thesis findings of the near-side ridge structure in the two-particle angular correlation function correspond to the ATLAS observation of the striking signal of collectivity in high-multiplicity $p + p$ collisions. Calculated two-particle cumulants qualitatively describe the experimental increase of azimuthal correlations with event multiplicity and transverse momentum of particles.

7. This thesis demonstrates that the proper time of the transverse evolution of the system of strings in an event, dynamically defined from the initial 3D string configuration, appeared to be the major parameter that controls the separation of core-corona regions of string density corresponding to the significantly different regimes of particle production in the model.

Summarising the results of the dissertation, it is necessary to emphasise that this study manifests the possibility to describe many collective effects seen in proton-proton interactions at high energies in the framework of the phenomenological model of interacting colour strings limited in rapidity. The obtained results on rapidity-azimuthal correlations make the proposed mechanism of particle boosts arising from

string fusion a competitor to the frequently used hydrodynamic description. It is important to mention that the model can be refined in all directions outlined in this dissertation. The modular structure of the Monte-Carlo workflow allows each mechanism to be developed separately, which increases the flexibility of the proposed approach. The possible comparison of the results obtained in the more sophisticated model will allow us to draw more solid conclusions about the properties of particle sources and the types of their interactions, thus, to improve our knowledge about the physical processes that determine the strong interaction. In the future, the developed model can be used to obtain predictions at the energies of the NICA collider and to be generalised to the description of nucleus-nucleus collisions.

List of abbreviations and designations

RHIC	Relativistic Heavy Ion Collider
LHC	Large Hadron Collider
QGP	Quark-Gluon Plasma
QCD	Quantum Chromodynamics
CERN	Conseil Européen pour la Recherche Nucléaire
SPS	Super Proton Synchrotron
ALICE	A Large Ion Collider Experiment
EPOS	Energy-conserving quantum mechanical multiple scattering approach, based on Partons (parton ladders), Off-shell remnants, and Splitting of parton ladders
HIJING	Heavy Ion Jet INteraction Generator
AMPT	A Multi-Phase Transport
QED	Quantum Electrodynamics
NICA	Nuclotron-based Ion Collider fAcility
ATLAS	A Toroidal LHC ApparatuS
CPU	Central Processing Unit
2D, 3D	2-, 3-dimensional
F-B	Forward-Backward
PDF	Parton Distribution Function
CTEQ	Coordinate Theoretical-Experimental Project on QCD
CT10nnlo	CTEQ version 10 next-to-next-to-leading order
LHAPDF	Les Houches Accord Parton Density Functions
PDG	Particle Data Group
TPC	Time-Projection Chamber
CR	Colour Reconnection

Bibliography

[1] Shuryak E. V. Theory of Hadronic Plasma // Sov. Phys. JETP. — 1978. — Vol. 47. — P. 212–219.

[2] Gross D. J., Wilczek F. Ultraviolet Behavior of Nonabelian Gauge Theories // Phys. Rev. Lett. — 1973. — Vol. 30. — P. 1343–1346.

[3] Politzer H. D. Reliable Perturbative Results for Strong Interactions? // Phys. Rev. Lett. — 1973. — Vol. 30. — P. 1346–1349.

[4] Busza W., Rajagopal K., van der Schee W. Heavy Ion Collisions: The Big Picture, and the Big Questions // Ann. Rev. Nucl. Part. Sci. — 2018. — Vol. 68. — P. 339–376.

[5] Cooper F., Frye G. Comment on the Single Particle Distribution in the Hydrodynamic and Statistical Thermodynamic Models of Multiparticle Production // Phys. Rev. D. — 1974. — Vol. 10. — P. 186.

[6] Heinz U. W., Jacob M. Evidence for a new state of matter: An Assessment of the results from the CERN lead beam program. — 2000. — 1. — nucl-th/0002042.

[7] Arsene I. et al. Quark gluon plasma and color glass condensate at RHIC? The Perspective from the BRAHMS experiment // Nucl. Phys. A. — 2005. — Vol. 757. — P. 1–27.

[8] Back B. B. et al. The PHOBOS perspective on discoveries at RHIC // Nucl. Phys. A. — 2005. — Vol. 757. — P. 28–101.

[9] Adams J. et al. Experimental and theoretical challenges in the search for the quark gluon plasma: The STAR Collaboration's critical assessment of the

evidence from RHIC collisions // Nucl. Phys. A. — 2005. — Vol. 757. — P. 102–183.

[10] Adcox K. et al. Formation of dense partonic matter in relativistic nucleus-nucleus collisions at RHIC: Experimental evaluation by the PHENIX collaboration // Nucl. Phys. A. — 2005. — Vol. 757. — P. 184–283.

[11] Harris J. W., Muller B. The Search for the quark-gluon plasma // Ann. Rev. Nucl. Part. Sci. — 1996. — Vol. 46. — P. 71–107.

[12] Koch P., Muller B., Rafelski J. Strangeness in Relativistic Heavy Ion Collisions // Phys. Rept. — 1986. — Vol. 142. — P. 167–262.

[13] Gyulassy M., Plumer M. Jet Quenching in Dense Matter // Phys. Lett. B. — 1990. — Vol. 243. — P. 432–438.

[14] Wang X.-N., Gyulassy M. Gluon shadowing and jet quenching in A+A collisions at $\sqrt{s} = 200A$ GeV // Phys. Rev. Lett. — 1992. — Vol. 68. — P. 1480–1483.

[15] Sorge H. Elliptical flow: A Signature for early pressure in ultrarelativistic nucleus-nucleus collisions // Phys. Rev. Lett. — 1997. — Vol. 78. — P. 2309–2312.

[16] Csernai L. P., Rohrich D. Third flow component as QGP signal // Phys. Lett. B. — 1999. — Vol. 458. — P. 454.

[17] Demoulins M. et al. Measurement of a baryon azimuthal emission pattern in Ne + (NaF, Nb, Pb) collisions at 800-MeV per nucleon // Phys. Lett. B. — 1990. — Vol. 241. — P. 476–480.

[18] A New Component of the Collective Flow in Relativistic Heavy Ion Collisions / Gutbrod H. H., Kolb B. W., Schmidt H. R., Poskanzer A. M., Ritter H. G., and Kampert K. H. // Phys. Lett. B. — 1989. — Vol. 216. — P. 267–271.

[19] Voloshin S., Zhang Y. Flow study in relativistic nuclear collisions by Fourier expansion of Azimuthal particle distributions // Z. Phys. C. — 1996. — Vol. 70. — P. 665–672.

[20] Elliptic flow at SPS and RHIC: From kinetic transport to hydrodynamics / Kolb P. F., Huovinen P., Heinz U. W., and Heiselberg H. // Phys. Lett. B. — 2001. — Vol. 500. — P. 232–240.

[21] Adam J. et al. Enhanced production of multi-strange hadrons in high-multiplicity proton-proton collisions // Nature Phys. — 2017. — Vol. 13. — P. 535–539.

[22] Rafelski J., Muller B. Strangeness Production in the Quark-Gluon Plasma // Phys. Rev. Lett. — 1982. — Vol. 48. — P. 1066.

[23] Khachatryan V. et al. Observation of Long-Range Near-Side Angular Correlations in Proton-Proton Collisions at the LHC // JHEP. — 2010. — Vol. 09. — P. 091.

[24] Aad G. et al. Observation of Long-Range Elliptic Azimuthal Anisotropies in $\sqrt{s}$ =13 and 2.76 TeV pp Collisions with the ATLAS Detector // Phys. Rev. Lett. — 2016. — Vol. 116, no. 17. — P. 172301.

[25] Aaboud M. et al. Measurements of long-range azimuthal anisotropies and associated Fourier coefficients for pp collisions at $\sqrt{s} = 5.02$ and 13 TeV and p+Pb collisions at $\sqrt{s_{\mathrm{NN}}} = 5.02$ TeV with the ATLAS detector // Phys. Rev. C. — 2017. — Vol. 96, no. 2. — P. 024908.

[26] Weller R. D., Romatschke P. One fluid to rule them all: viscous hydrodynamic description of event-by-event central p+p, p+Pb and Pb+Pb collisions at $\sqrt{s} = 5.02$ TeV // Phys. Lett. B. — 2017. — Vol. 774. — P. 351–356.

[27] One fluid might not rule them all / Zhou Y., Zhao W., Murase K., and Song H. // Nucl. Phys. A. — 2021. — Vol. 1005. — P. 121908.

[28] Ambrus V. E., Schlichting S., Werthmann C. Establishing the Range of Applicability of Hydrodynamics in High-Energy Collisions // Phys. Rev. Lett. — 2023. — Vol. 130, no. 15. — P. 152301.

[29] Glasma flux tubes and the near side ridge phenomenon at RHIC / Dumitru A., Gelis F., McLerran L., and Venugopalan R. // Nucl. Phys. A. — 2008. — Vol. 810. — P. 91–108.

[30] Dual parton model / Capella A., Sukhatme U., Tan C.-I., and Tran Thanh Van J. // Phys. Rept. — 1994. — Vol. 236. — P. 225–329.

[31] Braun M., Pajares C. A Probabilistic model of interacting strings // Nucl. Phys. B. — 1993. — Vol. 390. — P. 542–558.

[32] Gelis F. Color Glass Condensate and Glasma // Int. J. Mod. Phys. A. — 2013. — Vol. 28. — P. 1330001.

[33] Gurvich E. G. The quark anti-quark pair production mechanism in a quark jet // Phys. Lett. B. — 1979. — Vol. 87. — P. 386–388.

[34] Casher A., Neuberger H., Nussinov S. Chromoelectric Flux Tube Model of Particle Production // Phys. Rev. D. — 1979. — Vol. 20. — P. 179–188.

[35] Werner K. Revealing a deep connection between factorization and saturation: New insight into modeling high-energy proton-proton and nucleus-nucleus scattering in the EPOS4 framework // Phys. Rev. C. — 2023. — Vol. 108, no. 6. — P. 064903.

[36] Sjöstrand T. The PYTHIA Event Generator: Past, Present and Future // Comput. Phys. Commun. — 2020. — Vol. 246. — P. 106910.

[37] Wang X.-N., Gyulassy M. HIJING: A Monte Carlo model for multiple jet production in p p, p A and A A collisions // Phys. Rev. D. — 1991. — Vol. 44. — P. 3501–3516.

[38] A multiphase transport model for nuclear collisions at RHIC / Zhang B., Ko C. M., Li B.-A., and Lin Z.-w. // Phys. Rev. C. — 2000. — Vol. 61. — P. 067901.

[39] Gribov V. N. A Reggeon diagram technique // Zh. Eksp. Teor. Fiz. — 1967. — Vol. 53. — P. 654–672.

[40] Chew G. F., Frautschi S. C. Principle of Equivalence for All Strongly Interacting Particles Within the S Matrix Framework // Phys. Rev. Lett. — 1961. — Vol. 7. — P. 394–397.

[41] Gribov V. N., Migdal A. A. Strong Coupling in the Pomeranchuk Pole Problem // Zh. Eksp. Teor. Fiz. — 1968. — Vol. 55. — P. 1498–1520.

[42] Gribov V. N., Migdal A. A. Properties of the pomeranchuk pole and the branch cuts related to it at low momentum transfer // Yad. Fiz. — 1968. — Vol. 8. — P. 1002–1015.

[43] Veneziano G. Regge Intercepts and Unitarity in Planar Dual Models // Nucl. Phys. B. — 1974. — Vol. 74. — P. 365–377.

[44] Veneziano G. Large N Expansion in Dual Models // Phys. Lett. B. — 1974. — Vol. 52. — P. 220–222.

[45] Veneziano G. Some Aspects of a Unified Approach to Gauge, Dual and Gribov Theories // Nucl. Phys. B. — 1976. — Vol. 117. — P. 519–545.

[46] Werner K. Strings, pomerons, and the VENUS model of hadronic interactions at ultrarelativistic energies // Phys. Rept. — 1993. — Vol. 232. — P. 87–299.

[47] Jets in Small p(T) Hadronic Collisions, Universality of Quark Fragmentation, and Rising Rapidity Plateaus / Capella A., Sukhatme U., Tan C., and Tran Thanh Van J. // Phys. Lett. B. — 1979. — Vol. 81. — P. 68–74.

[48] Kaidalov A. B. The Quark-Gluon Structure of the Pomeron and the Rise of Inclusive Spectra at High-Energies // Phys. Lett. B. — 1982. — Vol. 116. — P. 459–463.

[49] Artru X. Classical String Phenomenology. How Strings Work // Phys. Rept. — 1983. — Vol. 97. — P. 147.

[50] The Spectrum of Charmonium / Eichten E., Gottfried K., Kinoshita T., Kogut J. B., Lane K. D., and Yan T. // Phys. Rev. Lett. — 1975. — Vol. 34. — P. 369–372.

[51] Artru X., Mennessier G. String model and multiproduction // Nucl. Phys. B. — 1974. — Vol. 70. — P. 93–115.

[52] Bialas A. Fluctuations of string tension and transverse mass distribution // Phys. Lett. B. — 1999. — Vol. 466. — P. 301–304.

[53] Ferreres-Solé S., Sjöstrand T. The space–time structure of hadronization in the Lund model // Eur. Phys. J. C. — 2018. — Vol. 78, no. 11. — P. 983.

[54] Schwinger J. On gauge invariance and vacuum polarization // Phys. Rev. — 1951. — Vol. 82. — P. 664–679.

[55] Andersson B., Gustafson G., Soderberg B. A General Model for Jet Fragmentation // Z. Phys. C. — 1983. — Vol. 20. — P. 317.

[56] Belokurova S., Vechernin V. Long-Range Correlations between Observables in a Model with Translational Invariance in Rapidity // Symmetry. — 2020. — Vol. 12, no. 7. — P. 1107.

[57] Kaidalov A. B., Ter-Martirosian K. A. Pomeron as Quark-Gluon Strings and Multiple Hadron Production at SPS Collider Energies // Phys. Lett. B. — 1982. — Vol. 117. — P. 247–251.

[58] Iritani T., Cossu G., Hashimoto S. Partial restoration of chiral symmetry in the color flux tube // Phys. Rev. D. — 2015. — Vol. 91, no. 9. — P. 094501.

[59] Kalaydzhyan T., Shuryak E. Collective interaction of QCD strings and early stages of high multiplicity pA collisions // Phys. Rev. C. — 2014. — Vol. 90, no. 1. — P. 014901.

[60] Kalaydzhyan T., Shuryak E. Self-interacting QCD strings and string balls // Phys. Rev. D. — 2014. — Vol. 90, no. 2. — P. 025031.

[61] The confining color field in SU(3) gauge theory / Baker M., Cea P., Chelnokov V., Cosmai L., Cuteri F., and Papa A. // Eur. Phys. J. C. — 2020. — Vol. 80, no. 6. — P. 514.

[62] Johnson K. The M.I.T. Bag Model // Acta Phys. Polon. B. — 1975. — Vol. 6. — P. 865.

[63] Type of dual superconductivity for the $SU(2)$ Yang–Mills theory / Nishino S., Kondo K.-I., Shibata A., Sasago T., and Kato S. // Eur. Phys. J. C. — 2019. — Vol. 79, no. 9. — P. 774.

[64] Flux tubes in the SU(3) vacuum: London penetration depth and coherence length / Cea P., Cosmai L., Cuteri F., and Papa A. // Phys. Rev. D. — 2014. — Vol. 89, no. 9. — P. 094505.

[65] Kharzeev D. E., Loshaj F. Partial restoration of chiral symmetry in a confining string // Phys. Rev. D. — 2014. — Vol. 90. — P. 037501.

[66] Cea P., Cosmai L., Papa A. Chromoelectric flux tubes and coherence length in QCD // Phys. Rev. D. — 2012. — Vol. 86. — P. 054501.

[67] Luscher M., Munster G., Weisz P. How Thick Are Chromoelectric Flux Tubes? // Nucl. Phys. B. — 1981. — Vol. 180. — P. 1–12.

[68] Braun M. A., Pajares C., Ranft J. Fusion of strings versus percolation and the transition to the quark gluon plasma // Int. J. Mod. Phys. A. — 1999. — Vol. 14. — P. 2689–2704.

[69] Bali G. S. Casimir scaling of SU(3) static potentials // Phys. Rev. D. — 2000. — Vol. 62. — P. 114503.

[70] Braun M. A., Del Moral F., Pajares C. Percolation of strings and the first RHIC data on multiplicity and tranverse momentum distributions // Phys. Rev. C. — 2002. — Vol. 65. — P. 024907.

[71] Long Range Azimuthal Correlations in Multiple Production Processes at High-energies / Abramovsky V. A., Gedalin E. V., Gurvich E. G., and Kancheli O. V. // JETP Lett. — 1988. — Vol. 47. — P. 337–339.

[72] Altsybeev I. Mean transverse momenta correlations in hadron-hadron collisions in MC toy model with repulsing strings // AIP Conf. Proc. — 2016. — Vol. 1701, no. 1. — P. 100002.

[73] Bierlich C., Gustafson G., Lönnblad L. Collectivity without plasma in hadronic collisions // Phys. Lett. B. — 2018. — Vol. 779. — P. 58–63.

[74] Braun M. A., Pajares C. Elliptic flow from color strings // Eur. Phys. J. C. — 2011. — Vol. 71. — P. 1558.

[75] Braun M. A., Pajares C., Vechernin V. V. Anisotropic flows from colour strings: Monte-Carlo simulations // Nucl. Phys. A. — 2013. — Vol. 906. — P. 14–27.

[76] Braun M. A., Pajares C., Vechernin V. V. Ridge from Strings // Eur. Phys. J. A. — 2015. — Vol. 51, no. 4. — P. 44.

[77] Observation of Charged Particle Correlations Between the Forward and Backward Hemispheres in *pp* Collisions at ISR Energies / Uhlig S., Derado I., Meinke R., and Preissner H. // Nucl. Phys. B. — 1978. — Vol. 132. — P. 15–28.

[78] Capella A., Tran Thanh Van J. Long Range Rapidity Correlations in Hadron-Nucleus Interactions // Phys. Rev. D. — 1984. — Vol. 29. — P. 2512.

[79] Gorenstein M. I., Gazdzicki M. Strongly Intensive Quantities // Phys. Rev. C. — 2011. — Vol. 84. — P. 014904.

[80] Andronov E. V. Influence of the quark–gluon string fusion mechanism on long-range rapidity correlations and fluctuations // Theor. Math. Phys. — 2015. — Vol. 185, no. 1. — P. 1383–1390.

[81] Non-Gaussian particle number fluctuations in vicinity of the critical point for van der Waals equation of state / Vovchenko V., Poberezhnyuk R. V., Anchishkin D. V., and Gorenstein M. I. // J. Phys. A. — 2016. — Vol. 49, no. 1. — P. 015003.

[82] Skewness of mean transverse momentum fluctuations in heavy-ion collisions / Giacalone G., Gardim F. G., Noronha-Hostler J., and Ollitrault J.-Y. // Phys. Rev. C. — 2021. — Vol. 103, no. 2. — P. 024910.

[83] Ferreiro E. G., del Moral F., Pajares C. Transverse momentum fluctuations and percolation of strings // Phys. Rev. C. — 2004. — Vol. 69. — P. 034901.

[84] Pruneau C., Gavin S., Voloshin S. Methods for the study of particle production fluctuations // Phys. Rev. C. — 2002. — Vol. 66. — P. 044904.

[85] Adams J. et al. Minijet deformation and charge-independent angular correlations on momentum subspace (eta, phi) in Au-Au collisions at $\sqrt{s_{NN}} =$ 130 GeV // Phys. Rev. C. — 2006. — Vol. 73. — P. 064907.

[86] Chatrchyan S. et al. Centrality Dependence of Dihadron Correlations and Azimuthal anisotropy Harmonics in PbPb Collisions at $\sqrt{s_{NN}} = 2.76$ TeV // Eur. Phys. J. C. — 2012. — Vol. 72. — P. 2012.

[87] Measurement of collective flow in heavy ion collisions using particle pair correlations / Wang S., Jiang Y. Z., Liu Y. M., Keane D., Beavis D., Chu S. Y., Fung S. Y., Vient M., Hartnack C., and Stoecker H. // Phys. Rev. C. — 1991. — Vol. 44. — P. 1091–1095.

[88] Jia J., Zhou M., Trzupek A. Revealing long-range multiparticle collectivity in small collision systems via subevent cumulants // Phys. Rev. C. — 2017. — Vol. 96, no. 3. — P. 034906.

[89] Prokhorova D. S., Kovalenko V. N. Study of Forward-Backward Multiplicity Fluctuations and Correlations with Pseudorapidity // Phys. Part. Nucl. — 2020. — Vol. 51, no. 3. — P. 323–326.

[90] Prokhorova D. S., Kovalenko V. N. Pseudorapidity Dependence of Multiplicity Fluctuations in a Model of Interacting Quark–Gluon Strings of Finite Rapidity Length // Bull. Russ. Acad. Sci. Phys. — 2020. — Vol. 84, no. 10. — P. 1261–1265.

[91] Correlations between multiplicities and average transverse momentum in the percolating color strings approach / Braun M. A., Kolevatov R. S., Pajares C., and Vechernin V. V. // Eur. Phys. J. C. — 2004. — Vol. 32. — P. 535–546.

[92] Braun M. A., Pajares C., Vechernin V. V. On the forward - backward correlations in a two stage scenario // Phys. Lett. B. — 2000. — Vol. 493. — P. 54–64.

[93] Derrick M. et al. Charged Particle Multiplicity Distributions in e^+e^- Annihilation at 29-GeV: A Comparison With Hadronic Data // Z. Phys. C. — 1987. — Vol. 35. — P. 323.

[94] Kutschera M., Werner K. Negative binomial multiplicity distributions for proton-nucleus collisions from a string model // Z. Phys. C. — 1989. — Vol. 45. — P. 91.

[95] Belokurova S., Vechernin V. Using a Strongly Intense Observable to Study the Formation of Quark-Gluon String Clusters in pp Collisions at LHC Energies // Symmetry. — 2022. — Vol. 14, no. 8. — P. 1673.

[96] Andronov E., Vechernin V. Strongly intensive observable between multiplicities in two acceptance windows in a string model // Eur. Phys. J. A. — 2019. — Vol. 55, no. 1. — P. 14.

[97] Gazdzicki M., Gorenstein M. I., Mackowiak-Pawlowska M. Normalization of strongly intensive quantities // Phys. Rev. C. — 2013. — Vol. 88, no. 2. — P. 024907.

[98] Belokurova S. N., Vechernin V. V. Strongly Intensive Variables and Long-Range Correlations in the Model with a Lattice in the Transverse Plane // Theor. Math. Phys. — 2019. — Vol. 200, no. 2. — P. 1094–1109.

[99] Adam J. et al. Forward-backward multiplicity correlations in pp collisions at $\sqrt{s} = 0.9$, 2.76 and 7 TeV // JHEP. — 2015. — Vol. 05. — P. 097.

[100] Sputowska I. A. Event-by-Event correlations and fluctuations with strongly intensive quantities in heavy-ion and // PoS. — 2022. — Vol. CPOD2021. — P. 027.

[101] Erokhin A. Forward-Backward Multiplicity Correlations with Strongly Intensive Observables in pp Collisions // Available online: https://indico.cern.ch/event/854124/contributions/4134683/, (accessed on 12 January 2021). — 2021. — Vol. 10-15 January.

[102] Andronov E. V., Prokhorova D. S., Belousov A. A. Influence of quark–gluon string interactions on particle correlations in p+p collisions // Theor. Math. Phys. — 2023. — Vol. 216, no. 3. — P. 1265–1277.

[103] Prokhorova D., Andronov E., Feofilov G. Interacting Colour Strings Approach in Modelling of Rapidity Correlations // MDPI Physics. — 2023. — Vol. 5, no. 2. — P. 636–654.

[104] Prokhorova D., Andronov E. Study of Multiplicity and Transverse Momentum Fluctuations in the Monte-Carlo Model of Interacting Quark-Gluon Strings // Phys. Part. Nucl. — 2023. — Vol. 54, no. 3. — P. 412–417.

[105] Prokhorova D., Andronov E. Role of String Fusion Mechanism in Fluctuation Studies // Phys. Atom. Nucl. — 2022. — Vol. 85, no. 6. — P. 1063–1070.

[106] Prokhorova D. S., Andronov E. V. String Fusion Mechanism and Studies of Correlations // Phys. Part. Nucl. Lett. — 2023. — Vol. 20, no. 6. — P. 1496–1499.

[107] Vechernin V., Lakomov I. The dependence of the number of pomerons on the impact parameter and the long-range rapidity correlations in pp collisions // PoS. — 2012. — Vol. Baldin-ISHEPP-XXI. — P. 072.

[108] Vechernin V. V., Belokurova S. N. The strongly intensive observable in *pp* collisions at LHC energies in the string fusion model // J. Phys. Conf. Ser. — 2020. — Vol. 1690, no. 1. — P. 012088.

[109] Armesto N., Derkach D. A., Feofilov G. A. p(t)-multiplicity correlations in a multi-Pomeron-exchange model with string collective effects // Phys. Atom. Nucl. — 2008. — Vol. 71. — P. 2087–2095.

[110] Kovalenko V. Modelling of exclusive parton distributions and long-range rapidity correlations for pp collisions at the LHC energy // Phys. Atom. Nucl. — 2013. — Vol. 76. — P. 1189–1195.

[111] Wilson K. G. Confinement of Quarks // Phys. Rev. D. — 1974. — Vol. 10. — P. 2445–2459.

[112] Iritani T., Cossu G., Hashimoto S. Analysis of topological structure of the QCD vacuum with overlap-Dirac operator eigenmode // PoS. — 2014. — Vol. LATTICE2013. — P. 376.

[113] Bugaev K. A., Zinovjev G. M. On Relation Between the Quark Gluon Bag Surface Tension and the Colour Tube String Tension // Nucl. Phys. A. — 2010. — Vol. 848. — P. 443–453.

[114] Shen C., Schenke B. Dynamical initial state model for relativistic heavy-ion collisions // Phys. Rev. C. — 2018. — Vol. 97, no. 2. — P. 024907.

[115] Vechernin V. V., Kolevatov R. S. Long-range correlations between transverse momenta of charged particles produced in relativistic nucleus-nucleus collisions // Phys. Atom. Nucl. — 2007. — Vol. 70. — P. 1809–1818.

[116] Biro T. S., Nielsen H. B., Knoll J. Color Rope Model for Extreme Relativistic Heavy Ion Collisions // Nucl. Phys. B. — 1984. — Vol. 245. — P. 449–468.

[117] De-Confinement and Clustering of Color Sources in Nuclear Collisions / Braun M. A., Dias de Deus J., Hirsch A. S., Pajares C., Scharenberg R. P., and Srivastava B. K. // Phys. Rept. — 2015. — Vol. 599. — P. 1–50.

[118] Multi-pomeron exchange model for pp and $p\bar{p}$ collisions at ultra-high energy / Bodnia E., Derkach D., Feofilov G., Kovalenko V., and Puchkov A. // PoS. — 2013. — Vol. QFTHEP2013. — P. 060.

[119] Correlation between mean transverse momentum and multiplicity of charged particles in pp and $p\bar{p}$ collisions: from ISR to LHC / Bodnya E. O., Kovalenko V. N., Puchkov A. M., and Feofilov G. A. // AIP Conf. Proc. — 2015. — Vol. 1606, no. 1. — P. 273–282.

[120] Andronov E. V., Kovalenko V. N. Strongly Intensive Fluctuations Between the Multiplicity and the Total Transverse Momentum in pp Interactions in the Multipomeron Exchange Approach // Theor. Math. Phys. — 2019. — Vol. 200, no. 3. — P. 1282–1293.

[121] Multipomeron Model with Collective Effects for High-Energy Hadron Collisions / Kovalenko V., Feofilov G., Puchkov A., and Valiev F. // Universe. — 2022. — Vol. 8, no. 4. — P. 246.

[122] Vechernin V. V. Forward–backward correlations between multiplicities in windows separated in azimuth and rapidity // Nucl. Phys. A. — 2015. — Vol. 939. — P. 21–45.

[123] An introduction to PYTHIA 8.2 / Sjöstrand T., Ask S., Christiansen J. R., Corke R., Desai N., Ilten P., Mrenna S., Prestel S., Rasmussen C. O., and Skands P. Z. // Comput. Phys. Commun. — 2015. — Vol. 191. — P. 159–177.

[124] Bierlich C. et al. A comprehensive guide to the physics and usage of PYTHIA 8.3 // SciPost Phys. Codeb. — 2022. — Vol. 2022. — P. 8.

[125] Skands P., Carrazza S., Rojo J. Tuning PYTHIA 8.1: the Monash 2013 Tune // Eur. Phys. J. C. — 2014. — Vol. 74, no. 8. — P. 3024.

[126] Sjostrand T., Mrenna S., Skands P. Z. PYTHIA 6.4 Physics and Manual // JHEP. — 2006. — Vol. 05. — P. 026.

[127] Abelev B. I. et al. Growth of Long Range Forward-Backward Multiplicity Correlations with Centrality in Au+Au Collisions at $\sqrt{s_{NN}} = 200$ GeV // Phys. Rev. Lett. — 2009. — Vol. 103. — P. 172301.

[128] Aamodt K. et al. Charged-particle multiplicity measurement in proton-proton collisions at $\sqrt{s} = 7$ TeV with ALICE at LHC // Eur. Phys. J. C. — 2010. — Vol. 68. — P. 345–354.

[129] Aamodt K. et al. Transverse momentum spectra of charged particles in proton-proton collisions at $\sqrt{s} = 900$ GeV with ALICE at the LHC // Phys. Lett. B. — 2010. — Vol. 693. — P. 53–68.

[130] Bjorken J. D. Highly Relativistic Nucleus-Nucleus Collisions: The Central Rapidity Region // Phys. Rev. D. — 1983. — Vol. 27. — P. 140–151.

[131] Aamodt K. et al. The ALICE experiment at the CERN LHC // JINST. — 2008. — Vol. 3. — P. S08002.

[132] Multivariate cumulants in flow analyses: The next generation / Bilandzic A., Lesch M., Mordasini C., and Taghavi S. F. // Phys. Rev. C. — 2022. — Vol. 105, no. 2. — P. 024912.

[133] Borghini N., Dinh P. M., Ollitrault J.-Y. A New method for measuring azimuthal distributions in nucleus-nucleus collisions // Phys. Rev. C. — 2001. — Vol. 63. — P. 054906.

[134] Pruneau C. A. Data Analysis Techniques for Physical Scientists. — Cambridge University Press, 2017.

[135] Kitazawa M., Luo X. Properties and uses of factorial cumulants in relativistic heavy-ion collisions // Phys. Rev. C. — 2017. — Vol. 96, no. 2. — P. 024910.

[136] Back B. B. et al. Forward-backward multiplicity correlations in $\sqrt{s_{NN}}$ = 200 GeV Au + Au collisions // Phys. Rev. C. — 2006. — Vol. 74. — P. 011901.

[137] Haussler S., Abdel-Aziz M., Bleicher M. Forward-Backward Charge Fluctuations at RHIC Energies // Nucl. Phys. A. — 2007. — Vol. 785. — P. 253–256.

[138] Brogueira P., Dias de Deus J. Forward-backward rapidity correlations in a two-step scenario // Phys. Lett. B. — 2007. — Vol. 653. — P. 202–205.

[139] Bzdak A., Wozniak K. Forward-backward multiplicity fluctuations in heavy nuclei collisions in the wounded nucleon model // Phys. Rev. C. — 2010. — Vol. 81. — P. 034908.

[140] Prokhorova D., Andronov E. Emergent Flow Signal and the Colour String Fusion // MDPI Physics. — 2024. — Vol. 6, no. 1. — P. 264–289.

[141] Dias de Deus J., Pajares C. Percolation of color sources and critical temperature // Phys. Lett. B. — 2006. — Vol. 642. — P. 455–458.

[142] Shen C., Schenke B. Longitudinal dynamics and particle production in relativistic nuclear collisions // Phys. Rev. C. — 2022. — Vol. 105, no. 6. — P. 064905.

[143] Bresenham J. E. Algorithm for computer control of a digital plotter // IBM Systems Journal. — 1965. — Vol. 4, no. 1. — P. 25–30.

[144] Kovalenko V. Azimuthal anisotropy of long-range correlations at LHC energy in Monte Carlo model with string fusion // EPJ Web Conf. — 2017. — Vol. 137. — P. 07012.

[145] Anisotropic parton escape is the dominant source of azimuthal anisotropy in transport models / He L., Edmonds T., Lin Z.-W., Liu F., Molnar D., and Wang F. // Phys. Lett. B. — 2016. — Vol. 753. — P. 506–510.

[146] Aaboud M. et al. Charged-particle distributions at low transverse momentum in $\sqrt{s} = 13$ TeV pp interactions measured with the ATLAS detector at the LHC // Eur. Phys. J. C. — 2016. — Vol. 76, no. 9. — P. 502.

[147] Braun M. A., Pajares C. Elliptic and triangular flows in dAu collisions at 200 GeV in the fusing color string model // Eur. Phys. J. A. — 2020. — Vol. 56, no. 2. — P. 41.

[148] Braun M. A., Pajares C. Flow coefficients in O-O Al-Al and Cu-Cu collisions at 200 GeV in the fusing color string model // Phys. Rev. C. — 2021. — Vol. 103, no. 5. — P. 054902.

[149] Poskanzer A. M., Voloshin S. A. Methods for analyzing anisotropic flow in relativistic nuclear collisions // Phys. Rev. C. — 1998. — Vol. 58. — P. 1671–1678.

[150] Luzum M., Ollitrault J.-Y. Eliminating experimental bias in anisotropic-flow measurements of high-energy nuclear collisions // Phys. Rev. C. — 2013. — Vol. 87, no. 4. — P. 044907.

[151] Adamczyk L. et al. Centrality dependence of identified particle elliptic flow in relativistic heavy ion collisions at $\sqrt{s_{NN}}$=7.7–62.4 GeV // Phys. Rev. C. — 2016. — Vol. 93, no. 1. — P. 014907.

[152] Aad G. et al. Measurement of the centrality and pseudorapidity dependence of the integrated elliptic flow in lead-lead collisions at $\sqrt{s_{\mathrm{NN}}} = 2.76$ TeV with the ATLAS detector // Eur. Phys. J. C. — 2014. — Vol. 74, no. 8. — P. 2982.

[153] Aaboud M. et al. Measurement of multi-particle azimuthal correlations in pp, p+Pb and low-multiplicity Pb+Pb collisions with the ATLAS detector // Eur. Phys. J. C. — 2017. — Vol. 77, no. 6. — P. 428.

[154] Graczykowski L. K., Janik M. A. Unfolding the effects of final-state interactions and quantum statistics in two-particle angular correlations // Phys. Rev. C. — 2021. — Vol. 104, no. 5. — P. 054909.

[155] Aaboud M. et al. Measurement of long-range multiparticle azimuthal correlations with the subevent cumulant method in pp and $p + Pb$ collisions with the ATLAS detector at the CERN Large Hadron Collider // Phys. Rev. C. — 2018. — Vol. 97, no. 2. — P. 024904.

[156] Acharya S. et al. Long- and short-range correlations and their event-scale dependence in high-multiplicity pp collisions at $\sqrt{s} = 13$ TeV // JHEP. — 2021. — Vol. 05. — P. 290.

[157] Kanakubo Y., Tachibana Y., Hirano T. Interplay between core and corona from small to large systems // EPJ Web Conf. — 2023. — Vol. 276. — P. 01017.

[158] Parkkila J. E. Long-range correlations in low-multiplicity pp collisions at $\sqrt{s} = 13\,\text{TeV}$ // 57th Rencontres de Moriond on QCD and High Energy Interactions. — 2023. — 6.

[159] Werner K., Karpenko I., Pierog T. The 'Ridge' in Proton-Proton Scattering at 7 TeV // Phys. Rev. Lett. — 2011. — Vol. 106. — P. 122004.

[160] CT10 next-to-next-to-leading order global analysis of QCD / Gao J., Guzzi M., Huston J., Lai H.-L., Li Z., Nadolsky P., Pumplin J., Stump D., and Yuan C. P. // Phys. Rev. D. — 2014. — Vol. 89, no. 3. — P. 033009.

[161] New parton distributions for collider physics / Lai H.-L., Guzzi M., Huston J., Li Z., Nadolsky P. M., Pumplin J., and Yuan C. P. // Phys. Rev. D. — 2010. — Vol. 82. — P. 074024.

[162] LHAPDF6: parton density access in the LHC precision era / Buckley A., Ferrando J., Lloyd S., Nordström K., Page B., Rüfenacht M., Schönherr M., and Watt G. // Eur. Phys. J. C. — 2015. — Vol. 75. — P. 132.

APPENDIX A

Developed algorithm of partons' permutations

This Appendix contains the short summary of the developed algorithm that allows one to prepare a set of protons, each containing the given number of partons with the certain fractions of the proton momentum and energy.

First step is to prepare extensive sets of protons for each possible number of partons, n_{part}. For each parton its momentum is sampled as proton momentum fraction, x_i (where i denotes the i-th parton), according to the parton distribution functions (PDFs). In this work, the parametrization was used from CT10nnlo, next-to-next-to-leading order approximation [160] developed by the CTEQ (Coordinate Theoretical-Experimental Project on QCD) group based on CT10 PDFs [161], set 1, of LHAPDF (Les Houches Accord Parton Density Functions) [162] at the momentum transferred, $Q^2 = 1$ GeV^2. A parton is assigned with the current quark mass of a certain flavour that is found from the probability distribution for a given x_i. At this point, there is no restriction to the parton content in terms of x_i.

At the second stage, the generated partons are rearranged between protons to limit the total partons' momentum and energy from above for each proton:

$$\sum_i x_i \leq 1, \quad \sum_i e_i \leq 1, \tag{A.1.1}$$

where e_i is the proton energy fraction carried by the i-th parton and defined as

$$e_i = \sqrt{\frac{m_i^2}{m_{\text{p}}^2 \cosh^2 y_{\text{beam}}} + x_i^2 \tanh^2 y_{\text{beam}}}, \tag{A.1.2}$$

where m_i is a mass of the ith parton, m_{p} is the mass of the proton, and y_{beam} is the proton beam rapidity

$$y_{\text{beam}} = \cosh^{-1}\left(\frac{\sqrt{s}}{2m_{\text{p}}}\right). \tag{A.1.3}$$

It is done to ensure that the total energy and momentum of the partons does not exceed the proton's energy and momentum. To perform this, two protons (necessarily with the same number of partons) are selected and two randomly chosen partons, one taken from each proton, are exchanged between them. The purpose of parton permutation is to bring the sums of x_i and e_i closer to unity. Therefore, if the sums are larger than 1, then the permutation will be accepted only if it decreases $\sum_i x_i$ and $\sum_i e_i$. If, on the contrary, the sums are smaller than 1, the permutation will be accepted only if such a rearrangement increases $\sum_i x_i$ and $\sum_i e_i$. This condition must be satisfied simultaneously for both considered protons.

The computation time of such an algorithm grows crucially with the number of considered partons. Therefore, in reality, one cannot reach exactly the value of 1 for $\sum_i x_i$ and $\sum_i e_i$. Thus, the procedure of permutations stops at some reasonable number of iterations (i.e. when the improvement caused by the exchange of the pair of partons becomes negligible), which leads to the inevitable lack of $\sum_i x_i$ and $\sum_i e_i$ compared to 1. To compensate it, an object called a gluon cloud with the momentum and energy fractions of those of a proton defined as

$$x_{g\text{cloud}} = 1 - \sum_i x_i, \tag{A.1.4}$$

$$e_{g\text{cloud}} = 1 - \sum_i e_i. \tag{A.1.5}$$

is introduced. It is assigned the mass,

$$m_{g\text{cloud}} = \sqrt{E^2_{g\text{cloud}} - p^2_{g\text{cloud}}}, \tag{A.1.6}$$

with $E_{g\text{cloud}}$ the energy and $p_{g\text{cloud}}$ the momentum of the gluon cloud. Gluon cloud is from this moment considered a parton that later is also used to form strings.

APPENDIX B

Improved algorithm for determining the parton composition of protons

In the following subsections, we present the new procedure for simulating a proton with $n_{\rm part} \geq 2$.

B.1 Valence quarks and diquark

We start with the creation of valence u and d quarks by sampling their proton momentum fractions, $x_u^{\rm val}$ and $x_d^{\rm val}$, from their valence parton distribution functions (PDFs), $x \cdot f_u^{\rm val}(x)$ and $x \cdot f_d^{\rm val}(x)$. We find $f_{u,d}^{\rm val}(x)$ as the difference between PDFs for u (d) quark and $\overline{u}$ ($\overline{d}$) antiquark taken from CT10nnlo approximation [160] based on CT10 PDFs [161], set 1 by LHAPDF [162] at the momentum transferred, $Q^2 = 1$ GeV^2.

We consider three possible combinations of selecting 2 out of 3 valence quarks in order to create a diquark (either uu or ud). We define diquark momentum, $x_{\rm di}$, as the sum of the proton momentum fractions of the two selected valence quarks, $x_u^{\rm val} + x_{u,d}^{\rm val}$. The three combinations are ordered by the largest $x_{u,d}^{\rm val}$ of the valence quark that is not included in the diquark.

We put the diquark mass, $m_{\rm di}$, equal to 0.1185 GeV. For quarks, both valence and sea, we start with the current (not constituent) masses: $m_u = 0.0022$ GeV, $m_d = 0.0048$ GeV, $m_s = 0.0950$ GeV, and $m_c = 1.2750$ GeV that are dynamically changed later, see Appendix B.3.

For each parton representing a quark or a diquark and enumerated by $1 \leq i \leq n_{\rm part}$, we calculate its energy, E_i, and its fraction of proton energy, e_i, as

$$E_i = \sqrt{m_i^2 + (x_i \cdot p_{\rm beam})^2}, e_i = \frac{E_i}{E_{\rm proton}}, \tag{B.1.1}$$

where $p_{\text{beam}} = \sqrt{s/4 - m^2_{\text{proton}}}$, $m_{\text{proton}} = 0.938$ GeV, $E_{\text{proton}} = \sqrt{s}/2$.

B.2 Sea quarks

In case of a number of pomeron exchanges greater than one, we take into account the presence of sea quarks that participate in the interaction. We sample the proton momentum fraction for each sea quark, x_i^{sea}, where i runs over values from 1 to $(n_{\text{part}} - 2)$, using the sum of PDFs for all flavours, $\sum_{\text{fl}} x \cdot f_{\text{fl}}(x)$. For a given sea quark (sampled x_i^{sea}) we define its flavour from the relative probability that is known at any given x (i.e. from the ratio between PDFs for different flavours, $f_{\text{fl}}(x)$, at x). Gluons are not considered at this stage because they are accounted for differently (see Appendix B.3). For each sea quark we also calculate e_i according to Eq. (B.1.1).

B.3 Energy-momentum conservation for a proton

At this point we take a step back and verify that the sums of partons' x_i and e_i are less than one. Otherwise we regenerate a proton from scratch.

Once it is achieved, one has to respect the energy-momentum conservation law within a proton. Namely, the sums for both x_i and e_i for all n_{part} should be equal to 1. However, at this step one cannot guarantee these conditions to be fulfilled. Therefore, we find the deficiencies, x_0 and e_0, as

$$x_0 = 1 - \sum_{i=1}^{n_{\text{part}}} x_i, e_0 = 1 - \sum_{i=1}^{n_{\text{part}}} e_i. \tag{B.3.1}$$

In this study, we distribute x_0 and e_0 between all the created partons (both valence and sea), which may be interpreted as a gluon contribution. For example, in the event with $n_{\text{pom}} = 1$ we split x_0 and e_0 in half between valence quark and diquark. Thus, for the bare valence quark and diquark (in equations below the subscript i is replaced by the notation q/di) one gets the modified fractions of proton momentum, $x_{q/\text{di}}^{\text{dressed}}$, and proton energy, $e_{q/\text{di}}^{\text{dressed}}$, from

$$x_{q/\text{di}}^{\text{dressed}} = x_{q/\text{di}}^{\text{bare}} + 0.5 \cdot x_0, \tag{B.3.2}$$

$$e_{q/\text{di}}^{\text{dressed}} = e_{q/\text{di}}^{\text{bare}} + 0.5 \cdot e_0. \tag{B.3.3}$$

Once we take into account the gluon contributions, we can define the initial parton momentum as

$$p_{\text{part}} = x_{\text{part}}^{\text{dressed}} \cdot p_{\text{beam}} \tag{B.3.4}$$

and the initial parton energy as

$$E_{\text{part}} = e_{\text{part}}^{\text{dressed}} \cdot E_{\text{proton}}. \tag{B.3.5}$$

This modification changes their masses from "bare" (current) values, m_{di} or $m_{\text{u/d/s/c}}$, to the "dressed" ones, $m_{q/\text{di}}^{\text{dressed}}$, according to

$$m_{q/\text{di}}^{\text{dressed}} = \sqrt{E_{\text{part}}^2 - p_{\text{part}}^2}. \tag{B.3.6}$$

This approach can be naturally extrapolated to any arbitrary number of sea quarks. Namely, we assign $1/3 \cdot x_0$ and $1/3 \cdot e_0$ to each of the valence quark and the diquark and split the remaining $1/3$ between all the sea quarks in a proton. This procedure increases the masses of quarks and diquark (for valence ones to a greater extent), which makes the distributions of the string ends' rapidities more realistic.

However, it is also possible that after this procedure, parton's energy decreases compared to parton's momentum. Therefore, one cannot calculate it's dressed mass, $m_{q/\text{di}}^{\text{dressed}}$. To solve this we check all the three possible combinations of valence quarks combined into a diquark, preferring to have the largest $x_{u,d}^{\text{val}}$ for the valence quark that is not included in a diquark. If the aforementioned difficulty makes it impossible, we will opt for the next combination. If this cannot be arranged anyhow, we will regenerate the proton from scratch.